University of Rhode Island
DigitalCommons@URI

Open Access Dissertations

2014

DYNAMIC RESPONSE OF TAILORED CARBONBASED MULTIFUNCTIONAL COMPOSITES

Nicholas J. Heeder
University of Rhode Island, nicholas.heeder@gmail.com

Follow this and additional works at: https://digitalcommons.uri.edu/oa_diss

Terms of Use
All rights reserved under copyright.

Recommended Citation
Heeder, Nicholas J., "DYNAMIC RESPONSE OF TAILORED CARBONBASED MULTIFUNCTIONAL COMPOSITES" (2014). *Open Access Dissertations.* Paper 236.
https://digitalcommons.uri.edu/oa_diss/236

This Dissertation is brought to you by the University of Rhode Island. It has been accepted for inclusion in Open Access Dissertations by an authorized administrator of DigitalCommons@URI. For more information, please contact digitalcommons-group@uri.edu. For permission to reuse copyrighted content, contact the author directly.

DYNAMIC RESPONSE OF TAILORED CARBON-BASED MULTIFUNCTIONAL COMPOSITES

BY

NICHOLAS J. HEEDER

A DISSERTATION SUBMITTED IN PARTIAL FULFILLMENT OF THE

REQUIREMENTS FOR THE DEGREE OF

DOCTOR OF PHILOSOPHY

IN

MECHANICAL, INDUSTRIAL AND SYSTEMS ENGINEERING

UNIVERSITY OF RHODE ISLAND

2014

DOCTOR OF PHILOSOPHY DISSERTATION

BY

NICHOLAS J. HEEDER

APPROVED:

Thesis Committee:

Major Professor Arun Shukla

David G. Taggart

Arijit Bose

Nasser H. Zawia
DEAN OF THE GRADUATE SCHOOL

UNIVERSITY OF RHODE ISLAND
2014

ABSTRACT

The importance of nanotechnology in the world has dramatically increased in the recent years as miniaturization has become more important in areas such as computing, sensing, biomedicine and many others. Advancements in these disciplines depend largely on the ability to synthesize nanoparticles of various shapes and sizes, as well as to assemble them efficiently into complex architectures. Currently, materials reinforced with nanoparticles have an enormous range of applications owing to their superb mechanical and physical properties. More specifically, recent progress has shown that using inorganic nanomaterials as fillers in polymer/inorganic composites has tremendous application potential in automotive, aerospace, construction and electronics industries. If properly incorporated into a polymeric matrix, conductive nanofillers such as carbon nanotubes (CNTs) and graphene can be assembled into a three-dimensional electrical network. Furthermore, these highly intricate networks can be utilized as an internal sensory mechanism capable of detecting information such as material deformation and various forms of damage. Fundamental investigation into the mechanical and electrical properties of nanomaterial-based polymer composites when subjected to loading is paramount before they can be incorporated into high performance applications. For this purpose, a comprehensive study was conducted to understand the electro-mechanical behavior of both CNT-based and graphene-based composites under static and dynamic loading conditions. Moreover, novel strategies were developed to produce designer graphene-based composites that possess tailored transport and mechanical properties.

A series of dynamic compressive experiments were performed to experimentally investigate the electrical response of multi-wall carbon nanotube (MWCNT) reinforced epoxy nanocomposites subjected to split Hopkinson pressure bar (SHPB) loading. Low-resistance CNT/epoxy specimens were fabricated using a combination of shear mixing and ultrasonication. Utilizing the carbon nanotube network within, the electrical resistance of the nanocomposites was monitored using a high-resolution four-point probe method during each compressive loading event. In addition, real-time deformation images were captured using high-speed photography. The percent change in resistance was correlated to both strain and real-time damage. The results were then compared to previous work conducted by the authors (quasi-static and drop-weight impact) in order to elucidate the strain rate sensitivity on the electrical behavior of the material. In addition, the percent change in conductivity was determined using a Taylor expansion model to investigate the electrical response based upon both dimensional change as well as resistivity change during mechanical loading within the elastic regime. Experimental findings indicate that the electrical resistance is a function of both the strain and deformation mechanisms induced by the loading. The bulk electrical resistance of the nanocomposites exhibited an overall decrease of 40-65% for quasi-static and drop-weight experiments and 65-85% for SHPB experiments.

An experimental investigation was conducted to understand the electro-mechanical response of graphene reinforced polystyrene composites under static and dynamic loading. Graphene-polystyrene composites were fabricated using a solution mixing approach followed by hot-pressing. Absolute resistance values were measured with a high-resolution four-point probe method for both quasi-static and dynamic

loading. A modified split Hopkinson (Kolsky) pressure bar apparatus, capable of simultaneous mechanical and electrical characterization, was developed and implemented to investigate the dynamic electro-mechanical response of the composites. In addition to measuring the change in electrical resistance as well as the dynamic constitutive behavior, real-time surface damage and global deformation was captured using high-speed photography. The real-time damage was correlated to both stress-strain and percent change in resistance profiles. The experimental findings indicate that the bulk electrical resistance of the composite increased significantly due to the brittle nature of the polystyrene matrix and the presence of relative agglomerations of graphene platelets which resulted in micro-crack formations.

A novel capillary-driven particle-level templating technique along with hot melt pressing was developed and utilized to disperse few-layer graphene (FLG) flakes within a polystyrene matrix to enhance the electrical conductivity of the polymer. The conducting pathways provided by the graphene located at the particle surfaces through contact of the bounding surfaces allow percolation at a loading of less than 0.01% by volume. This method of distributing graphene within a matrix overcomes the need to disperse the sheet-like conducting fillers isotropically within the polymer, and can be scaled up easily.

The novel capillary-driven particle-level templating technique was then extended to allow for distribution of conductive sheet-like particles, such as graphite nanoplatelets (GNPs) into specially constructed architectures throughout a polystyrene matrix to form multi-functional composites with tailored electro-mechanical properties. By precisely controlling the temperature and pressure during a melt

compression process, highly conductive segregated composites were formed using very low loadings of graphene particles. Since the graphene flakes form a honeycomb percolating network along the boundaries between the polymer matrix particles, the composites show very high electrical conductivity but poor mechanical strength. To improve the mechanical properties, a new processing technique was developed that uses rotary shear through fixed angles to gradually evolve the honeycomb graphene network into a concentric band structure over the dimensions of the sample. An experimental investigation was conducted to understand the effect of GNP loading as well as the rotary shear angle on the mechanical strength and electrical conductivity of the composites. The experimental results show that both the electrical and mechanical properties of the composites are significantly altered using this very simple technique, which allows rational co-optimization of competing mechanical and electrical performance as appropriate for a given target application .

Flexible multi-functional composites with tailored electro-mechanical properties were produced using a modified capillary-driven particle-level templating technique. A fixed-angle rotary shear technique was utilized during the melt compression process to distribute GNPs into specially constructed architectures throughout a styrene-butadiene matrix. An experimental investigation was conducted to understand the effect of GNP loading as well as rotary shear angle on the mechanical strength and electrical conductivity of the composites. The experimental results show that this technique can be used to produce flexible composites that possess exceptional conductivity while still maintaining the salient mechanical characteristics the copolymer has to offer.

ACKNOWLEDGEMENTS

First and foremost I would like to thank Dr. Arun Shukla for his continuous guidance and support throughout this research. His patience and adamant work ethic has truly been inspirational and motivating throughout my graduate studies. I cannot thank him enough for all of the positive things he has instilled into me to help me grow as an engineer, a researcher and most of all an individual. He is not only an outstanding professor and mentor but a truly inspirational human being. It has been an honor for me to be one of his graduate students.

I would also like to sincerely thank Dr. Sze Yang, Dr. Vijaya Chalivendra, Dr. Arijit Bose, Dr. Robert Hurt, and Dr. Anubhav Tripathi for their continued support throughout this research. Furthermore, I would like to thank Dr. David G. Taggart, Dr. Arijit Bose, Dr. Carl-Ernst Rousseau and Dr. Sze Yang for agreeing to serve as my committee members.

The help and encouragement from my friends and colleagues are greatly appreciated. I would like to thank all of my lab mates in the Dynamic Photo Mechanics Laboratory that have been by my side and influenced me along the way: Sachin Gupta, Ryan Sekac, Nathaniel Gardner, Erheng Wang, Sandeep Abotula, Puneet Kumar, Jefferson Wright, Daniel Gracia, Alexander Escher, Chris O'Connell, Emad Makki, Prathmesh Parrikar, Payam Fahr, Frank LiVolsi, Abayomi Yussuf, Chris Shillings, Murat Yazici, Venkitanarayanan Parameswaran, İdris Karen, Kim McCarthy and Anil Rajesh Kumar C. I would also like to thank Indrani Chakraborty, Fei Guo, Michael Godfrin, and Kaushal Purohit for all of their continued support throughout my research. The time spent with everyone has made it an incredible

experience as well as provided me with many great friendships. In addition, I would also like to thank Dave Ferreira, Joe Gomez, Jim Byrnes, Rob D'Ambrosca, AJ Bothun, Jen Cerullo, Nancy Dubee and the rest of the mechanical engineering department faculty and staff.

I would like to acknowledge the financial support provided by the Rhode Island Science & Technology Advisory Council as well as Research Experiences for Undergraduates National Science Foundation (CMMI 1233887).

Last but not least, I would like to thank my parents Craig and Mary, my grandparents Bob and Jane Cola, my sisters Katie, Jamie, and Jenna and my extended family for their understanding nature and endless support throughout my studies.

PREFACE

An experimental investigation has been conducted to investigate the electro-mechanical behavior of multifunctional materials under static and dynamic loading. Additionally, novel strategies to develop multifunctional materials with tunable properties have also been developed. Understanding the overall electro-mechanical response of these multifunctional composites will lead to the development of improved smart materials capable of sensing crucial information such as material deformation and damage within the material. Due to the increased demand for high performance materials that possess multi-functionalities, a comprehensive understanding of the dynamic electro-mechanical response of multi-functional composites is pivotal. This dissertation addresses the dynamic electro-mechanical behavior of both carbon nanotube (CNT) and graphene reinforced composites under compressive loadings. This dissertation is prepared using the manuscript format.

Chapter 1 provides an overview of previous and current published literature of subject matter relevant to this dissertation. Topics include a brief background of CNTs and graphene, the use of these types of filler material as reinforcement of polymer composites, various methods of incorporating conductive nanofillers into polymers, the characterization of multifunctional composites, as well as the mechanical and electrical response of such composites under different forms of mechanical loading. This chapter serves to provide a review of the relevant research in literature, the possible data gaps that exist, as well as an introduction to the studies within this dissertation.

Chapter 2 investigates the electrical behavior of CNT/epoxy nanocomposites subjected to split Hopkinson pressure bar (SHPB) loading. An SHPB apparatus was utilized to load the specimens while the resistance history and high speed deformation images were both captured. In addition, the percent change in conductivity was determined using a Taylor expansion model to investigate the electrical response based upon both dimensional change as well as resistivity change during mechanical loading within the elastic regime. This chapter will follow the formatting guidelines specified by the *Journal of Material Science*.

Chapter 3 focuses on the electro-mechanical behavior of graphene/polystyrene composites under dynamic loading. An experimental investigation was conducted to understand the electro-mechanical response of graphene reinforced polystyrene composites under static and dynamic loading. Graphene-polystyrene composites were fabricated using a solution mixing approach followed by hot-pressing. Absolute resistance values were measured with a high-resolution four-point probe method for both quasi-static and dynamic loading. A modified split Hopkinson (Kolsky) pressure bar apparatus, capable of simultaneous mechanical and electrical characterization, was developed and implemented to investigate the dynamic electro-mechanical response of the composites. In addition to measuring the change in electrical resistance as well as the dynamic constitutive behavior, real-time surface damage and global deformation was captured using high-speed photography. The real-time damage was correlated to both stress-strain and percent change in resistance profiles. This chapter will follow the formatting guidelines specified by the *Journal of Experimental Mechanics*.

Chapter 4 details a novel strategy developed for producing highly conductive graphene-based segregated composites prepared by particle templating. A capillary-driven particle-level templating technique and hot melt pressing was used to disperse few-layer graphene (FLG) flakes within a polystyrene matrix to enhance the electrical conductivity of the polymer. The conducting pathways provided by the graphene located at the particle surfaces through contact of the bounding surfaces allow percolation at a loading of less than 0.01% by volume. This chapter will follow the formatting guidelines specified by the *Journal of Materials Science*.

Chapter 5 details a novel method for tailoring the electro-mechanical properties of templated graphene/polymer composites by using fixed-angle rotary shear. A capillary-driven particle-level templating technique was utilized to distribute graphite nanoplatelets (GNPs) flakes into specially constructed architectures throughout a polystyrene matrix to form multi-functional composites with tailored electro-mechanical properties. By precisely controlling the temperature and pressure during a melt compression process, highly conductive segregated composites were formed using very low loadings of graphene particles. Since the graphene flakes form a honeycomb percolating network along the boundaries between the polymer matrix particles, the composites show very high electrical conductivity but poor mechanical strength. To improve the mechanical properties, a novel processing technique was developed that uses rotary shear through fixed angles to gradually evolve the honeycomb graphene network into a concentric band structure over the dimensions of the sample. An experimental investigation was conducted to understand the effect of GNP loading as well as rotary shear angle on the mechanical strength and electrical

conductivity of the composites. This chapter will follow the formatting guidelines specified by the *Journal of Composites Science and Technology.*

Chapter 6 provides the details of utilizing the novel fabrication technique to produce tunable flexible graphene/polymer composites with enhanced exceptional electrical and mechanical performance. Flexible multi-functional composites with tailored electro-mechanical properties were produced using a capillary-driven particle-level templating technique. A fixed-angle rotary shear technique was utilized during the melt compression process to distribute graphite nanoplatelets (GNPs) into specially constructed architectures throughout a styrene-butadiene matrix. An experimental investigation was conducted to understand the effect of GNP loading as well as rotary shear angle on the mechanical strength and electrical conductivity of the composites. This chapter will follow the formatting guidelines specified by the *Journal of Composites Part A: Applied Science and Manufacturing.*

Chapter 7 provides a summary of the major experimental findings obtained during the investigation of the various types of multifunctional materials when subjected to various rates of loading. Suggestions for future designs, as well as experiments and analysis will also be provided.

TABLE OF CONTENTS

LIST OF FIGURES

CHAPTER 2

CHAPTER 3

CHAPTER 6

CHAPTER 1

INTRODUCTION AND LITERATURE REVIEW

The importance of nanotechnology in the world has dramatically increased in the recent years as miniaturization has become more important in areas such as computing, sensing, biomedicine and many others. Advancements in these disciplines depend largely on the ability to synthesize nanoparticles of various shapes and sizes, as well as to assemble them efficiently into complex architectures. Currently, materials reinforced with nanoparticles have an enormous range of applications owing to their superb mechanical and physical properties. More specifically, recent progress has shown that using inorganic nanomaterials as fillers in polymer/inorganic composites has tremendous application potential in industries such as automotive, aerospace, construction and electronics [1-7]. If properly incorporated into a polymeric matrix, conductive nanofillers such as CNTs and graphene can be assembled into a three-dimensional electrical network. Furthermore, these highly intricate networks can be utilized as an internal sensory mechanism capable of detecting crucial information such as material deformation and various forms of damage. Despite recent progresses on the mechanical and electrical characterization of nanomaterial-based polymer composites, little results have been published regarding the electro-mechanical behavior of such composites when subjected to dynamic loading conditions. To meet this need, CNT-based composites as well as graphene-based composites will be investigated to study their electro-mechanical behavior under dynamic loading.

Extraordinary mechanical properties and excellent transport properties make CNTs and graphene a promising addition to the future of smart composite materials

[1-7]. CNTs are a promising addition to the future of developing novel materials capable of self-sensing and active response due to their extraordinary electrical conductivity and excellent transport properties. Unlike other smart materials, CNTs can provide both structural and functional capabilities simultaneously and have been used in many applications including actuation, sensing, and power generation [8-11]. Carbon nanotube-based polymeric nanocomposites have found new applications in various fields such as future spacecraft, anti-meteorite/anti-ballistic shields for satellites, anti-ballistic vests, explosion-proof blankets for aircraft cargo bays, and safety belts [12, 13].

Significant research has been performed to fundamentally understand the enhancement of mechanical properties due to CNT reinforcement of polymers [14, 15]. Allaoui et al. [16] investigated the influence of multi-walled carbon nanotubes (MWCNTs) in a rubbery epoxy matrix, and found that the addition of up to 4 wt.% MWCNTs could lead to a significant increase in the strength and Young's modulus [17]. Given the practical potential applications of CNTs in electromechanical devices, specifically as piezoresistive sensors, the effect of mechanical deformation on the electrical properties of individual CNTs has been studied theoretically [18-21] and experimentally [19, 21].

An increased amount of research has been conducted in studying the electrical response of CNT/polymer composites under mechanical loading. Alexopoulos et al. [18], Nofar et al. [20], and Gao et al. [22, 23] have studied damage detection and health monitoring of composites reinforced with CNT-embedded glass fibers. Alexopoulos et al. [18] performed various incremental tensile loading-unloading steps

as well as three-point bending tests on specimens with CNT fibers in the tensile region. Results indicated that CNT fibers provide unquestionable advantages for sensing and damage monitoring of non-conductive composites, when compared to the competitors, e.g. the embedded carbon fibers and a modified (doped) conductive network. Sensing ability for the investigated specimens with CNT fibers in the compressive region was also reported. Gao et al. [23] studied the sensing of damage development in composites using CNT networks utilizing two sensing techniques: electrical resistance and acoustic emission. Resistance change and acoustic emission counts showed a bi-linear relation in detecting damage in quasi-static and cyclic experiments which can be used to give additional insight toward damage evolution. Thostenson et al. [24] performed tensile experiments on CNT/epoxy samples and demonstrated a highly linear relationship between the specimen deformation and the electrical resistance. This result suggests that CNT networks formed in an epoxy polymer matrix could be utilized as highly sensitive sensors for detecting the evolution of damage in advanced polymer-based composites [24]. Later, Lim et al. [25] experimentally investigated the mechanical and electrical response of CNT-based fabric composites to Hopkinson bar loading, further demonstrating the effectiveness of a percolating carbon nanotube network being capable of sensing damage caused by impact. In their previous work, the authors experimentally investigated the electrical response of multi-walled carbon nanotube reinforced nanocomposites under quasi-static and dynamic loading. The results indicated that the electrical resistance of the nanocomposite decreased under both quasi-static and dynamic loading due to the

formation of more efficient carbon nanotube networks caused by the compression of the epoxy matrix [25, 26].

Although carbon nanotubes (CNTs) possess excellent physical and mechanical properties, graphene amazingly possesses superior electrical and thermal properties, as well as a higher specific surface area [4, 27]. Its reinforcement can also offer exceptional properties in future high performance novel composites. In recent years, graphene based composites have become a topic of significant academic and industrial interest. While a number of studies have shown that the presence of graphene within polymers can enhance the mechanical properties of the bulk composite [27-33], other studies have shown that graphene can also have adverse effects on the mechanical properties [34-36]. Fang et al. [28] investigated the effect of low concentrations of graphene on the mechanical strength of graphene/polystyrene composites. The results showed a substantial increase in tensile strength as graphene loadings were increased from 0.1 wt. % to 0.9 wt. % in comparison to pristine polystyrene. The increase in strength was attributed to effective load transfer between the graphene and polymer. Alternatively, the addition of certain filler materials can also have adverse effects on the mechanical properties of the resulting composite due to factors such as reinforcement phase concentration, dispersion quality, interface bonding, aspect ratio, surface-to-volume ratio of filler, etc. [27, 34-39]. Wang et al. [39] compared the use of graphite nanosheets to carbon black as a filler material in high density polyethylene. They reported a gentle increase in both tensile strength and impact strength of the composite with low loadings of graphene (0.5 to 2.0 wt. %) but a sharp reduction when the graphene content was greater than 2 wt. %. Due to the high surface energy of

graphene, as well as the weak interaction between the graphene and polyethylene, an inhomogeneous dispersion in the polymer matrix was formed when the content of graphene was high, leading to adverse effects on the properties of the composites.

Due to the exceptional electrical properties of graphene, several researchers in the past have also studied the utilization of graphene as an electrically conductive additive in composites [3, 38, 40, 41]. The electrical conductivity of graphene-based composites has been studied theoretically [42] as well as experimentally [38, 41, 43, 44]. Studies have shown remarkable increases in composite electrical properties with graphene reinforcement. More recently, Qi et al. [41] demonstrated a substantial enhancement of electrical properties of polystyrene (PS) with the addition of graphene. The conductivity of the graphene/polystyrene composite was shown to be ~ 2–4 orders of magnitude higher than that of multi-walled-carbon-nanotube/polystyrene composites.

The combination of the remarkable mechanical properties and the exceptional electrical properties make graphene another ideal candidate for use as a filler material in fabricating multi-functional composites capable of sensing material behavior. Many reports demonstrate the effectiveness of utilizing graphene in providing strain sensing functions [45-47]. Eswaraiah et al. [45] demonstrated the real time strain response of functionalized graphene-polyvinylidene fluoride (f-G-PVDF) composites on the macro-scale under tensile loads and the use of the composite as a strain sensor. The analysis of the change in voltage of various composite films revealed that the graphene-based composite showed better strain sensing performance compared to carbon nanotube-based polymer composites. In their previous work, the authors

experimentally investigated the electrical response of multi-walled carbon nanotube reinforced nanocomposites under quasi-static and dynamic loading. The results indicated that the electrical resistance of the nanocomposite decreased under both quasi-static and dynamic loading due to the formation of more efficient carbon nanotube networks caused by the compression of the epoxy matrix [26, 48].

Apart from this, it was identified that the practical use of graphene has been heavily restricted because current polymer processing technologies distribute graphene in a highly anisotropic fashion within polymer matrices, undermining some of the key advantages of using graphene as a filler material. The predicted percolation threshold for randomly aligned and uniformly dispersed 2-dimensional sheets such as graphene (aspect ratio ~ 4000) in a matrix is 0.01 % by volume [49]. Achieving this threshold is difficult, because strong van der Waals interactions between these sheets lead to aggregation [50, 51]. In addition, most processing techniques, especially at the pilot and commercial scales result in highly anisotropic flows, which tend to align sheets along the direction of flow, thereby inhibiting the formation of a percolating network. Achieving the theoretical percolation limit for scalable techniques has therefore been difficult. Because of the energy demand for removing solvents, and sometimes their potentially hazardous nature, melt processing is often chosen over solvent based mixing of filler and polymer, despite the increased viscosity of a melt. Dispersing high aspect ratio sheets isotropically in a melt of high viscosity is a major challenge.

An alternate method for creating a connected pathway for conductive particles is to make segregated composites. The conductive particles within segregated composites are only permitted to reside on the surfaces of the polymer matrix

particles. When consolidated into a monolith, these conductive particles become connected in a three-dimensional network, dramatically increasing the conductivity of the composite [52-55]. Sheets do not have to be distributed isotropically throughout a matrix to achieve percolation, overcoming a major limitation. This way of achieving three-dimensional connectivity of the particles also decreases the contact resistance between the particles [52]. Du et al. prepared multi-walled carbon nanotube (MWCNT)/high density polyethylene (HDPE) and graphene nanosheets (GNS)/HDPE composites with a segregated network structure by alcohol-assisted dispersion and hot-pressing. The electrical properties of the GNS/HDPE and MWCNT/HDPE composites were compared and it was found that the percolation threshold of the GNS/HDPE composites (1 % v/v) was much higher than that of the MWCNT/HDPE composites (0.15 % v/v) while the MWCNT/HDPE composite showed higher electrical conductivity than the GNS/HDPE composite at the same filler content. They concluded that, due to crimp, rolling and aggregation of the GNSs in the HDPE matrix, the two dimensional GNSs were not as effective as MWCNTs in forming conductive networks. Later, Hu et al. prepared graphene/polyethylene segregated composites using a two-step process. A combination of sonication and mechanical mixing was used to first coat the ultrahigh molecular weight polyethylene (UHMWPE) with graphene oxide (GO) sheets. The excess solvent was removed from the system and then the coated powders were added to a hydrazine solution and stirred at 95 º C to reduce the GO to graphene. All coated powders were compressively molded and hot pressed to form composite sheets. This two-step process was shown to effectively prevent aggregation, leading to composites exhibiting high electrical

conductivity at a very low percolation threshold (0.028 % v/v). To date, there have been no studies reported on the electro-mechanical behavior of either CNT- or graphene-reinforced polymers when subjected to dynamic loading.

REFERENCES

[1] R. Frazier, D. Daly, R. Swatloski, K. Hathcock and C. South, Recent progress in graphene-related nanotechnologies, in "Recent Patents on Nanotechnology" (2009) p. 164.

[2] D. Y. Godovsky, in "Biopolymers Â• PVA Hydrogels, Anionic Polymerisation Nanocomposites" (Springer Berlin Heidelberg, 2000) p. 163.

[3] H. Kim, Y. Miura and C. W. Macosko, Chemistry of Materials 22 (2010) 3441.

[4] T. Kuilla, S. Bhadra, D. Yao, N. H. Kim, S. Bose and J. H. Lee, Progress in Polymer Science 35 (2010) 1350.

[5] T. Ramanathan, A. A. Abdala, StankovichS, D. A. Dikin, M. Herrera Alonso, R. D. Piner, D. H. Adamson, H. C. Schniepp, ChenX, R. S. Ruoff, S. T. Nguyen, I. A. Aksay, R. K. Prud'Homme and L. C. Brinson, Nat Nano 3 (2008) 327.

[6] C. Soldano, A. Mahmood and E. Dujardin, Carbon 48 (2010) 2127.

[7] Y. Zhu, S. Murali, W. Cai, X. Li, J. W. Suk, J. R. Potts and R. S. Ruoff, Advanced Materials 22 (2010) 3906.

[8] M. Dash, M. Tripathy, A. Sasmal, G. Mohanty and P. L. Nayak, Journal of Materials Science 45 (2010) 3858.

[9] I. Kang, Y. Y. Heung, J. H. Kim, J. W. Lee, R. Gollapudi, S. Subramaniam, S. Narasimhadevara, D. Hurd, G. R. Kirikera, V. Shanov, M. J. Schulz, D. Shi, J. Boerio, S. Mall and M. Ruggles-Wren, Composites Part B: Engineering 37 (2006) 382.

[10] J. Sumfleth, S. Buschhorn and K. Schulte, Journal of Materials Science 46 (2011) 659.

[11] K. You, S. Park, C. Lee, J. Kim, G. Park and W. Kim, Journal of Materials Science 46 (2011) 6850.

[12] A. B. Dalton, S. Collins, J. Razal, E. Munoz, V. H. Ebron, B. G. Kim, J. N. Coleman, J. P. Ferraris and R. H. Baughman, Journal of Materials Chemistry 14 (2004) 1.

[13] C. Park, Z. Onuaies, K. Watson, K. Pawlowski, S. Lowther, J. Connell, E. Siochi, J. Harrison and T. St. Clair, Polymer-Single Wall Carbon Nanotube Composites for Potential Spacecraft Applications. Material Research Society, in "Material Research Society " (2010).

[14] C. Li, E. T. Thostenson and T.-W. Chou, Composites Science and Technology 68 (2008) 1227.

[15] E. T. Thostenson, Z. Ren and T.-W. Chou, Composites Science and Technology 61 (2001) 1899.

[16] A. Allaoui, S. Bai, H. M. Cheng and J. B. Bai, Composites Science and Technology 62 (2002) 1993.

[17] P. Guo, X. Chen, X. Gao, H. Song and H. Shen, Composites Science and Technology 67 (2007) 3331.

[18] N. D. Alexopoulos, C. Bartholome, P. Poulin and Z. Marioli-Riga, Composites Science and Technology 70 (2009) 260.

[19] A. Bezryadin, A. R. M. Verschueren, S. J. Tans and C. Dekker, Physical Review Letters 80 (1998) 4036.

[20] M. Nofar, S. V. Hoa and M. D. Pugh, Composites Science and Technology 69 (2009) 1599.

[21] S. Paulson, M. R. Falvo, N. Snider, A. Helser, T. Hudson, A. Seeger, R. M. T. II, R. Superfine and S. Washburn, Applied Physics Letters 75 (1999) 2936.

[22] L. Gao, T.-W. Chou, E. T. Thostenson and Z. Zhang, Carbon 48 (2010) 3788.

[23] L. Gao, E. T. Thostenson, Z. Zhang and T.-W. Chou, Carbon 47 (2009) 1381.

[24] E. T. Thostenson and T. W. Chou, Advanced Materials 18 (2006) 2837.

[25] A. S. Lim, Q. An, T.-W. Chou and E. T. Thostenson, Composites Science and Technology 71 (2011) 616.

[26] N. J. Heeder, A. Shukla, V. Chalivendra, S. Yang and K. Park, Experimental Mechanics 52 (2012) 315.

[27] V. Singh, D. Joung, L. Zhai, S. Das, S. I. Khondaker and S. Seal, Progress in Materials Science 56 (2011) 1178.

[28] M. Fang, K. Wang, H. Lu, Y. Yang and S. Nutt, Journal of Materials Chemistry 19 (2009) 7098.

[29] U. Khan, P. May, A. O'Neill and J. N. Coleman, Carbon 48 (2011) 4035.

[30] J. Liang, Y. Huang, L. Zhang, Y. Wang, Y. Ma, T. Guo and Y. Chen, Advanced Functional Materials 19 (2009) 2297.

[31] T. Rath and Y. Li, Composites Part A: Applied Science and Manufacturing 42 (2011) 1995.

[32] S. Vadukumpully, J. Paul, N. Mahanta and S. Valiyaveettil, Carbon 49 (2011) 198.

[33] S. Yang, W. Lin, Y. Huang, H. Tien, J. Wang, C. Ma, S. Li and Y. Wang, Carbon 49 (2011) 793.

[34] G. Goncalves, P. A. A. P. Marques, A. Barros-Timmons, I. Bdkin, M. K. Singh, N. Emami and J. Gracio, Journal of Materials Chemistry 20 (2010) 9927.

[35] H. Kim and C. W. Macosko, Macromolecules 41 (2008) 3317.

[36] A. Yasmin and I. M. Daniel, Polymer 45 (2004) 8211.

[37] H. Sahrim, A. Mou'ad, S. Yahya and R. Rozaidi, in "Carbon Nanotubes - Synthesis, Characterization, Applications", edited by S. Yellampalli (InTech, 2011).

[38] S. Stankovich, D. A. Dikin, G. H. B. Dommett, K. M. Kohlhaas, E. J. Zimney, E. A. Stach, R. D. Piner, S. T. Nguyen and R. S. Ruoff, Nature 442 (2006) 282.

[39] L. Wang, J. Hong and G. Chen, Polymer Engineering & Science 50 (2010) 2176.

[40] H. Kim and C. W. Macosko, Polymer 50 (2009) 3797.

[41] X.-Y. Qi, D. Yan, Z. Jiang, Y.-K. Cao, Z.-Z. Yu, F. Yavari and N. Koratkar, ACS Applied Materials & Interfaces 3 (2011) 3130.

[42] I.-H. Kim and Y. G. Jeong, Journal of Polymer Science Part B: Polymer Physics 48 (2010) 850.

[43] C. Ramirez, F. M. Figueiredo, P. Miranzo, P. Poza and M. I. Osendi, Carbon 50 (2012) 3607.

[44] H.-B. Zhang, W.-G. Zheng, Q. Yan, Y. Yang, J.-W. Wang, Z.-H. Lu, G.-Y. Ji and Z.-Z. Yu, Polymer 51 (2010) 1191.

[45] V. Eswaraiah, K. Balasubramaniam and S. Ramaprabhu, Journal of Materials Chemistry 21 (2011) 12626.

[46] W. Li, A. Dichiara and J. Bai, Composites Science and Technology 74 (2013) 221.

[47] S. Qu and S.-C. Wong, Composites Science and Technology 67 (2007) 231.

[48] N. Heeder, A. Shukla, V. Chalivendra and S. Yang, Journal of Materials Science 47 (2012) 3808.

[49] H. Kim, A. A. Abdala and C. W. Macosko, Macromolecules 43 (2010) 6515.

[50] B. Li and W.-H. Zhong, Journal of Materials Science 46 (2011) 5595.

[51] J. R. Potts, D. R. Dreyer, C. W. Bielawski and R. S. Ruoff, Polymer 52 (2011) 5.

[52] J. Du, L. Zhao, Y. Zeng, L. Zhang, F. Li, P. Liu and C. Liu, Carbon 49 (2011) 1094.

[53] H. Hu, G. Zhang, L. Xiao, H. Wang, Q. Zhang and Z. Zhao, Carbon 50 (2012) 4596.

[54] Y. Mamunya, in "Carbon Nanotubes-Polymer Nanocomposites", edited by D. S. Yellampalli (InTech, 2011).

[55] H. Pang, Y. Bao, J. Lei, J.-H. Tang, X. Ji, W.-Q. Zhang and C. Chen, Polymer-Plastics Technology and Engineering 51 1483.

CHAPTER 2

SENSITIVITY AND DYNAMIC ELECTRICAL RESPONSE OF CNT REINFORCED NANOCOMPOSITES

by

Nicholas Heeder, Arun Shukla, Vijaya Chalivendra, Sze Yang

has been published in the Journal of Materials Science

Corresponding Author: Arun Shukla

Dynamic Photo Mechanics Laboratory

Department of Mechanical, Industrial and Systems Engineering

University of Rhode Island

206 Wales Hall, 92 Upper College Rd

Kingston, RI, 02881, USA

Phone: +1-401-874-2283

Email Address: shuklaa@egr.uri.edu

Abstract

A series of dynamic compressive experiments were performed to experimentally investigate the electrical response of multi-wall carbon nanotube (MWCNT) reinforced epoxy nanocomposites subjected to split Hopkinson pressure bar (SHPB) loading. Low-resistance CNT/epoxy specimens were fabricated using a combination of shear mixing and ultrasonication. Utilizing the carbon nanotube network within, the electrical resistance of the nanocomposite was monitored using a high-resolution four-point probe method during each compressive loading event. In addition, real-time deformation images were captured using high-speed photography. The percent change in resistance was correlated to both strain and real-time damage. The results were then compared to previous work conducted by the authors (quasi-static and drop-weight impact) in order to elucidate the strain rate sensitivity on the electrical behavior of the material. In addition, the percent change in conductivity was determined using a Taylor expansion model to investigate the electrical response based upon both dimensional change as well as resistivity change during mechanical loading within the elastic regime. Experimental findings indicate that the electrical resistance is a function of both the strain and deformation mechanisms induced by the loading. The bulk electrical resistance of the nanocomposites exhibited an overall decrease of 40-65% and 65-85% during quasi-static/drop-weight and SHPB experiments respectively.

Keywords: Electrical response, carbon nanotube/polymer composites, dynamic response, four-point probe method

1. Introduction

Carbon nanotubes (CNTs) are a promising addition to the future of developing novel materials capable of self-sensing and active response due to their extraordinary electrical conductivity and excellent transport properties. Unlike other smart materials, CNTs can provide both structural and functional capabilities simultaneously and have been used in many applications including actuation, sensing, and power generation [1-4]. Carbon nanotube-based polymeric nanocomposites have found new applications in various fields such as future spacecraft, anti-meteorite/anti-ballistic shields for satellites, anti-ballistic vests, explosion-proof blankets for aircraft cargo bays, and safety belts in industries [5, 6].

Significant research has been performed to fundamentally understand the enhancement of mechanical properties due to CNT reinforcement of polymers [7, 8]. Allaoui et al. [9] investigated the influence of multi-walled carbon nanotubes (MWCNTs) in a rubbery epoxy matrix, and found that the addition of up to 4 wt.% MWCNTs could lead to a significant increase in the strength and Young's modulus [10]. Given the practical potential applications of CNTs in electromechanical devices, specifically as piezoresistive sensors, the effect of mechanical deformation on the electrical properties of individual CNTs has been studied theoretically [11-14] and experimentally [11, 12].

An increased amount of research has been conducted in studying the electrical response of CNT/polymer composites under mechanical loading. Alexopoulos et al. [13], Nofar et al. [14], and Gao et al. [15, 16] have studied damage detection and health monitoring of composites reinforced with CNT-embedded glass fibers.

Alexopoulos et al. [13] performed various incremental tensile loading-unloading steps as well as three-point bending tests on specimens with CNT fibers in the tensile region. Results indicated that CNT fibers provide unquestionable advantages for sensing and damage monitoring of non-conductive composites, when compared to the competitors, e.g. the embedded carbon fibers and a modified (doped) conductive network. Sensing ability for the investigated specimens with CNT fibers in the compressive region was also reported [13]. Gao et al. [15] studied the sensing of damage development in composites using CNT networks utilizing two sensing techniques: electrical resistance and acoustic emission. Resistance change and acoustic emission counts showed a bi-linear relation in detecting damage in quasi-static and cyclic experiments which can be used to give additional insight toward damage evolution. Thostenson et al. [17] performed tensile experiments on CNT/epoxy samples and demonstrated a highly linear relationship between the specimen deformation and the electrical resistance. This result suggests that CNT networks formed in an epoxy polymer matrix could be utilized as highly sensitive sensors for detecting the evolution of damage in advanced polymer-based composites [17]. Later, Lim et al. [18] experimentally investigated the mechanical and electrical response of CNT-based fabric composites to Hopkinson bar loading further demonstrating the effectiveness of a percolating carbon nanotube network being capable of sensing damage caused by impact. In their previous work, the authors experimentally investigated the electrical response of multi-walled carbon nanotube reinforced nanocomposites under quasi-static and dynamic loading. The results indicated that the electrical resistance of the nanocomposite decreased under both quasi-static and

dynamic loading due to the formation of more efficient carbon nanotube networks caused by the compression of the epoxy matrix [18, 19].

The aforementioned studies revealed that when properly dispersed within a given matrix, an internal sensory network can be formed and utilized to detect important information such as strain and damage within the material. To further this investigation, it is crucial to understand the electrical response of the nanocomposites under dynamic loading conditions. The present paper experimentally investigates the electrical response of MWCNT reinforced nanocomposites subjected to dynamic split Hopkinson pressure bar loading. A modified four-point probe method, using line and face contacts rather than point contacts, was implemented to measure more consistent and accurate results during mechanical loading [19]. Fabricated nanocomposites were loaded using a split Hopkinson pressure bar equipped with solid steel bars. The history between the electrical resistance change, the mechanical loading, and the high-speed deformation photography are correlated to characterize the electrical response of CNT reinforced epoxy under compressive loading. For the sake of completeness, results corresponding to static and drop weight impact experiments previously performed by the authors will be presented for comparison purposes [19].

It was observed that the overall bulk resistance decreased significantly when subjected to SHPB loading, demonstrating a similar electrical response as seen during quasi-static and drop weight loading. A 65 – 85% decrease of resistance was observed. This is due to a more efficient carbon nanotube network forming under compressive loading caused by the compression of the epoxy matrix.

2. Material and Specimen

2.1 Material Fabrication

Due to the simplicity of casting and low curing temperature, a two-part epoxy, consisting of bisphenol-A resin (Buehler Epothin 20-8140-032) and an epoxy hardener (Buehler Epothin 20-8142-016) with a mixing ratio of 50g/18g, was chosen as a polymeric matrix. CNTs used for this study were multi-wall carbon nanotubes (Nanolab, purity > 95%). The MWCNTs have outside diameters of 30 ± 15 nm, lengths of 5 to 20 microns and a specific surface area of 200 to 400 m^2/g. Various weight fractions of CNTs were used in the production of samples ranging from 0.1 to 0.5 wt%.

The general procedure of material fabrication is shown in Fig. 1. High surface energy of carbon nanotubes causes the agglomeration of nanotubes when dispersed, adversely affecting the electrical transport properties of the material [20]. In order to address the agglomeration issue and effectively disperse the CNTs, the present work implemented high-intensity ultrasonication and high-speed shear mixing. Pre-measured amounts of Epothin Part-A Resin and carbon nanotubes were mechanically stirred for 5 minutes in a copper beaker. The mixture was then placed into a shear mixer (Ika Werke RW 16 Basic) outfitted with a 3-blade propeller stirrer (R1381 Propeller stirrer) and shear-mixed at 600 RPM for 30 minutes. Following shear mixing, the ultrasonication process was applied for one hour on pulse mode, 4.5 sec on 9 sec off, at 100 kHz (Sonics & Materials Inc. VCX750). The mixture was then placed into a vacuum chamber to remove any trapped air bubbles generated during the mechanical mixing process [21]. A pre-measured amount of Part B epoxy hardener, in

a separate container, was also placed inside the vacuum chamber. Both solutions were placed under vacuum for 1 hour. Once all air was removed from both solutions, they were combined and mechanically stirred for 2 minutes. The mixture was once again placed back into the vacuum chamber for 5 minutes. Finally, the CNT/epoxy solution was slowly poured into pre-manufactured wax molds and allowed to cure for 3 days under ambient conditions.

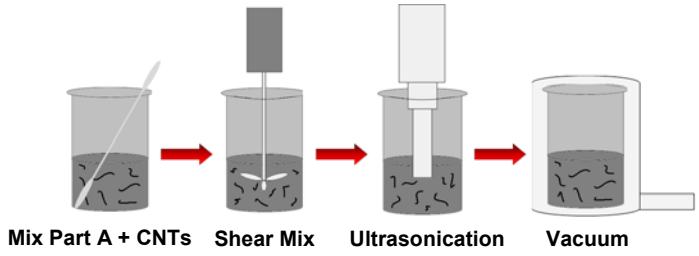

Fig. 1 Schematic of nanocomposite fabrication procedure

It is critically important to control the temperature of the mixture during the sonication process for the quality of the fabricated specimens. The sonication process generates substantial heat that may damage CNTs and deteriorate the electrical properties of the final composite [22]. Moreover, too much heat could cause the epoxy to reach the flash point. To control the temperature of the mixture during sonication, a cooling apparatus was designed and built as shown in Fig. 2. While the mixture in the copper breaker is sonicated, liquid nitrogen flows through a copper-tube coil submerged in an anti-freeze solution under the beaker to maintain the mixture temperature. The flow rate of liquid nitrogen is precisely controlled while temperatures of the beaker and anti-freeze solution are real-time monitored by thermocouples. The required cooling rate for proper temperature control depends primarily on the weight fraction of CNTs in the solution. For the present fabrication,

the mixture temperature was maintained in between 18°C - 30°C, depending on the sonication duration. A percolation study on the material was previously performed by the authors which resulted in an electrical percolation threshold occurring between 0.1 and 0.2 wt.% of CNTs for the particular CNTs and polymer used [19]. Nanotube concentration greater than 0.2 wt.% does not provide better electrical conduction. Therefore, the concentration of CNTs was set to 0.2 wt.% for all experiments in the present study.

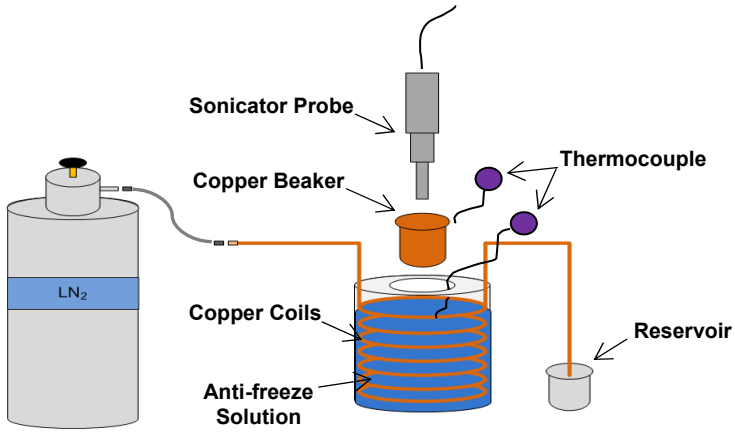

Fig. 2 Schematic of cooling apparatus used to control temperature during the ultrasonication process

2.2 Specimen

Fig. 3 illustrates specimens prepared for the dynamic compressive loading experiments. Specimens have cylindrical geometry measuring 8.8 mm in diameter and 11.7 mm in length. Two V-notch channels with a depth of 0.3 mm were machined in the middle section of the specimen. The channels were used to implement a modified four-point probe method. Each channel was located 3 mm from each end. The loading is exerted in the longitudinal direction along the length of the specimen. The left face,

right face, and the two inner channels of the specimen served as four probes to obtain a four point probe measurement. All four probes were coated with silver paint (SPI-Paint 05001-AB) and lead wires were attached using an adhesive (M-Coat A Air-Drying Polyurethane Coating).

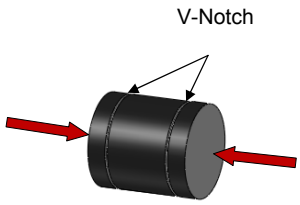

Fig. 3 Specimen geometry and loading direction used in SHPB compressive experiments

3. Experimental Setup and Procedure

3.1 Electrical Characterization

In order to effectively capture the change in electrical resistance of the cylindrical specimen, a novel approach utilizing the four-point probe method was implemented. The four probes consisted of the left face, right face, and the two inner channels. To allow a constant current flow through the entire bulk of the specimen, a constant current was supplied through the right and left faces of the specimen. The two inner channels served as the two peripheral electrodes that measure the voltage drop across the middle section of the specimen. The electrical resistance of the middle section can be easily determined from the input current and the voltage drop across the inner probes. As the specimen underwent deformation, the instantaneous resistance of the middle section changed. Percent change in the resistance was calculated for each experiment. Due to the complex dispersion pattern of nanotubes inside, the initial

resistance of the individual specimens varies slightly. Therefore, the initial resistance of each specimen served as the baseline for each experiment. Based on previous studies [19], this method better provides the means to detect changes in the resistance caused by strain and damage mechanisms in the material as compared to the classical four-point probe method. Since the current uniformly flows through the cross sectional area, the measured resistance is an estimation of the bulk resistance of the inner section. By using this average voltage measurement technique, more consistent and accurate results were obtained during a wide range of mechanical loading schemes and consequent specimen deformations.

A sketch of the experimental setup used to capture the electrical resistance change during the dynamic compressive experiments is shown in Fig. 4(a). A constant current source with high frequency response (Keithley Instruments Model 6221) was used to generate a constant DC current flow under the high rate deformation while the voltage drop between the two inner probes was measured by a differential amplifier (Tektonix ADA 400A) and recorded by a digital oscilloscope (Tektronix TDS 3014).

3.2 Split Hopkinson Pressure Bar Loading

A split Hopkinson bar, equipped with a solid maraging steel incident and transmission bar, was used to apply a dynamic load to the specimens. A sketch of the SHPB device and typical pulse profiles are given in Fig. 4(a) and (b), respectively. The incident and transmission bar were 12.7 mm in diameter and measured 1220 mm in length. For the SHPB dynamic loading, the incident pulse length is related to the projectile length. To induce sufficient strain in the specimen, a 355 mm striker was used. A layer of electrical tape was placed at the ends of the incident and transmission

bars to insulate the specimen from the loading apparatus. A high-speed camera (Photron SA1) captured high-speed deformation images at a frame rate of 100,000 fps. The high-speed images were used to calculate the strain history of the specimen under dynamic loading as well as capture major damage mechanisms.

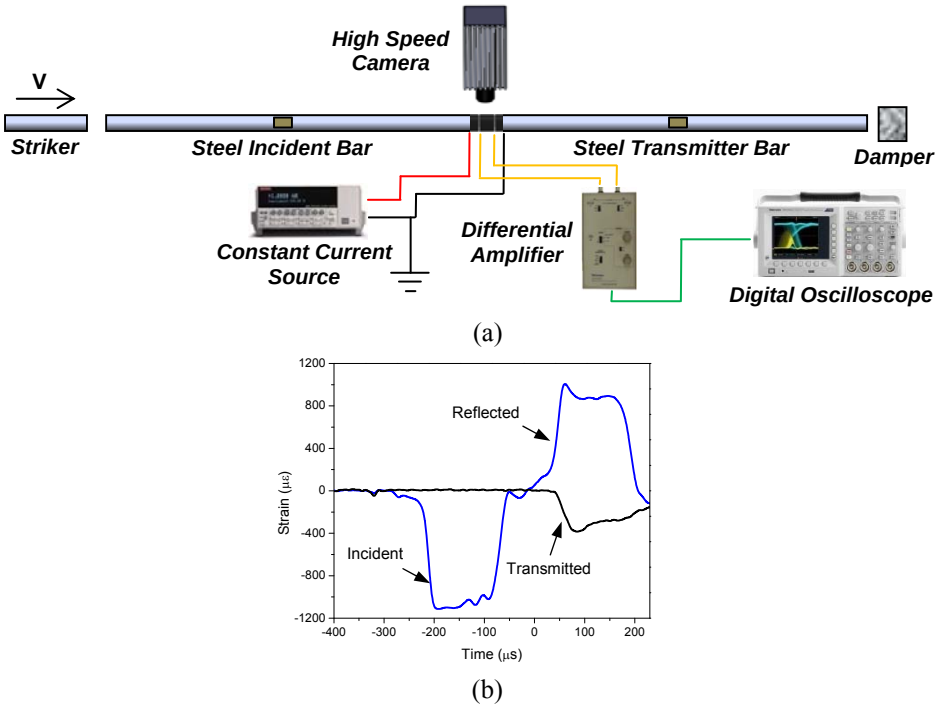

Fig. 4 (a) Experimental set-up used for measuring resistance change during SHPB compressive experiments and (b) typical pulse profile

4. Experimental Results and Discussion

4.1 Quasi-Static Loading

Fig. 5 shows a typical result of the electrical resistance and stress changes of a specimen as a function of engineering strain during a quasi-static loading experiment. The stress within the specimen monotonically increases to ~75 MPa at 4% engineering strain and then gradually decreases. As the compressive strain increases to ~12%, the electrical resistance decreases ~56%. The electrical resistance of the specimen is

dependent on two factors: a geometrical factor and the specific resistance of the material. Since the resistance of the matrix material is very high, the CNTs exclusively conduct the electrical current within the material. Therefore, the change in the material's specific resistance is based exclusively on the CNT networks present within the composite. The effective inter-nanotube gap becomes closer during compression, thus forming a more efficient conductive network. A strain threshold, εt, in which no prominent change in resistance is demonstrated until surpassed, occurs at approximately 3% engineering strain. Once this threshold is surpassed, the rate of change in resistance increases significantly due to the increased number of electrical connections between CNTs. As the specimen reaches its elastic limit, the material begins to spread, causing a bulging phenomenon located in the middle section. The combination of the material compression and spreading causes less resistance change following elastic deformation.

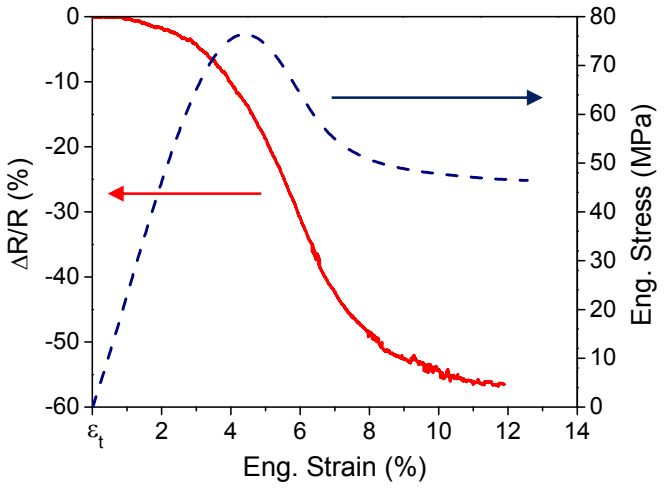

Fig. 5 Typical electrical response of CNT/epoxy nanocomposite under quasi-static loading

4.2 Drop Weight Impact

Impact experiments, using a drop weight apparatus, were performed to study the electrical response of the nanocomposites under intermediate strain rate loadings (10^1/s). A typical electrical response and the real-time deformation images of a rectangular CNT/epoxy nanocomposite under high mass, low velocity impact loading are shown in Fig. 6. In general, the response of the nanocomposites under drop weight loading is more brittle than under quasi-static loading due to the increased strain rate. The overall resistance change follows a similar trend as under quasi-static loading. A strain threshold, lasting approximately 250 μs, is evident. Once surpassed, the resistance monotonically decreases as the specimen deforms uniformly. At 600 μs, it can be observed that the right and left sides of the specimen demonstrate an expansion. As the material reaches this critical strain value, the decrease in electrical resistance quickly arrests and shows very little change due to the combination of the material compression and spreading. Damage then quickly initiates and propagates throughout the specimen resulting in a sharp increase in resistance. Overall, the resistance of the material decreases approximately 65% during drop weight impact loading.

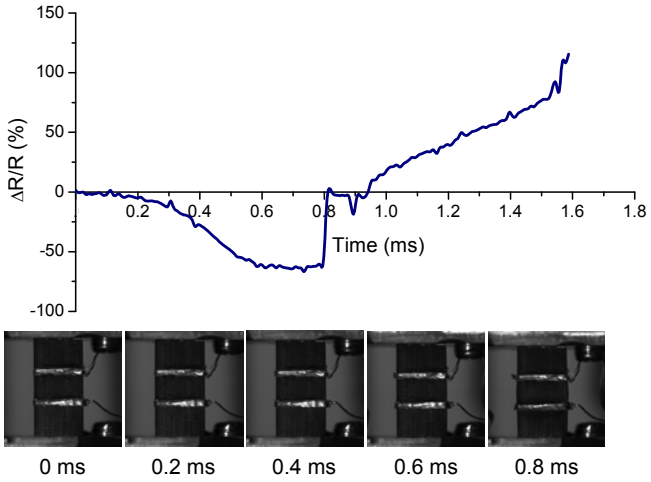

Fig. 6 Percent change in conductivity of 0.2 wt.% CNT/epoxy nanocomposite under drop weight loading with real-time deformation

4.3 Split Hopkinson Pressure Loading

To investigate the electrical response of the nanocomposites under higher strain rates, a SHPB apparatus was utilized to load the specimens. A typical result of the actual resistance, as a function of engineering strain during a SHPB experiment, is shown in Fig. 7. The initial resistance of the inner section of the specimen can be seen to be approximately 13.5 kΩ prior to loading. As the specimen undergoes dynamic compression at a strain rate of approximately 2000/s, the electrical resistance change is inversely proportional to the change in strain. As the stress of the specimen monotonically increases to 160 MPa at 8% engineering strain, a small decrease in electrical resistance from 13.5 kΩ to 11 kΩ is observed. Once the material begins to yield, the resistance begins to decrease at a higher rate up until the strain reaches 12 % engineering strain. As the compressive strain increases, the electrical resistance begins to decrease at a slower rate due to the spreading of the material (larger cross-sectional area). The electrical response of the nanocomposites under SHPB loading shows a

similar response to that seen during quasi-static compression as well as drop weight impact compression [19]. When considering the negligible change in CNT geometry during compression, the resistance change is primarily attributed to the rearrangement of the CNT networks present within the material, thus causing new tube-to-tube contacts and a decrease in electrical resistance.

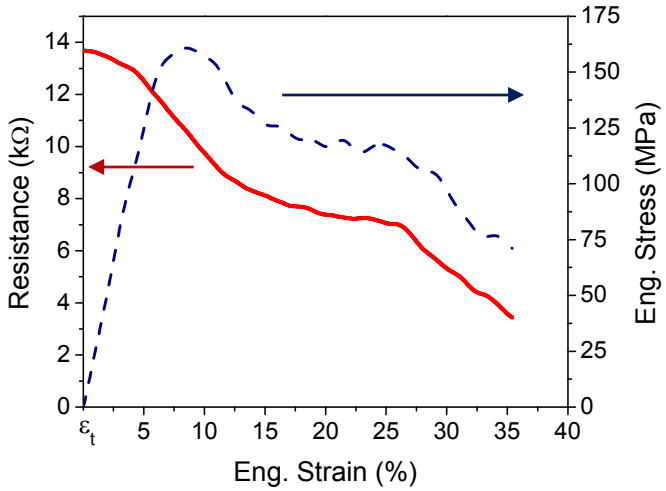

Fig. 7 Typical electrical response of CNT/epoxy nanocomposites under SHPB compressive loading

A typical electrical response along with the real-time deformation images of a CNT/epoxy nanocomposite subjected to SHPB loading are shown in Fig. 8. The time frames used in the loading event are chosen in a manner such that they can be correlated to the time at which certain deformation mechanisms were first observed. A schematic representing the deformed configurations of the specimen and damage mechanisms induced by mechanical compression is shown in Fig. 9. During the first 60 μs, the specimen undergoes a uniform compression. This axial compression, shown in Fig. 9 (I), causes more efficient electrical pathways by decreasing the inter-tube gaps between the CNTs present within the matrix and increasing the number of new

contacts thus causing a sharp decrease in resistance. At approximately 60 μs, evidence of barreling conveyed by the radial expansion of the middle section can be seen. This barreling occurred due to the friction present between the insulating electrical tape and specimen interfaces. In spite of having smooth surface, this barreling could not be avoided during the Hopkinson pressure bar experiments. As the compressive strain increases, the radial expansion of the matrix decreases the efficiency of the CNT network as shown in Fig. 8. The rearrangement of the CNT network caused by the radial expansion of the matrix is schematically represented in Fig. 9(II). As observed in Fig. 9(III), voids and cracks are later formed within the material further decreasing the electrical efficiency between CNTs. It can be seen that the rate of resistance change in turn changes drastically, showing a less overall decrease in resistance due to the combinative effect of both axial compression and radial expansion. The material reaches its maximum strain given the loading conditions at approximately 140 μs. The electrical resistance of the nanocomposite decreases approximately 54% during the entire loading event.

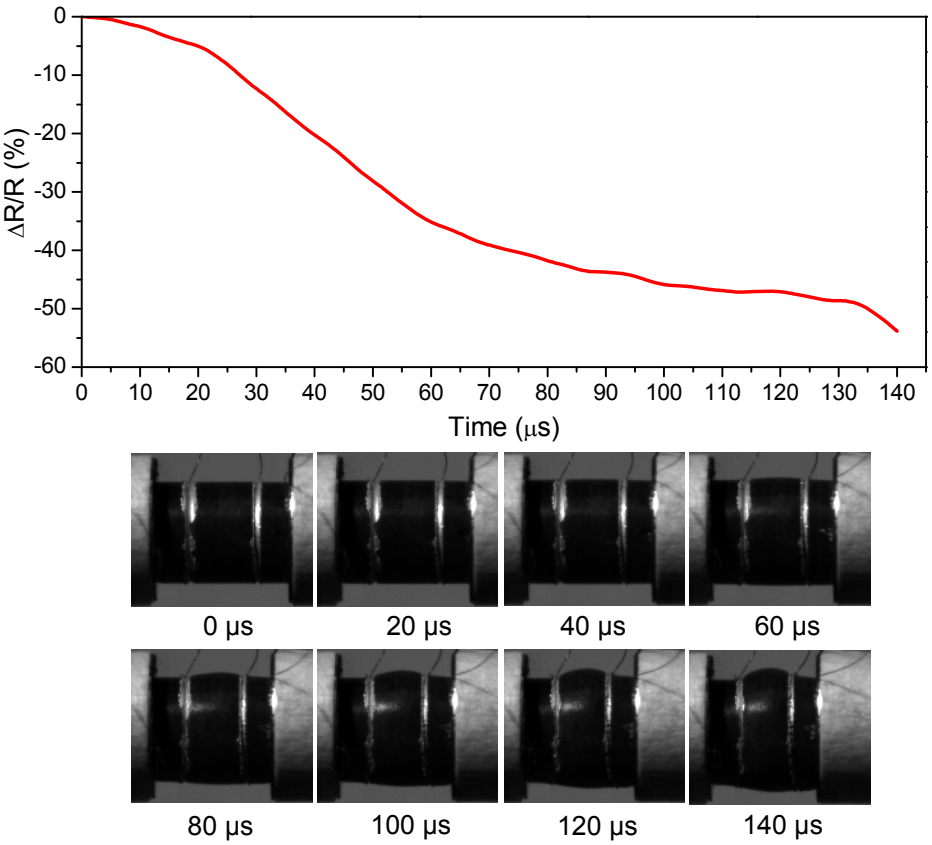

Fig. 8 Percent change in electrical resistance of 0.2 wt.% CNT/epoxy nanocomposite subjected to SHPB loading with real-time deformation images

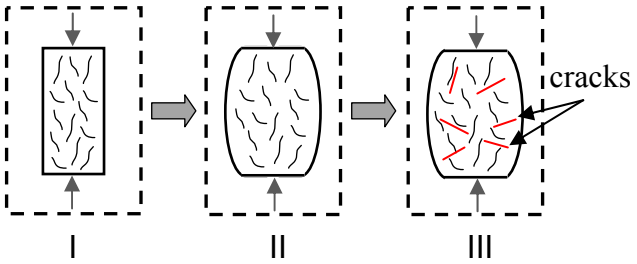

Fig. 9 Schematic of CNT rearrangement due to different damage mechanisms during mechanical compression

A series of experiments were carried out and the change in electrical resistance demonstrated by all specimens was repeatable. The resistance changes of four different specimens are shown in Fig. 10. The difference between the curves can be

attributed to the variability and complexity of the CNT networks present within each specimen. As the material compresses, new tube-to-tube contacts were made with non-linear deformation of the epoxy matrix, which increases the electrical conductivity of the embedded CNT network. As seen in Fig. 7, specimens subjected to dynamic compressive loading using a split Hopkinson pressure bar apparatus showed a 65 - 85% decrease in material resistance during compression. Hence there exists rate sensitivity of electrical response of embedded CNT network with matrix deformation.

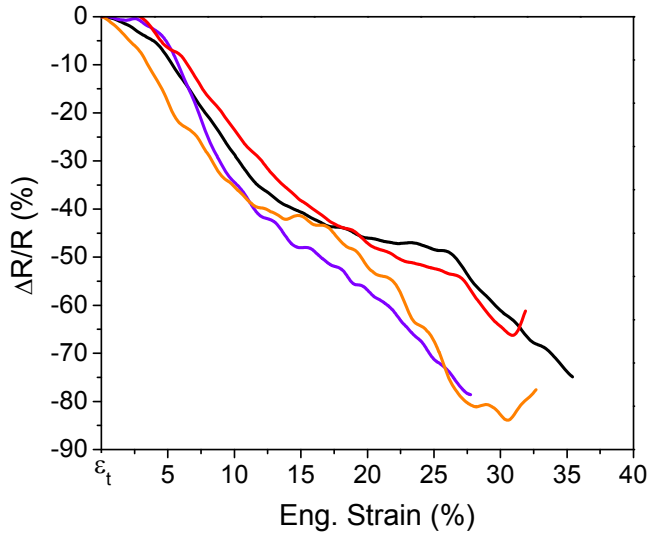

Fig. 10 Percent change in resistance of 0.2 wt.% CNT/epoxy nanocomposites under SHPB loading

4.4 CNT Sensitivity in the Elastic Region

To better understand the electrical response of the material, the change in electrical conductivity of the nanocomposite was determined. To calculate the change in conductivity of the material from the obtained results, it was assumed that the conductivity c of the nanocomposite with a length L, cross-sectional area A, and a resistance R is given by $c = l/RA$. Since large changes in resistance were measured

during experimentation, higher order terms are necessary in order to account for the large changes in material conductivity. Taylor Expansion for multiple variables was applied.

$$c(l+dl,R+dR,A+dA)=c(l,R,A)+\frac{\partial c}{\partial l}dl+\frac{\partial c}{\partial R}dR+\frac{\partial c}{\partial A}dA+\frac{\partial^2 c}{\partial l^2}\frac{dl^2}{2!}+\frac{\partial^2 c}{\partial R^2}\frac{dR^2}{2!}+\frac{\partial^2 c}{\partial A^2}\frac{dA^2}{2!}+\frac{\partial^3 c}{\partial l^3}\frac{dl^3}{3!}+\frac{\partial^3 c}{\partial R^3}\frac{dR^3}{3!}+\frac{\partial^3 c}{\partial A^3}\frac{dA^3}{3!}+\cdots \quad (1)$$

Replacing $dl = \Delta l$, $dR = \Delta R$, $dA = \Delta A$, Eq. (1) can be written as

$$c(L+\Delta l,R+\Delta R,A+\Delta A)=c(l,R,A)+\left(\frac{1}{RA}\right)\Delta l+\left(\frac{-l}{R^2A}\right)\Delta R+\left(\frac{-l}{RA^2}\right)\Delta A+\left(\frac{2l}{R^3A}\right)\frac{\Delta R^2}{2!}+\left(\frac{2l}{RA^3}\right)\frac{\Delta A^2}{2!}+\left(\frac{-6l}{R^4A}\right)\frac{\Delta R^3}{3!}+\left(-\frac{6l}{RA^4}\right)\frac{\Delta A^3}{3!} \quad (2)$$

The change in electrical conductivity, $\Delta c/c$, is then

$$\frac{\Delta c}{c}=\left(\frac{\Delta l}{l}-\frac{\Delta R}{R}-\frac{\Delta A}{A}\right)+\left(\left(\frac{\Delta R}{R}\right)^2+\left(\frac{\Delta A}{A}\right)^2\right)-\left(\left(\frac{\Delta R}{R}\right)^3+\left(\frac{\Delta A}{A}\right)^3\right) \quad (3)$$

The change in area is related to the change in length by $dA/A = -2\upsilon\varepsilon$ where υ is the Poison's ratio of the material. Thus,

$$\frac{\Delta c}{c}=\left[\varepsilon\left(1+2\upsilon+4\upsilon^2\varepsilon+8\upsilon^3\varepsilon^2\right)\right]-\left[\left(\frac{\Delta R}{R}\right)-\left(\frac{\Delta R}{R}\right)^2+\left(\frac{\Delta R}{R}\right)^3\right] \quad (4)$$

Eq. (4) is thus used to obtain the change in electrical conductivity of the nanocomposite while subjected to a mechanical load (under small mechanical strains within the elastic regime). The change in electrical conductivity is a function of two factors: a geometrical factor and a resistance factor. During compression, the geometrical factor which is denoted as $\varepsilon(1+2\upsilon+4\upsilon^2\varepsilon+8\upsilon^3\varepsilon^2)$, estimates the conductivity change based on the change in overall geometry. Since the resistance of the matrix

material is very high, the CNTs exclusively conduct the electrical current within the material. Therefore, the change in conductivity, denoted $\Delta c/c$, comprises of the change in material conductivity based exclusively on the CNT networks present within the composite. During compression, the carbon nanotube networks change due to the non-linear (large) deformation of the epoxy matrix. This re-orientation of nanotubes within the matrix thus changes the specific resistance of the nanocomposite. In contrast to typical strain gages, geometry plays a much smaller role than the actual resistivity of the material. Using a Poisson's ratio of 0.375 during a typical SHPB experiment and a for a strain value of 5% the geometrical factor only contributes approximately 36% of the total resistance change observed while the change in material conductivity contributes 64%. Using Eq. (4), an approximate value of $\Delta c/c$ is determined and thus used to characterize the change in electrical properties of a nanocomposite material itself under compressive loading. Fig.11 shows the change in electrical conductivity as a function of engineering strain within the elastic regime for both quasi-static as well as SHPB loading experiment. The rate of increase in electrical conductivity increases as the material becomes closer to yield for both types of loading scenarios. It can be postulated that the difference between the two curves is due to an increase in matrix stiffness occurring over a very brief period of time in SHPB loadings. This phenomenon may cause a slight delay in the change in electrical conductivity based on the time it takes for the internal networks to rearrange. The electrical conductivity of the nanocomposites under quasi-static and SHPB compressive loading increased approximately 25% and 20% respectively.

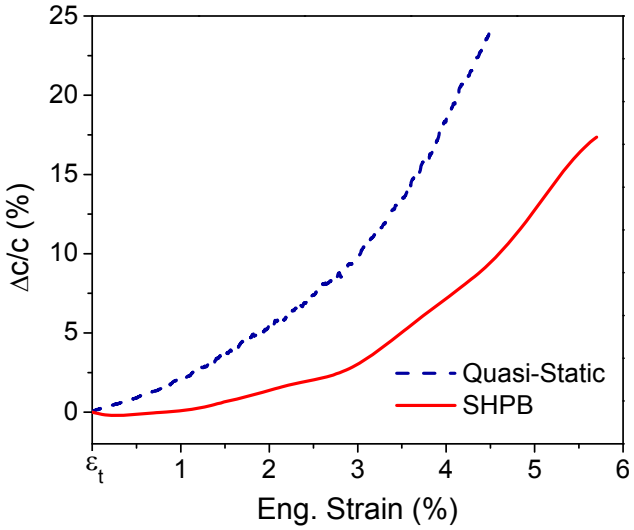

Fig. 11 Percent change in conductivity of CNT/epoxy nanocomposites under quasi-static and SHPB loading

5. Conclusions

The obtained results provide further insights on the electrical behaviors of CNT reinforced nanocomposites under compressive loading conditions, and will thus be beneficial in the development of improved smart materials capable of sensing crucial information. The electrical response of MWCNT reinforced nanocomposites subjected to compressive loading under various strain rates was investigated. From these experiments, we conclude:

1. The electrical resistance of the nanocomposite is a function of both the strain and deformation mechanisms induced by the loading.

2. The bulk electrical resistance of the nanocomposites exhibited an overall decrease of 65-85% during SHPB experiments.

3. The electrical response observed during SHPB loading demonstrated a similar response as previously observed during both quasi-static and drop weight loading

where the bulk electrical resistance of the nanocomposites decreased during compression and then increased as damage initiated and propagated.

4. The change in electrical conductivity of the material due to the CNT rearrangement for small strains was determined using a Taylor expansion model to better characterize the electrical response demonstrated by the material.

5. It was observed that the changes in CNT networks within the nanocomposite contributed approximately 64% to the overall resistance change of the material while only 36% was due to dimensional changes. This phenomenon differs from a typical strain gage measurement where the change in electrical resistance is based primarily on the dimensional changes rather than the change in material conductivity.

Acknowledgements

This work was supported by the National Science Foundation (NSF) under grant number CMMI 0856133.

References

1. Kang I, Heung YY, Kim JH, Lee JW, Gollapudi R, Subramaniam S, Narasimhadevara, S, Hurd D, Kirikera GR, Shanov V, Schulz MJ, Shi D, Boerio J, Mall S, Ruggles-Wren M (2006) Introduction to carbon nanotube and nanofiber smart materials. Composites Pt B 37(6): 382-394

2. You KM, Park SS, Lee CS, Kim JM, Park GP, Kim WN (2011) Preparation and characterization of conductive carbon nanotube-polyurethane foam composites. Journal of Material Science 46(21): 6850-6855

3. Sumfleth J, Buschhorn ST, Schulte K (2011) Comparison of rheological and electrical percolation phenomena in carbon black and carbon nanotube filled epoxy polymers. Journal of Material Science 46(3): 659-669

4. Dash MP, Tripathy M, Sasmal A, Mohanty GC, Nayak PL (2010) Poly(anthranilic acid)/multi-walled carbon nanotube composites: spectral, morphological, and electrical properties. Journal of Material Science 45(14):3858-3865

5. Park C, Onuaies Z, Watson KA, Pawlowski K, Lowther SE, Connell JW, Siochi EJ, Harrison JS, St. Clair TL (2002) Polymer-Single Wall Carbon Nanotube Composites for Potential Spacecraft Applications. Material Research Society 706

6. Dalton AB, Collins S, Razal J, Munoz E, Ebron VH, Kim BG, Coleman JN, Ferraris JP, Baughman RH (2004) Continuous carbon nanotube composite fibers: properties, potential applications, and problems. Journal of Materials Chemistry 14: 1-3

7. Li C, Thostenson ET, Chou TW (2008) Sensors and actuators based on carbon nanotubes and their composites: A review. Composites Science and Technology 68(6): 1227-1249

8. Thostenson ET, Ren Z, Chou TW (2001) Advances in the science and technology of carbon nanotubes and their composites: A review. Composites Science and Technology 61(13): 1899-1912

9. Allaoui A, Bai S, Cheng HM, Bai JB (2002) Mechanical and electrical properties of a MWNT/epoxy composite. Composites Science and Technology 62(15): 1993-1998

10. Guo P, Chen X, Gao X, Song H, Shen H (2007) Fabrication and mechanical properties of well-dispersed multiwalled carbon nanotubes/epoxy composites. Composites Science and Technology 67(15-16): 3331-3337

11. Bezryadin A, Verschueren A, Tans S, Dekker C (1998) Multiprobe transport experiments on individual single-wall carbon nanotubes. Physical Review Letters 80: 4036-4039

12. Paulson S. et al (1999) In situ resistance measurements of strained carbon nanotubes. Applied Physics Letters 75: 2936-2938

13. Alexopoulos ND, Bartholome C, Poulin P, Marioli-Riga Z (2009) Structural health monitoring of glass fiber reinforced composites using embedded carbon nanotube (CNT) fibers. Composites Science and Technology 70(2): 260-271

14. Nofar M, Hoa SV, Pugh MD (2009) Failure detection and monitoring in polymer matrix composites subjected to static and dynamic loads using carbon nanotube networks. Composites Science and Technology 69(10): 1599-1606

15. Gao L, Thostenson ET, Zhang Z, Chou TW (2009) Coupled carbon nanotube network and acoustic emission monitoring for sensing of damage development in composites. Carbon 47(5): 1381-1388

16. Gao L, Chou TW, Thostenson ET, Zhang Z (2010) A comparative study of damage sensing in fiber composites using uniformly and non-uniformly dispersed carbon nanotubes. Carbon 48 (13): 3788-3794

17. Thostenson ET, Chou TW (2006) Carbon Nanotube Networks: Sensing of Distributed Strain and Damage for Life Prediction and Self Healing. Advanced Materials 18: 2837-2841

18. Lim AS, An Q, Chou TW, Thostenson ET (2011) Mechanical and electrical response of carbon nanotube-based fabric composites to Hopkinson bar loading. Composites Science and Technology

19. Heeder N, Shukla A, Chalivendra V, Yang S, Park K (2011) Electrical Response of Carbon Nanotube Reinforced Nanocomposites under Static and Dynamic Loading. Experimental Mechanics, doi:10.1007/s11340-011-9488-x.

20. Kabir ME, Saha MC, Jeelani S (2007) Effect of ultrasound sonication in carbon nanofibers/polyurethane foam composite. Materials Science and Engineering A 459(1-2): 111-116

21. Evora VMF, Shukla A (2003) Fabrication, characterization, and dynamic behavior of Polyester/TiO2 nanocomposites. Materials Science and Engineering A 361(1-2): 358- 366

22. Ma P, Siddiqui NA, Marom G, Kim J (2010) Dispersion and functionalization of carbon nanotubes for polymer-based nanocomposites: A review. Composites Part A: Applied Science and Manufacturing 41(10): 1345-1367

CHAPTER 3

ELECTRO-MECHANICAL BEHAVIOR OF GRAPHENE/POLYSTYRENE COMPOSITES UNDER DYNAMIC LOADING

by

Nicholas Heeder, Indrani Chakraborty, Fei Guo, Michael P. Godfrin, Robert Hurt, Anubhav Tripathi, Arijit Bose and Arun Shukla

Under preparation for submission to the Journal of Experimental Mechanics

Corresponding Author: Arun Shukla

Dynamic Photo Mechanics Laboratory

Department of Mechanical, Industrial and Systems Engineering

University of Rhode Island

206 Wales Hall, 92 Upper College Rd

Kingston, RI, 02881, USA

Phone: +1-401-874-2283

Email Address: shuklaa@egr.uri.edu

Abstract

An experimental investigation was conducted to understand the electro-mechanical response of graphene reinforced polystyrene composites under static and dynamic loading. Graphene-polystyrene composites were fabricated using a solution mixing approach followed by hot-pressing. Absolute resistance values were measured with a high-resolution four-point probe method for both quasi-static and dynamic loading. A modified split Hopkinson (Kolsky) pressure bar apparatus, capable of simultaneous mechanical and electrical characterization, was developed and implemented to investigate the dynamic electro-mechanical response of the composites. In addition to measuring the change in electrical resistance as well as the dynamic constitutive behavior, real-time surface damage and global deformation was captured using high-speed photography. The real-time damage was correlated to both stress-strain and percent change in resistance profiles. The experimental findings indicate that the bulk electrical resistance of the composite increased significantly due to the brittle nature of the polystyrene matrix and the presence of relative agglomerations of graphene platelets which resulted in micro-crack formations.

Keywords: Electrical response, graphene/polymer composites, dynamic response, quasi-static response, four-point probe method

1. Introduction

A comprehensive series of experiments were conducted to experimentally investigate the electro-mechanical response of graphene-PS composites subjected to static as well as dynamic loading. A novel split Hopkinson pressure bar (SHPB) apparatus, capable of simultaneous mechanical and electrical characterization, was

developed to effectively investigate the electro-mechanical response of the graphene reinforced PS composites under dynamic loading. The history between the electrical resistance change, mechanical loading, and the high-speed deformation photography are correlated to characterize the electrical-mechanical response of the fabricated composites.

Owing to extraordinary physical and mechanical properties, graphene has the potential to be an ideal filler material in developing novel composites with multifunctional capabilities such as self-sensing and active response. Recent progress has shown that inorganic nanomaterials as fillers in polymer/inorganic composites have tremendous application potential in industries such as automotive, aerospace, construction and electronics [1-7]. Although carbon nanotubes (CNTs) posses comparable mechanical properties, graphene still has superior electrical and thermal properties, as well as a higher surface area [1, 8]. Its reinforcement can offer exceptional properties in future high performance novel composites.

In recent years, graphene based composites have become a topic of significant academic and industrial interest. While a number of studies have shown that the presence of graphene within polymers can enhance the mechanical properties of the bulk composite [8-14], other studies have shown that graphene can also have adverse effects on the mechanical properties [8, 15-17]. Fang et al. [9] investigated the effect of low concentrations of graphene on the mechanical strength of graphene/polystyrene composites. The results showed a substantial increase in tensile strength as graphene loadings were increased from 0.1 wt %. to 0.9 wt. % in comparison to pristine polystyrene. The increase in strength was attributed to effective load transfer between

the graphene and polymer. Alternatively, the addition of certain filler materials can also have adverse effects on the mechanical properties of the resulting composite due to factors such as reinforcement phase concentration, dispersion quality, interface bonding, aspect ratio, surface-to-volume ratio of filler, etc. [8, 15-20]. Wang et al. [20] compared the use of graphite nanosheets to carbon black as a filler material in high density polyethylene. They reported a gentle increase in both tensile strength and impact strength of the composite with low loadings of graphene (0.5 to 2.0 wt. %) but a sharp reduction when the graphene content was greater than 2 wt. %. Due to the high surface energy of graphene, as well as the weak interaction between the graphene and polyethylene, an inhomogeneous dispersion in the polymer matrix was formed when the content of graphene was high, leading to adverse effects on the properties of the composites.

Due to the exceptional electrical properties of graphene, several researchers in the past have also studied the utilization of graphene as an electrically conductive additive in composites [7, 18, 22-23]. The electrical conductivity of graphene-based composites has been studied theoretically [21] as well as experimentally [18, 23, 25-26]. Studies have shown remarkable increases in composite electrical properties with graphene reinforcement. More recently, Qi et al. [23] demonstrated a substantial enhancement of electrical properties of polystyrene (PS) with the addition of graphene. The conductivity of the graphene/polystyrene composite was shown to be ~ 2–4 orders of magnitude higher than that of multi-walled-carbon-nanotube/polystyrene composites.

The combination of the remarkable mechanical properties and the exceptional electrical properties make graphene an ideal candidate for use as a filler material in fabricating multi-functional composites capable of sensing material behavior. Many reports demonstrate the effectiveness of utilizing CNT reinforced polymer composites as strain and damage sensors [27-30]. Thostenson et al. [27] performed tensile experiments on CNT/epoxy samples and demonstrated a highly linear relationship between the specimen deformation and the electrical resistance. This result suggested that CNT networks formed in an epoxy polymer matrix could be utilized as highly sensitive sensors for detecting the evolution of damage in advanced polymer-based composites [27-28]. More recently, similar studies have been conducted where graphene is utilized in providing strain sensing functions [31-33]. Eswaraiah et al. [31] demonstrated the real time strain response of f-G-PVDF composites on the macro-scale under tensile loads and the use of the composite as a strain sensor. The analysis of the change in voltage of various composite films revealed that the graphene-based composite showed better strain sensing performance compared to carbon nanotube-based polymer composites. In their previous work, the authors experimentally investigated the electrical response of multi-walled carbon nanotube reinforced nanocomposites under quasi-static and dynamic loading. The results indicated that the electrical resistance of the nanocomposite decreased under both quasi-static and dynamic loading due to the formation of more efficient carbon nanotube networks caused by the compression of the epoxy matrix [29-30].

The aforementioned studies revealed that when conductive filler materials are properly dispersed within a given matrix, an internal sensory network can be formed

and utilized to detect important information such as strain and damage within the material. To further this investigation, it is crucial to understand the electrical response of graphene reinforced composites under dynamic compressive loading conditions. The present study experimentally investigates the electro-mechanical response of graphene-PS composites subjected to static as well as dynamic split Hopkinson pressure bar (SHPB) loading. A novel SHPB apparatus, capable of simultaneous mechanical and electrical characterization, was developed to effectively investigate the electro-mechanical response of the graphene reinforced PS composites. The history between the electrical resistance change, mechanical loading, and the high-speed deformation photography are correlated to characterize the electrical-mechanical response of the fabricated composites.

2. Material and Specimen

2.1 Material Fabrication

The graphene platelets used in this study were xGnP^{TM} Nanoplatelets (XG Sciences). These unique nanoparticles consist of short stacks of one or more graphene sheets having a lateral dimension of ~25 μm. The edges of these sheets are sites for functionalization, which may help facilitate bonding within the polymer matrix. An SEM image of these platelets is shown in Fig. 1. The specific polymeric matrix chosen for this study was polystyrene (PS) (Crystal PS 1300) purchased from Styrolution. The PS had an average molecular weight of about 265,000 g/mol. Graphene's strong intrinsic van der Waals forces of attraction between sheets and high surface area make graphene very difficult to disperse uniformly within polymer materials [20]. In order to disperse the platelets throughout the PS matrix, a solution mixing process was

employed [23]. The general procedure used to disperse the graphene platelets is shown in Fig. 2. Briefly, 5 g of PS was first dissolved in 30 mL of dimethyl formamide (DMF). The desired amount of graphene platelets were dispersed in a separate DMF solution (~ 0.1 g graphene per 100 mL DMF) using ultrasonication. The graphene / DMF solution was sonicated for 1.5 h at 20 kHz on pulse mode, 30 s on 10 s off using a Sonics & Materials Inc. VCX750 probe sonicator. The graphene / DMF suspension was then added to the PS / DMF solution and mechanically stirred for ~ 2 h. Since the nanoplatelets tend to agglomerate during slow solvent evaporation, the solution was dropped into a large volume of methanol to coagulate the graphene-PS composites. The resulting composite was then filtered and dried in an oven at ~ 80 ºC for ~ 18 h. Finally, the dried graphene-PS composites were hot-pressed using a heated steel mold (~ 190 ºC) and a hydraulic press.

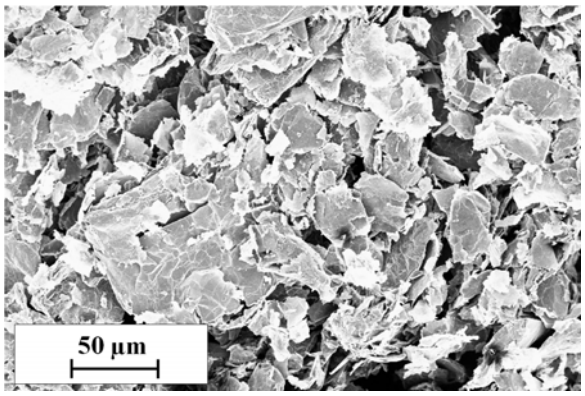

Fig. 1 SEM image of xGnP M-25 nanoplatelets

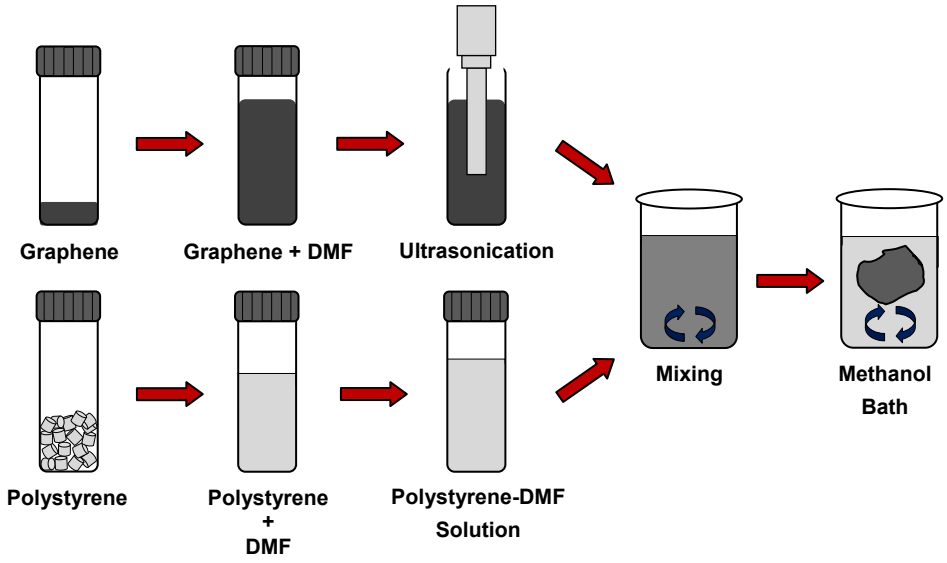

Fig. 2 Procedure for dispersing graphene platelets in polystyrene

2.2 Specimen

Fig. 3 illustrates specimens prepared for both quasi-static and dynamic compression loading experiments. 5 vol. % graphene-PS composites were fabricated for all experiments. Specimens used in quasi-static experiments were 10 mm in length and had a diameter of 6.35 mm, where the loading was exerted in the longitudinal direction of the 10 mm length. Specimens used in dynamic experiments were 8.68 mm in length and had a diameter of 15.87 mm. Two V-notch channels with a depth of 0.3 mm were machined in the middle section of both specimens located 1.9 mm from each face. The channels were used to implement a modified four-point probe method [29] in order to effectively measure the change in electrical resistance of the specimen during loading. The loading is exerted in the longitudinal direction along the length of the specimen. The left face, right face, and the two inner channels of the specimen served as four probes to obtain a four point probe measurement. All four probes were

coated with silver paint (SPI-Paint 05001-AB) and lead wires were attached using an adhesive (M-Coat A Air-Drying Polyurethane Coating).

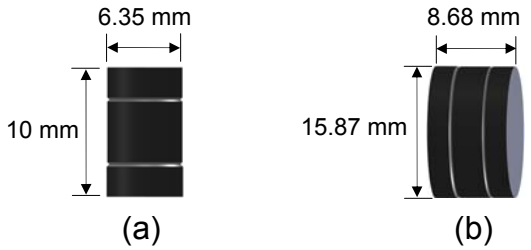

Fig. 3 Specimen geometry used for (a) quasi-static loading and (b) dynamic loading

3. Experimental Setup and Procedure

3.1 Electrical Characterization

In order to effectively capture the change in electrical resistance of the cylindrical specimen, a novel approach previously developed by the authors utilizing the four-point probe method was implemented [29]. The four probes consisted of the left face, right face, and the two inner channels. To allow a constant current flow through the entire bulk of the specimen, a constant current was supplied through the right and left faces of the specimen. The two inner channels served as the two peripheral electrodes that measure the voltage drop across the middle section of the specimen. The electrical resistance of the middle section can be easily determined from the input current and the voltage drop across the inner probes. As the specimen underwent deformation, the instantaneous resistance of the middle section changed. Percent change in the resistance was calculated for each experiment. Due to the complex dispersion pattern of graphene inside, the initial resistance of the individual specimens varies slightly. Therefore, the initial resistance of each specimen served as the baseline for each experiment. Based on previous studies [29], this method better

provides the means to detect changes in the resistance caused by strain and damage mechanisms in the material as compared to the classical four-point probe method. Since the current uniformly flows through the cross sectional area, the measured resistance is an estimation of the bulk resistance of the inner section. By using this average voltage measurement technique, more consistent and accurate results were obtained during a wide range of mechanical loading schemes and consequent specimen deformations.

3.2 Quasi-static Electro-Mechanical Characterization

The quasi-static loading was implemented by a screw-driven testing machine. A modified four-point probe method was utilized to measure the resistance change during the compression tests [29]. The experimental setup used to capture the resistance change of the composites under quasi-static loading is shown in Fig. 4. A constant current source was used to supply a DC current flow through the specimen. The graphene/PS specimen was sandwiched between two aluminum plates to establish uniform current flow through the specimen during the compressive loading. Silver paint was applied to the top and bottom of each specimen to minimize the contact resistance between the specimen and the plates. Each loading head was insulated from the electrical measurement system. Two electrometers were used to measure the voltage at each of the two individual inner probe rings. The difference between the two voltage readings, which corresponds to the voltage drop across the two inner probes, was measured using a digital multimeter and recorded using a LabView system.

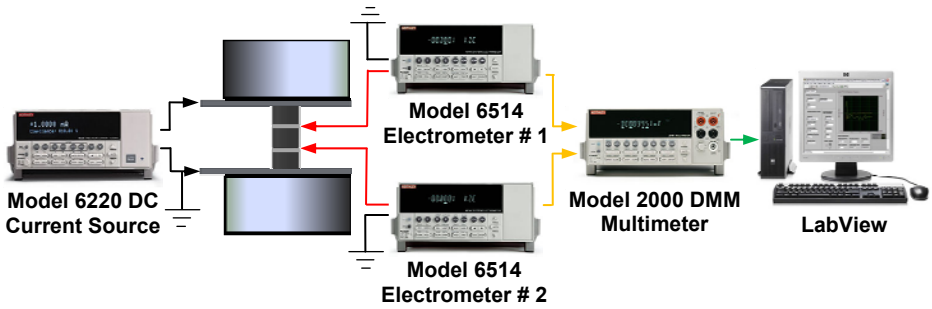

Fig. 4 Experimental setup for electrical characterization under quasi-static loading

3.3 Dynamic Electro-Mechanical Characterization

A modified split Hopkinson (Kolsky) pressure bar apparatus, capable of simultaneous mechanical and electrical characterization, was developed and implemented to investigate the dynamic electro-mechanical response of the graphene-PS composites.

A typical SHPB consists of a striker bar, a solid incident bar and a solid transmission bar. The striker bar is propelled using an air-operated gun. A pulse shaper is commonly placed at the impact end of the incident bar with a thin layer of lubricant to improve force equilibrium conditions at the specimen-bar interfaces. The theoretical details of SHPB can be obtained from Kolsky [34]. The specimen is sandwiched between the incident bar and the transmission bar. A lubricant is applied between the specimen and the bar interfaces to minimize friction.

When the striker bar impacts the incident bar, an elastic compressive stress pulse, referred to as the incident pulse, is generated and then propagates along the incident bar towards the specimen. When the incident pulse reaches the specimen, part of it reflects back into the incident bar (reflected pulse) in the form of a tensile pulse due to the impedance mismatch at the bar-specimen interface and the remaining pulse

is transmitted (transmission pulse) to the transmission bar. Axial strain gages mounted on the surfaces of the incident and transmission bar provide time-resolved measures of the elastic strain pulses in the bars. The amplitude and length of the incident pulse is related to the projectile velocity and projectile length which allows for variation in achievable strain rates.

Using one-dimensional wave theory, the engineering stress and engineering strain in the specimen can be determined from the reflected and transmitted strain pulses respectively, as given in Eqs. 1 and 2.

$$\sigma_s = E_b \frac{A_b}{A_s} \varepsilon_t(t) \tag{1}$$

$$\varepsilon_s = \frac{-2c_b}{L_s} \int_0^t \varepsilon_r(t) dt \tag{2}$$

The above equations were suitably modified to obtain the true stress and true strain in the specimen. The expressions for the forces at the specimen incident bar interface and at the specimen transmission bar interface are given in equations Eqs. 3 and 4 respectively.

$$F_i = A_b E_b (\varepsilon_i + \varepsilon_r) \tag{3}$$

$$F_t = A_b E_b \varepsilon_t \tag{4}$$

where ε_i, ε_r, ε_t are the time-resolved strain values of the incident, reflected and transmitted pulses respectively, c_b is the longitudinal bar wave speed, E_b is the Young's modulus of the bar material, L_s is the thickness of the specimen, A_b is the cross-sectional area of the bar and A_s is the cross-sectional area of the specimen.

Force equilibrium within the specimen during the wave loading is attained when the forces on each face of the specimen are equal.

Several modifications were made to the existing SHPB to simultaneously capture the electrical response as well as the mechanical behavior of the specimen during the dynamic loading. A sketch of the novel SHPB device is shown in Fig. 5. The aluminum incident and transmission bars were 19.05 mm in diameter and measured 1613 mm and 1220 mm in length respectively. Lead wires were securely attached to each bar to provide a means of supplying a DC current flow through the specimen during loading. In order to obtain an accurate electrical response of the specimen, nylon bushings were fabricated and installed to isolate the incident and transmission bars from the supports. A similar four-point probe technique, as described in quasi-static experiments, was implemented. To minimize the contact resistance as well as the frictional forces present at the specimen-bar interfaces, a conductive lubricant (AI Technology Inc. ELGR8501) was applied to the specimen faces. Additionally, a pulse shaper consisting of a single layer of electrical tape and clay (~ 2 mm thick) were used to isolate the incident bar from the gas gun apparatus and to improve the force equilibrium conditions at the specimen-bar interfaces. A constant current source with high frequency response (Keithley Instruments Model 6221) was used to supply the constant DC current flow under the high rate deformation while the voltage drop between the two inner probes was measured by a differential amplifier (Tektonix ADA 400A) and recorded by a digital oscilloscope (Tektronix TDS 3014).

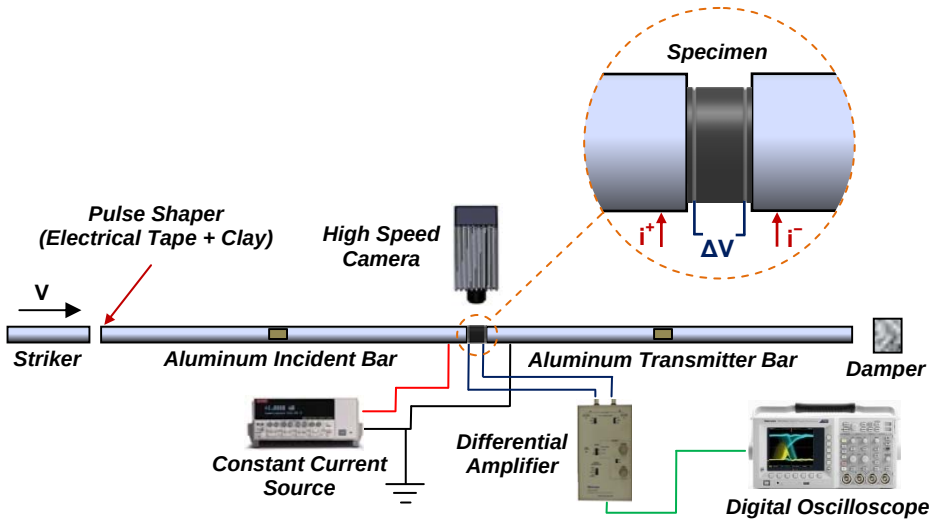

Fig. 5 Experimental setup of SHPB apparatus with dynamic electrical characterization setup

It is important to note that proper strain gage selection is critical in preventing any electrical interference in strain measurements while conducting these types of experiments. The particular strain gages chosen (Micro-Measurements C2A-13-250LW-350) consists of an encapsulated gage mounted on a thin high-performance laminated polyimide film backing. The polyimide film backing provides a layer of insulation between the actual gage and the bar surface and therefore prevents any voltage interference. A series of experiments were performed with and without supplying current through the bars, validating that the strain gages bonded to the bars remain unaffected. Fig. 6 shows typical pulses obtained from the strain gages for the two cases when the incident bar is in contact with the transmission bar without any specimen in between. Since there is no impedance mismatch at the bars interface, the entire incident pulse is transmitted to the transmission bar. It can be clearly seen that there is no effect on the pulses when a current of 1 mA was supplied through the bars.

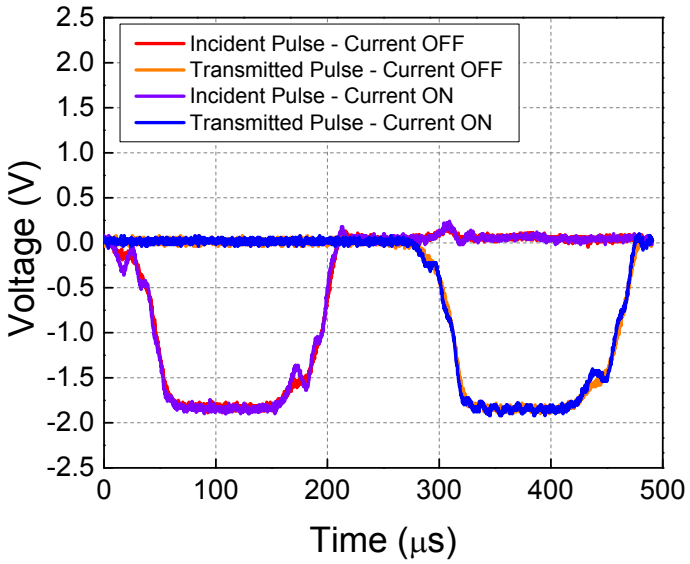

Fig. 6 Original pulses generated from the modified SHPB to ensure no current effect

A striker length of 406 mm was used in all experiments to achieve large strains in the specimen. A high-speed digital camera (Photron SA1) was used to capture the real time deformation of the specimen at a frame rate of 100,000 fps.

4. Experimental Results and Discussion

4.1 Quasi-Static Compressive Response

A typical electro-mechanical response of a 5 vol. % graphene-PS composite under compressive loading is shown in Fig. 7. During the quasi-static compression, the stress in the specimen monotonically increases to 47 MPa at 5 % strain and then gradually decreases. Initially, no significant change in resistance is observed up until ~ 1 % strain. Taking the initial resistance as a baseline, the percent change in electrical resistance increases proportionally with strain. Since the electrical resistance of the matrix material is very high, the graphene particles exclusively conduct the electrical current within the material. Due to the brittle nature of the PS matrix, small micro-

cracks begin to form as the compressive strain increases resulting in a significant increase in electrical resistance. When considering the negligible change in graphene particle geometry during the compressive event, the resistance change is caused by the interruptions of the electrical networks between the graphene particles.

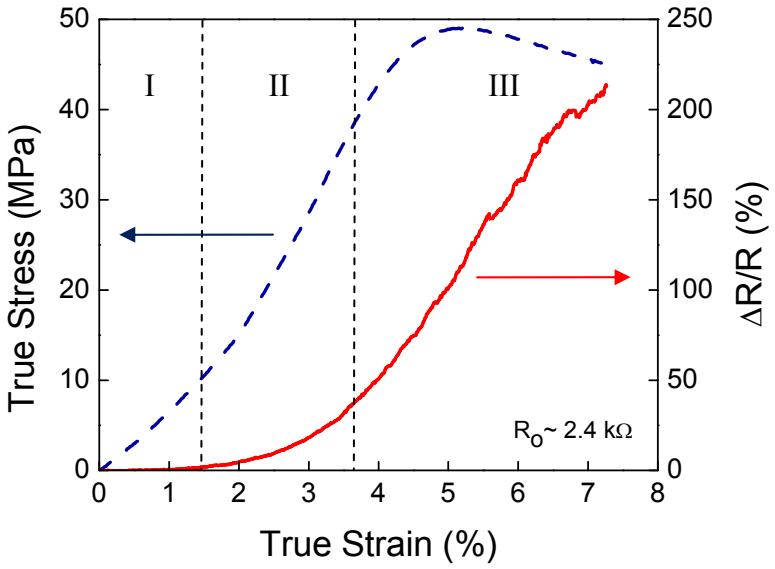

Fig.7 Typical electro-mechanical response of 5 vol% graphene-PS under quasi-static loading

A schematic representing the damage mechanisms induced by the mechanical compression is shown in Fig. 8. As observed in Fig 8-I, the electrical resistance of the composite begins to increase at ~ 1 % strain due to the disruption of the graphene network present throughout the volume of the composite. Scanning electron microscopy (SEM) was performed on the post-mortem specimens to provide more insight on the internal damage mechanisms occurring during the compressive event. As shown in Fig. 9, evidence of micro-cracks located primarily around small agglomerates of FLG. The small agglomerates of the graphene sheets appear to serve

as crack nucleation sites and due to poor interactions between the PS matrix and FLG paricles, damage tends to propagate along the graphene-polymer interfaces. A series of experiments were carried out in which and the change in resistance showed this similar behavior.

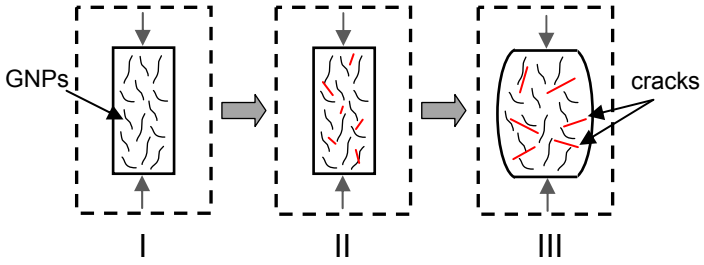

Fig. 8 Representation of a cross-section of a graphene-PS under compressive loading

The micro-cracks, formed primarily around the graphene agglomerations, continue to grow and propagate throughout the composite which leads to an increase in the rate of electrical resistance change. The formation of additional voids and cracks due to the increasing strain further decreases the electrical efficiency between graphene particles, which is illustrated in Fig 8II and Fig 8III.

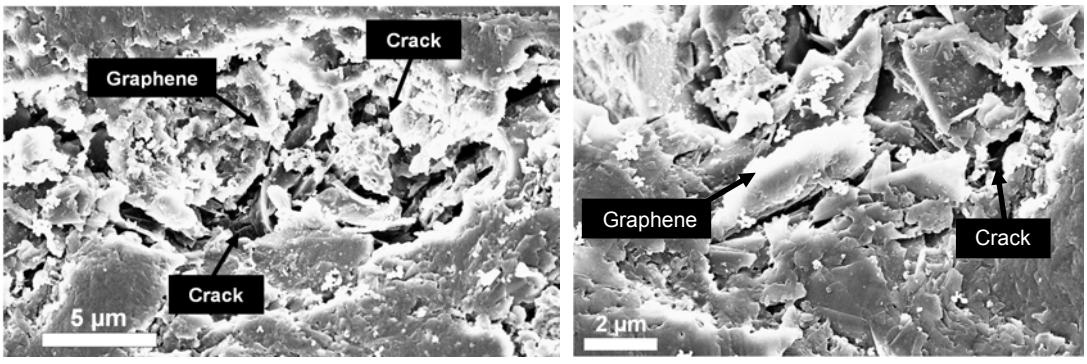

Fig. 9 SEM image of a cross-section of a post-mortem specimen loaded to 7% eng. strain.

The true stress versus true strain curves for pristine PS and PS reinforced with 5 vol. % graphene are shown in Fig 10. A significant decrease in yield strength (~47%) and modulus (~57%) is observed with the addition of graphene. This result differs from most reports where authors observed significant improvements in mechanical properties when graphene is used as a filler material within various polymers [8-11]. Generally, the enhancement of strength and modulus is attributed to high aspect ratio and high strength of the filler as well as the uniform distribution and good interfacial adhesion between the fillers and matrixes, which provide effective load transfer from the matrixes to the fillers [8, 20, 35]. When relatively high concentrations of graphene are used, an ineffective dispersion typically forms due to inevitable aggregation of the graphene particles. The heterogeneity of the polymer microstructure creates many structural flaws and weak interfaces between the graphene and PS resulting in a decrease in mechanical strength. This behavior has been previously reported and demonstrated for various types of particles, including graphene [8, 15-20].

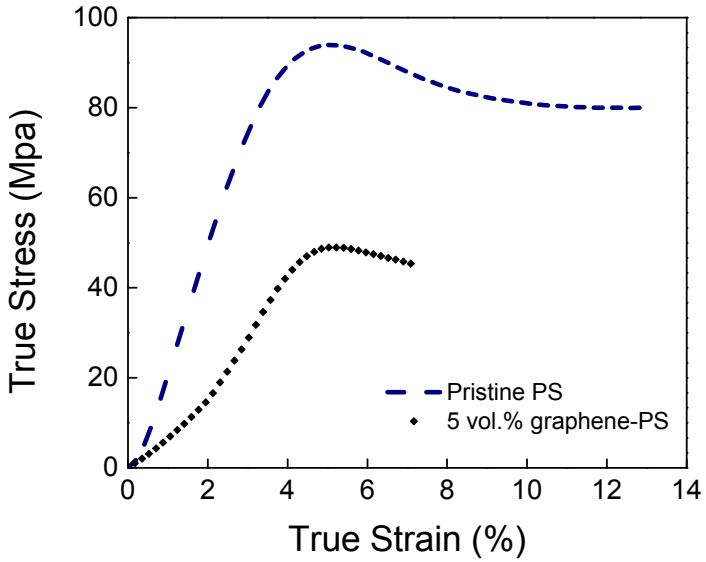

Fig. 10 True compressive stress-strain curve of polystyrene and graphene-PS under quasi-static loading.

4.2 Split Hopkinson Pressure Bar Loading

To investigate the electrical response of the graphene reinforced composites under higher strain rates, the electro-mechanical SHPB apparatus developed was utilized to load the specimens. The real time strain-pulses obtained for polystyrene at an average strain rate of $2000s^{-1}$ under dynamic compression are shown in Fig. 11. It can be observed from the Figure that the pulse shaper, consisting of a layer of electrical tape and clay, used in all experiments helped to reduce high frequency oscillations in the incident stress wave. The incident pulse length applied to the specimen was ~ 240 μs. Due to the brittle nature of the PS matrix, the transmitted pulse profile shows that the total loading event lasts only ~ 100 μs at which point the specimen fails.

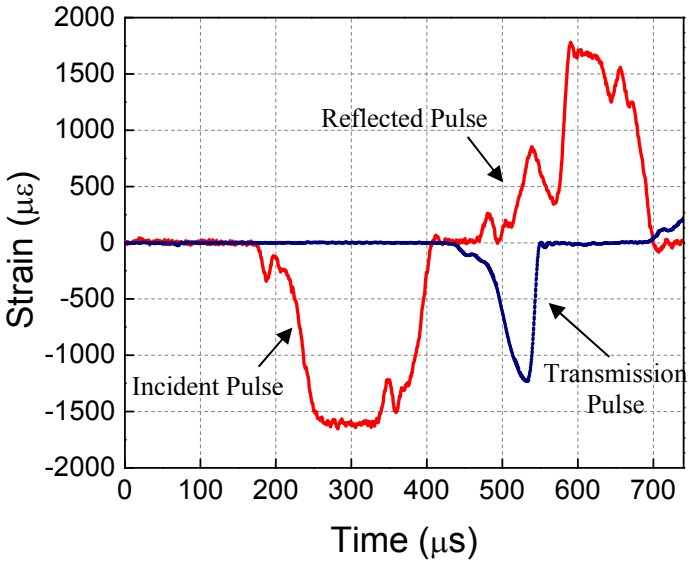

Fig. 11 Typical real-time strain pulses obtained from strain gages mounted on the bars for PS at an average strain rate of 2000 s^{-1}

It is important for the specimen to be in equilibrium under dynamic loading conditions for valid analysis of data. Fig 12 shows the typical force equilibrium of polystyrene at an average strain rate of 2000 s-1. The pulse shaper improved the force equilibrium conditions at the specimen-bar interfaces. The force equilibrium was maintained during the entire loading duration.

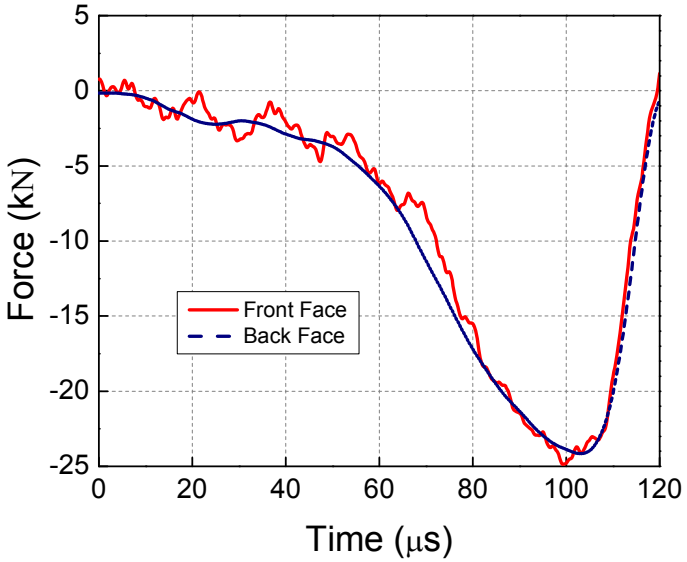

Fig. 12 Typical force equilibrium conditions at the specimen-bar interface at an average strain rate of 2000 s^{-1}

A typical electrical response along with the mechanical behavior of both neat PS and graphene reinforced composites is shown in Fig. 13. As the specimen undergoes dynamic compression, the electrical resistance increases proportional to the change in strain. As the stress of the specimen monotonically increases to 75 MPa at 5% strain, the bulk electrical resistance of the specimen increases ~ 85% due to the formation of micro-cracks within the matrix. As the internal damage grows, the electrical resistance continues to increase as the electrical efficiency of the composite is further diminished. The resistance does not abruptly jump but gradually increases as damage initiates and propagates throughout the composite. We believe that this difference may come from the non-uniform dispersion of graphene inside the matrix and complex initiation and propagation of damages.

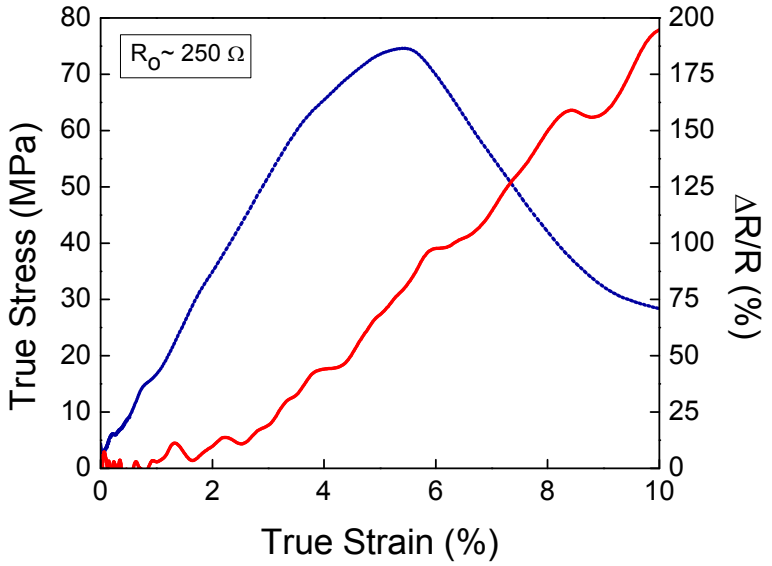

Fig. 13 Typical electro-mechanical response of 5 vol% graphene/PS under dynamic loading

A typical electrical response along with the real-time deformation images of a 5 vol.% graphene-PS composite subjected to dynamic loading are shown in Fig. 14. The time frames used in the loading event are chosen in a manner such that they can be correlated to the time at which certain deformation mechanisms were first observed. During the first 50 μs, the specimen undergoes a slight uniform compression. Since the strain of the material is very minimal during this time, no noticeable change in electrical resistance is observed. At ~ 60 μs, a crack is seen to initiate and propagate through the specimen consequently causing an increase in resistance. From 60 to 100 μs, damage further propagates throughout the specimen leading to larger increases in electrical resistance.

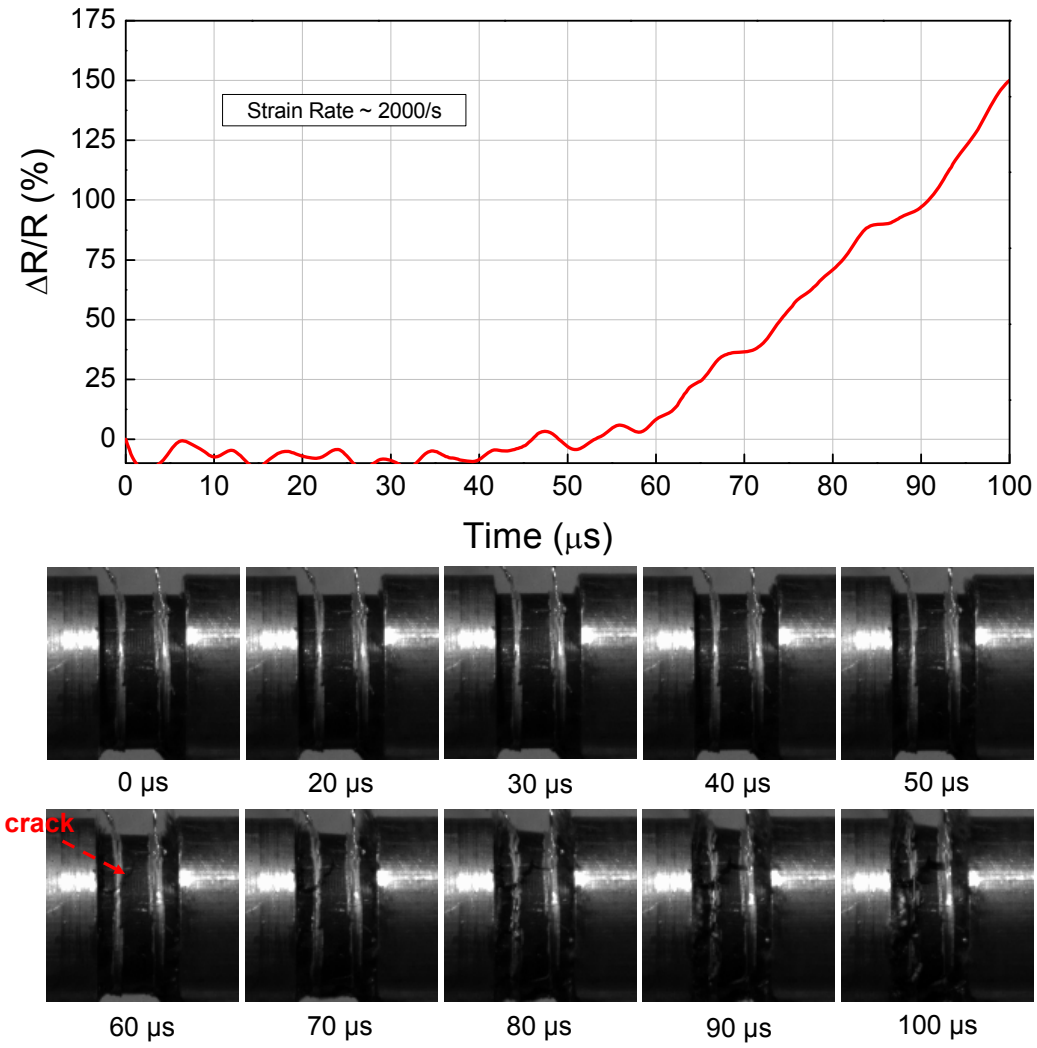

Fig. 14 Percent change in electrical resistance of a 5 vol. % graphene-PS composite subjected to SHPB loading with real-time deformation images

The dynamic true stress-strain curves for pristine PS and PS containing 5 vol. % graphene is shown in Fig. 15. The high strain-rate yield stresses were much higher than the quasi-static ones for both pristine PS as well as graphene reinforced PS. Similar to static loading, the graphene-PS composites demonstrated a reduced strength

and modulus in comparison to pristine polystyrene. The composite strength and modulus decreased ~ 47 % and ~ 66 % respectively. The reduced mechanical properties are again attributed to the presence of relative agglomerations of graphene particles within the PS matrix which prevent efficient load transfer to the graphene particles.

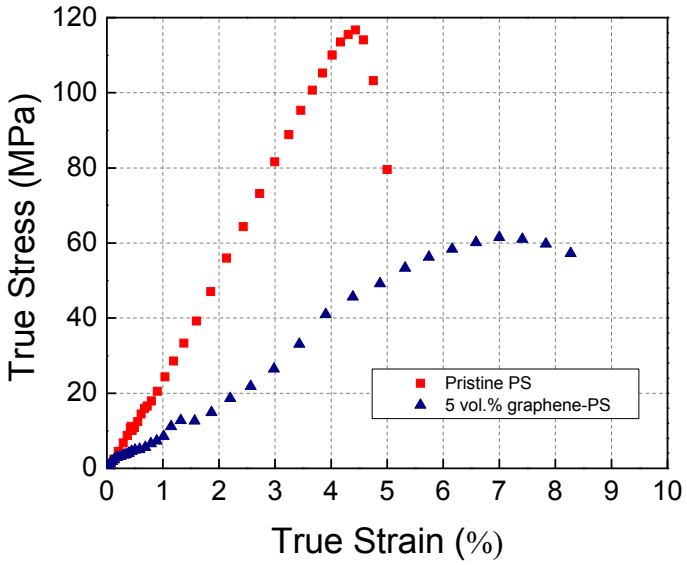

Fig. 15 True compressive stress-strain curve for pristine PS and 5 vol.% graphene/PS at an average strain rate of 2000 s^{-1}

Fig. 16 shows the effect of 5 vol. % graphene on the static and dynamic behavior of polystyrene. Despite an increase in yield stress for dynamic loading in comparison to static loading, the presence of graphene within the polystyrene matrix significantly diminishes the mechanical properties of the composite material under both static and dynamic compression.

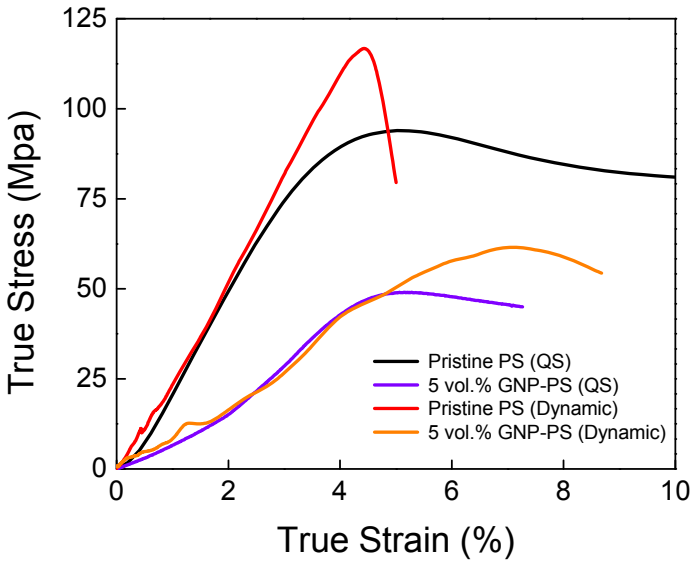

Fig. 16 Comparison of pristine PS vs. graphene-PS under static and dynamic loading

5. Conclusions

The present paper describes the electro-mechanical response of graphene reinforced polystyrene composites under quasi-static and dynamic compressive loading. Graphene-PS composites with low resistance were fabricated using a solution mixing approach followed by hot-pressing. A modified four-point probe method, using line and face contacts rather than point contacts, was implemented to accurately monitor the bulk electrical resistance of the composites. Moreover, a modified split Hopkinson (Kolsky) pressure bar apparatus, capable of simultaneous mechanical and electrical characterization, was developed and implemented to investigate the dynamic electro-mechanical response of the composites. In addition to measuring the change in electrical resistance as well as the dynamic constitutive behavior, real-time damage was captured using high-speed photography. The real-time damage was correlated to both stress-strain and percent change in resistance profiles. Due to a high

concentration of graphene particles, relative aggregations of the graphene were inevitably formed which resulted in inadequate load transfer between the graphene particles and the PS matrix. Consequently, a significant decrease in mechanical properties under both static and dynamic loading conditions with the presence of graphene was observed. The bulk electrical resistance of the composite increased significantly due to the brittle nature of the PS matrix as well as the presence of relative agglomerations of graphene platelets which resulted in micro-crack formations.

Acknowledgements

The authors acknowledge the financial support provided by the Rhode Island Science & Technology Advisory Council as well as Research Experiences for Undergraduates National Science Foundation (CMMI 1233887).

References

[1] Kuilla T, Bhadra S, Yao D, Kim NH, Bose S, Lee JH. Recent advances in graphene based polymer composites. Progress in Polymer Science 2010; 35(11): 1350-1375.

[2] Ramanathan T, Abdala AA, Stankovich S, Dikin DA, Herrera-Alonso M, Piner RD, et al. Functionalized graphene sheets for polymer nanocomposites 2008; 3(6): 327-331.

[3] Godovsky, D. Device applications of polymer-nanocomposites. Advances in Polymer Science 2000; 153: 163-205.

[4] Zhu Y, Murali S, Cai W, Li X, Suk JW, Potts JR, et al. Graphene and graphene oxide : synthesis, properties, and applications. Adv Mater 2010; 22(35): 3906–24.

[5] Frazier R, Daly D, Swatloski R, Hathcock K, and South C. Recent progress in graphene-related nanotechnologies. Recent Patents on Nanotechnology 2009; 3(3): 164-176.

[6] Soldano C, Mahmood A, Dujardin E. Production, properties and potential of graphene. Carbon 2010; 48(8): 2127-2150.

[7] Kim H, Miura Y, Macosco CW. Graphene/polyurethane nanocomposites for improved gas barrier and electrical conductivity. Chemistry of Materials 2010; 22(11): 3441-3450.

[8] Singh V, Joung D, Zhai L, Das S, Khondaker S, Seal S. Graphene based materials: Past, present and future. Progress in Materials Science 2011; 56(8): 1178-1271.

[9] Fang M, Wang K, Lu H, Yang Y, Nutt S. Covalent polymer functionalization of graphene nanosheets and mechanical properties of composites. J Mater Chem 2009; 19(38): 7098

[10] Rath T, Li Y. Nanocomposites Based on Polystyrene-b-poly(ethylene-r-butylene)-b-polystyrene and Exfoliated Graphite Nanoplates: Effect of Nanoplatelet Loading on Morphology and Mechanical Properties. Composites Part A: Applied Science and Manufacturing 2011; 42(12): 1995-2002.

[11] Liang JJ, Huang Y, Zhang L, Wang Y, Ma YF, Guo TY, and Chen Y. Molecular-Level Dispersion of Graphene into Poly(vinyl Alcohol) and Effective Reinforcement of Their Nanocomposites. Advanced Functional Materials 2011; 19(14): 2297-2302.

[12] Vadukumpully S, Paul J, Mahanta N, Valiyaveettil S. Flexible conductive graphene/poly(vinyl chloride) composite thin films with high mechanical strength and thermal stability. Carbon 2011; 49(1): 198-205.

[13] Yang S, Lin W, Huang Y, Tien H, Wang J, Ma CM, Li S, Wang Y. Synergetic effects of graphene platelets and carbon nanotubes on the mechanical and thermal properties of epoxy composites. Carbon 2011; 49(3): 793-803.

[14] Khan U, May P, O'Neill A, Coleman JN. Development of stiff, strong, yet tough composites by the addition of solvent exfoliated graphene to polyurethane. Carbon 2011; 49(1): 198-205.

[15] Kim H, Macosko CW. Morphology and properties of polyester/exfoliated graphite nanocomposites. Macromolecules 2008; 41(9): 3317-3327.

[16] Goncalves G, Marques P, Barros-Timmons A, Bdkin I, Singh MK, Emami N, Grácio J. Graphene oxide modified with PMMA via ATRP as reinforcement filler. Journal of Materials Chemistry 2010; 20(44): 9927-3327.

[17] Yasmin A, Daniel IM. Mechanical and thermal properties of graphite platelet/epoxy composites. Polymer 2004; 45(24): 8211-8219.

[18] Stankovich S, Dikin D, Dommett G, Kohlhaas K, Zimney E, Stach E, Piner R, Nguyen S, and Ruoff R. Graphene-based Composite Materials. Nature 2006; 442(7100): 282-286.

[19] Sahrim HA, Mou'ad AT, Yahya SY, and Rozaidi R.Ahmad SH, Tarawneh MA, Yahya SY and Rasid R (2011). Reinforced Thermoplastic Natural Rubber (TPNR) Composites with Different Types of Carbon Nanotubes (MWNTS), Carbon Nanotubes - Synthesis, Characterization, Applications, Dr. Siva Yellampalli (Ed.), ISBN: 978-953-307-497-9, InTech, DOI: 10.5772/16494.

[20] Wang L, Hong J, Chen G. Comparison study of graphite nanosheets and carbon black as fillers for high density polyethylene. Polymer Engineering & Science 2010; 50(11): 2176-2181.

[21] Kim I, Jeong YG. Polylactide/exfoliated graphite nanocomposites with enhanced thermal stability, mechanical modulus, and electrical conductivity. Journal of Polymer Science Part B: Polymer 2010; 48(8): 850-858.

[22] Kim H, Macosko CW. Processing-property relationships of polycarbonate/graphene composites. Polymer 2009; 50(15): 3797-3809.

[23] Qi XY, Yan D, Jiang Z, Cao YK, Yu ZZ, Yavari F, and Koratkar N. Enhanced Electrical Conductivity in Polystyrene Nanocomposites at Ultra-Low Graphene Content. ACS Applied Materials & Interfaces 2011; 3(8): 3130-3133.

[24] Xie SH, Liu YY, and Li JY. Comparison of effective conductivity between composites reinforced by graphene nanosheets and carbon nanotubes. Applied Physics Letters 2008; 92(24): 243121-3.

[25] Zhang H, Zheng W, Yan Q, Yang Y, Wang J, Lu Z, Ji G, Yu Z. Electrically Conductive Polyethylene Terephthalate/graphene Nanocomposites Prepared by Melt Compounding. Polymer 2010; 51(5): 1191-1196.

[26] Ramirez C, Figueiredo FM, Miranzo P, Poza P, Osendi MI. Graphene nanoplatelet/silicon nitride composites with high electrical conductivity. Carbon 2012; 50(10): 3607-3615.

[27] Thostenson ET, Chou TW Carbon Nanotube Networks: Sensing of Distributed Strain and Damage for Life Prediction and Self Healing. Advanced Materials 2006; 18(21): 2837-2841.

[28] Lim AS, An Q, Chou TW, Thostenson ET. Mechanical and electrical response of carbon nanotube-based fabric composites to Hopkinson bar loading. Composites Science and Technology 2011; 71(5): 616-621.

[29] Heeder N, Shukla A, Chalivendra V, Yang S, Park K. Electrical Response of Carbon Nanotube Reinforced Nanocomposites under Static and Dynamic Loading. Experimental Mechanics 2012; 52(3): 315-322.

[30] Heeder N, Shukla A, Chalivendra V, Yang S. Sensitivity and dynamic electrical response of CNT-reinforced nanocomposites. Journal of Materials Science 2012; 47(8): 3808-3816.

[31] Eswaraiah V, Balasubramani K, Ramaprabhu S. Functionalized graphene reinforced thermoplastic nanocomposites as strain sensors in structural health monitoring. Journal of Materials Chemistry 2011; 21(34): 12626-12628.

[32] Qu S, Wong S. Piezoresistive behavior of polymer reinforced by expanded graphite. Composites Science and Technology 2007; 67(2): 231-237.

[33] Li W, Dichiara A, Bai J. Carbon nanotube–graphene nanoplatelet hybrids as high-performance multifunctional reinforcements in epoxy composites. Composites Science and Technology 2013; 74(0): 221-227.

[34] Kolsky H. An Investigation of the Mechanical Properties of Materials at very High Rates of Loading. Proceedings of the Physical Science 1949; 62:676-700.

[35] Tjong SC. Structural and mechanical properties of polymer nanocomposites. Materials Science and Engineering R: Reports 2006; 53(3-4): 73-197.

CHAPTER 4

HIGHLY CONDUCTIVE GRAPHENE-BASED SEGREGATED COMPOSITES PREPARED BY PARTICLE TEMPLATING

by

Nicholas Heeder, Abayomi Yussuf, Fei Guo, Indrani Chakraborty, Michael P. Godfrin, Robert Hurt, Anubhav Tripathi, Arijit Bose and Arun Shukla

has been published in the Journal of Materials Science

Corresponding Author: Nicholas Heeder

Dynamic Photo Mechanics Laboratory

Department of Mechanical, Industrial and Systems Engineering

University of Rhode Island

110 Wales Hall, 92 Upper College Rd

Kingston, RI, 02881, USA

Phone: +1-401-874-2227

Email Address: heedern@egr.uri.edu

Abstract

We use capillary-driven particle level templating and hot melt pressing to disperse few-layer graphene (FLG) flakes within a polystyrene matrix to enhance the electrical conductivity of the polymer. The conducting pathways provided by the graphene located at the particle surfaces through contact of the bounding surfaces allow percolation at a loading of less than 0.01% by volume. This method of distributing graphene within a matrix overcomes the need to disperse the sheet-like conducting fillers isotropically within the polymer, and can be scaled up easily.

Keywords: Graphene; Polymer; Segregated Composites; Nanocomposites; Electrical Properties

1. Introduction

Electrical conductivity in polymers that are traditionally insulating can be achieved by dispersing conducting particles within the non-conducting matrix. The predicted percolation threshold for randomly aligned and uniformly dispersed 2-dimensional sheets such as graphene (aspect ratio ~ 4000) in a matrix is 0.01 % by volume [1]. Achieving this threshold is difficult, because strong van der Waals interactions between these sheets lead to aggregation [2-4]. In addition, most processing techniques, especially at the pilot and commercial scales, result in highly anisotropic flows, which tend to align sheets along the direction of flow and inhibit the formation of a percolating network. Achieving the theoretical percolation limit for scalable techniques has therefore been difficult. Because of the energy demand for removing solvents, and sometimes their potentially hazardous nature, melt processing is often chosen over solvent based mixing of filler and polymer, despite the increased

viscosity of a melt. Dispersing high aspect ratio sheets isotropically in a melt of high viscosity is a major challenge.

An alternate method for creating a connected pathway for conductive particles is to make segregated composites. The conductive particles within segregated composites are only permitted to reside on the surfaces of the polymer matrix particles. When consolidated into a monolith, these conductive particles get connected in a three-dimensional network, dramatically increasing the conductivity of the composite [5-8]. Sheets do not have to be distributed isotropically throughout a matrix to achieve percolation, overcoming a major limitation. This way of achieving three-dimensional connectivity of the particles also decreases the contact resistance between the particles [5]. Du et al. [5] prepared multi-walled carbon nanotube (MWCNT)/high density polyethylene (HDPE) and graphene nanosheets (GNS)/HDPE) composites with a segregated network structure by alcohol-assisted dispersion and hot-pressing. The electrical properties of the GNS/HDPE and MWCNT/HDPE composites were compared and it was found that the percolation threshold of the GNS/HDPE composites (1 % v/v) was much higher than that of the MWCNT/HDPE composites (0.15 % v/v) while the MWCNT/HDPE composite showed higher electrical conductivity than the GNS/HDPE composite at the same filler content. They concluded that, due to crimp, rolling and aggregation of the GNSs in the HDPE matrix, the two-dimensional GNSs were not as effective as MWCNTs in forming conductive networks. Later, Hu et al. [8] prepared graphene/polyethylene segregated composites using a two-step process. A combination of sonication and mechanical mixing was used to first coat the ultrahigh molecular weight polyethylene

(UHMWPE) with graphene oxide (GO) sheets. The excess solvent was removed from the system and then the coated powders were added to a hydrazine solution and stirred at 95 ºC to reduce the GO to graphene. All coated powders were compressively molded and hot pressed to form composite sheets. This two-step process was shown to effectively prevent aggregation, leading to composites exhibiting high electrical conductivity at a very low percolation threshold (0.028 % v/v).

In this work we use capillary interactions between polystyrene (PS) particles and few-layer graphene (FLG) particles to coat the FLG onto the polymer. Hot pressing these coated particles results in highly conductive composites. We obtain electrical percolation below 0.01 % v/v of FLG. A significant increase in electrical conductivity is observed for the composites between 0.01 % v/v and 0.3 % v/v. The fabrication technique demonstrated here is simple, commercially viable and does not require hazardous chemicals. It provides the means to form highly organized conductive networks throughout insulating polymeric materials.

2. Material and methods

The few-layer graphene flakes used in this study were xGnP^{TM} Nanoplatelets (XG Sciences, USA). These nanoparticles consist of short stacks of graphene layers having a lateral dimension of ~ 25 μm and a thickness of ~ 6 nm. The polymeric material chosen for this study was polystyrene (Crystal PS 1300, average molecular weight of 121,000 g/mol) purchased from Styrolution, USA. The PS pellets (~ 2 mm) used were elliptical prisms with a total surface area of 1.03 ± 0.01 cm2.

A two-step process was utilized to produce the FLG/PS segregated composites. First, the desired amount of graphene platelets were measured and added to 7 g of dry

PS pellets. The FLG spontaneously adheres to the dry polymer particles by physical forces, which may be van der Waals forces or electrostatic attraction associated with surface charges. Figure 1 shows PS pellets coated with various amounts of FLG using this dry coating process. This coating process works well for FLG loadings below 0.2 % v/v. However, at higher FLG loadings, this dry method leaves behind excess FLG because the charge on the pellets is neutralized after the initial coating.

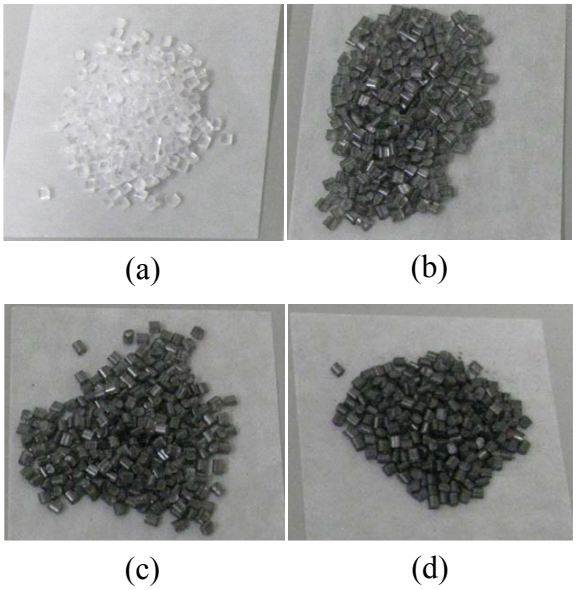

Fig. 1 (a) PS, (b) PS coated with 0.05 % v/v FLG, (c) PS coated with 0.1 % v/v FLG, and (d) PS with less than 0.2 % v/v FLG.

To provide a means of temporarily attaching larger quantities of the FLG to the surface of the PS, an additional step is implemented during the fabrication procedure, shown in Fig. 2. The PS is first soaked in a methanol bath and the excess methanol is drained from the PS pellets. FLG is added, and the mixture is then shaken vigorously, creating a dense coating of graphene on each PS pellet. The methanol temporarily moistens the polymer pellets forming small liquid bridges. The capillary pressure

created through these bridges allows the FLG sheets to stick easily to the surface of the pellets. During the subsequent hot melt pressing, the temperature and mold pressure are precisely controlled allowing the pellets to be consolidated into a monolith while maintaining boundaries. The methanol evaporates during the molding cycle. In our experiments, a stainless steel mold consisting of a lower base and a plunger was heated to 110 ºC. The graphene-coated PS was placed inside the cavity of the lower base and the plunger was placed on top. The temperature of both the plunger and the base mold was increased to 190 ºC at which point it was hot-pressed at 45 kN using a hydraulic press.

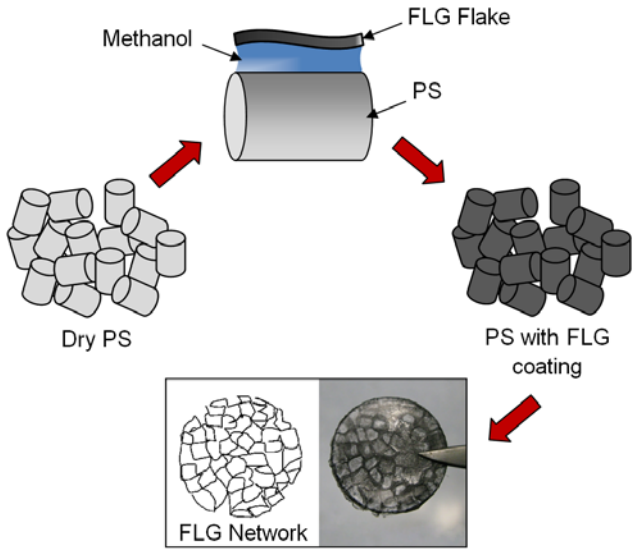

Fig. 2 Surface wetting fabrication procedure to obtain highly conductive FLG/PS composites.

Electrical conductivity measurements were made on the FLG/PS composites using a volumetric two-point probe measurement technique. The bulk electrical conductivity was measured across the thickness of the sample (perpendicular to pressing). The resistance of the material was experimentally determined by supplying

a constant current, ranging from 5 nA to 1 mA, through the specimen while simultaneously measuring the voltage drop across the specimen. A constant current source (Keithley Instruments Model 6221) was used to supply the DC current while two electrometers (Keithley Instruments Model 6514) were used to measure the voltage drop. The difference between the two voltage readings was measured using a digital multimeter (Keithley Instruments Model 2000 DMM).

3. Results and discussion

As seen in Fig. 2, the composite (with 0.3 % v/v FLG) has a foam-like structure in which the dark wall-like structures are FLG while the lighter domains are the PS. Images of a 0.05 % v/v FLG/PS composite exhibiting this segregated structure are shown in Fig. 3.

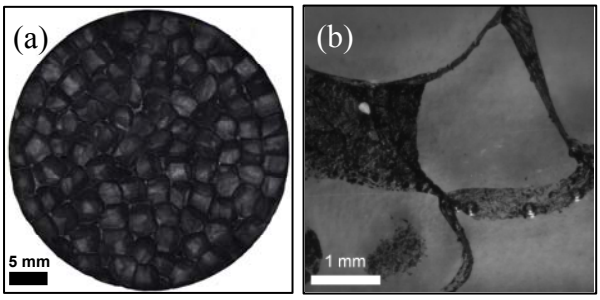

Fig. 3 Optical microscopic images of (a) top surface and (b) cross-section of a 0.05 % v/v FLG/PS composite.

Fig. 4 shows the electrical conductivity as a function of graphene loading. A significant enhancement in electrical conductivity is demonstrated when 0.01 % v/v FLG was added to the PS. Since the boundaries located between the pellets are maintained, the graphene particles become interconnected throughout the material thus causing a significant increase in conductivity while using very low loadings of

graphene. The capillary driven coating process enables more graphene to completely coat the surface of the PS, which in turn increases the electrical conductivity of the composite approximately 4-5 orders of magnitude from 0.01 to 0.3 % v/v.

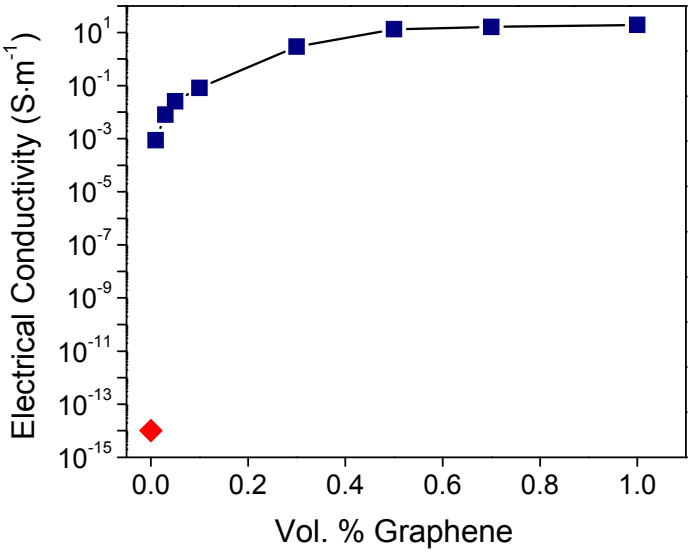

Fig. 4 Electrical conductivity of FLG/PS composite material as a function of graphene content.

A scanning electron microscope (SEM) image showing a section view of a 5 % v/v FLG/PS segregated composite is shown in Fig. 5. It appears that the majority of the graphene particles are oriented along the PS-PS interface. This alignment of the large graphene sheets enables efficient utilization of the high aspect ratio while also allowing for efficient electron transfer between the graphene particles. These micro-scale interactions further contribute to the exceptional conductivity demonstrated at very low loading fractions.

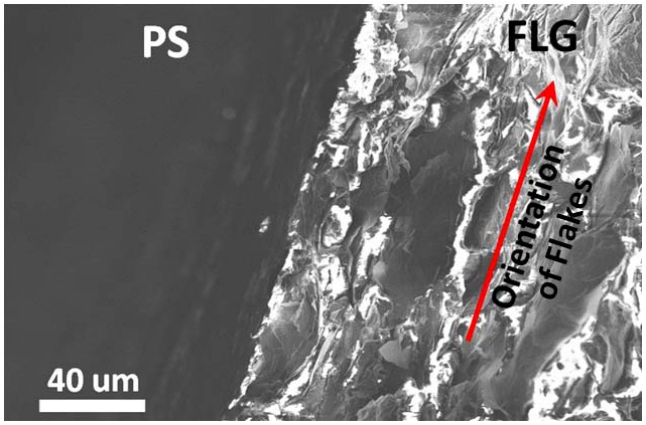

Fig. 5 SEM image of a 5 % v/v FLG/PS segregated composite prepared by the capillary-driven coating process.

4. Conclusions

We demonstrate a simple, inexpensive and commercially viable technique that can be used to disperse conductive sheet-like particles, such as graphene, into a highly organized pattern within polymeric materials on either the micro- or macro-scale. Utilizing capillary interactions between polymeric particles and few-layer graphene particles, liquid bridges on the surface of a polymeric material allows for coating of graphene onto the polymer surfaces. By precisely controlling the temperature and pressure during the melt compression process, highly conductive composites are formed using very low loadings of graphene particles. Applications for such composites could include sensing devices, coloring mechanisms, as well as barrier mechanisms.

Acknowledgements

The authors acknowledge the financial support provided by the Rhode Island Science & Technology Advisory Council as well as Research Experiences for Undergraduates National Science Foundation (CMMI 1233887).

References

[1] Kim H, Abdala A, Macosko C (2010) Graphene/Polymer Nanocomposites, Macromolecules 43: 6515-6530.

[2] Potts J, Dreyer D, Bielawski C, Ruoff R (2011) Graphene-based polymer nanocomposites, Polymer 52: 5-25.

[3] Li B, Zhong WH (2011) Review on polymer/graphite nanoplatelet nanocomposites, J Mater Sci 46: 5595-5614.

[4] Heeder N, Shukla A, Chalivendra V, Yang S, Park K (2012) Electrical Response of Carbon Nanotube Reinforced Nanocomposites under Static and Dynamic Loading, Experimental Mechanics 52: 315-322.

[5] Du J, Zhao L, Zeng Y, Zhang L, Li F, Liu P, Liu C (2011) Comparison of electrical properties between multi-walled carbon nanotube and graphene nanosheet/high density polyethylene composites with a segregated network structure, Carbon 49: 1094-1100.

[6] Mamunya BY (2011) Carbon Nanotubes as Conductive Filler in Segregated Polymer Composites-Electrical Properties. Ed. Yellampalli, S. Rijeka, Intech, Croatia, pp 173-196.

[7] Pang H, Bao Y, Lei J, Tang JH, Ji X, Zhang WQ, Chen C (2012) Segregated Conductive Ultrahigh-Molecular-Weight Polyethylene Composites Containing High-

Density Polyethylene as Carrier Polymer of Graphene Nanosheets, Polymer-Plastics Technology and Engineering 51: 1483-1486.

[8] Hu H, Zhang G, Xiao L, Wang H, Zhang Q, Zhao Z (2012) Preparation and electrical conductivity of graphene/ultrahigh molecular weight polyethylene composites with a segregated structure, Carbon 50: 4596-4599.

CHAPTER 5

FIXED-ANGLE ROTARY SHEAR AS A NEW METHOD FOR TAILORING ELECTRO-MECHANICAL PROPERTIES OF TEMPLATED GRAPHENE-POLYMER COMPOSITES

by

Nicholas Heeder, Abayomi Yussuf, Indrani Chakraborty, Michael P. Godfrin, Robert Hurt, Anubhav Tripathi, Arijit Bose and Arun Shukla

Under preparation for submission to the Journal Composites Science and Technology

Corresponding Author: Arun Shukla

Dynamic Photo Mechanics Laboratory

Department of Mechanical, Industrial and Systems Engineering

University of Rhode Island

206 Wales Hall, 92 Upper College Rd

Kingston, RI, 02881, USA

Phone: +1-401-874-2283

Email Address: shuklaa@egr.uri.edu

Abstract

A capillary-driven particle-level templating technique was utilized to distribute graphite nanoplatelets (GNPs) into specially constructed architectures throughout a polystyrene matrix to form multi-functional composites with tailored electro-mechanical properties. By precisely controlling the temperature and pressure during a melt compression process, highly conductive segregated composites were formed using very low loadings of graphene particles. Since the graphene flakes form a honeycomb percolating network along the boundaries between the polymer matrix particles, the composites show very high electrical conductivity but poor mechanical strength. To improve the mechanical properties, a new processing technique was developed that uses rotary shear through pre-set fixed angles to gradually evolve the honeycomb graphene network into a concentric band structure over the dimensions of the sample. An experimental investigation was conducted to understand the effect of GNP loading as well as rotary shear angle on the mechanical strength and electrical conductivity of the composites. The experimental results show that both the electrical and mechanical properties of the composites are significantly altered using this very simple technique, which allows rational co-optimization of competing mechanical and electrical performance as appropriate for a given target application.

Keywords: Graphene; Polymer; Functional Composites; Segregated Composites, Tailored Composites; Electro-mechanical Properties; Electrical Properties;

1. Introduction

The desire to produce light-weight, multi-functional composites has grown tremendously in recent years. Polymer nanocomposites, in particular, have attracted

significant attention in the past decades with the belief that they could become the next generation high performance materials with multifunctional capabilities [1-12]. Significant research has shown that carbon-based polymer nanocomposites have proven to demonstrate remarkable physical and mechanical properties by incorporating very small amounts of filler material [13-18]. One of the most compelling features of polymer nanocomposites is the ability to create a new class of materials with attributes that come both from the filler and the matrix. Having the ability to manipulate the degree and nature of the dispersion is key to the development of these types of novel composites [19]. Many studies have documented enhancement of properties such as stiffness and strength, thermal stability, electrical and thermal conductivities, dielectric performance and gas barrier properties of polymer composites with the incorporation of fillers [20-25].

Owing to its extraordinary mechanical and physical properties, graphene appears to be a very attractive filler material for the next generation of smart materials in batteries, supercapacitors, fuel cells, photovoltaic devices, sensing platforms and other devices [13, 14]. Although significant research has been performed to develop strategies to effectively incorporate nanoparticles into polymers, ability to control the dispersion and location of graphene-based fillers to fully exploit their intrinsic properties remains a challenge [26-29].

Along with the aspect ratio and the surface-to-volume ratio, the distribution of the filler in a polymer matrix has been shown to directly correlate with its effectiveness in improving material properties such as mechanical strength, electrical and thermal conductivity, and impermeability [19]. The critical content of a filler

material that characterizes a drastic increase in composite properties, such as electrical conductivity, is commonly termed the percolation threshold. From a physical standpoint, the predicted percolation threshold for randomly aligned and uniformly dispersed 2-dimensional sheets such as graphite nanoplatelets (aspect ratio ~ 4000) in a matrix is 0.01 % by volume [15]. Achieving this threshold is difficult, because strong van der Waals interactions between these sheets lead to aggregation, especially in the face-to-face configuration [4, 16, 17]. In addition, most processing techniques, especially at the pilot and commercial scales, result in highly anisotropic flows, which tend to align sheets along the direction of flow and inhibit the formation of a percolating network. Achieving the theoretical percolation limit for scalable techniques has therefore been difficult. Because of the energy demand for removing solvents, and sometimes their potentially hazardous nature, melt processing is often chosen over solvent based mixing of filler and polymer, despite the increased viscosity of a melt. Dispersing high aspect ratio sheets isotropically in a melt of high viscosity is a major challenge.

An alternate method for creating a connected pathway for conductive particles is to make segregated composites. The conductive particles within segregated composites are specially localized on the surfaces of the polymer matrix particles. When consolidated into a monolith, these conductive particles form a percolating three-dimensional network that dramatically increases the conductivity of the composite [30-35]. Sheets do not have to be distributed isotropically throughout a matrix to achieve percolation, overcoming a major limitation. This way of achieving three-dimensional connectivity of the particles also decreases the contact resistance

between the particles [30]. Du et al. [30] prepared multi-walled carbon nanotube (MWCNT)/high density polyethylene (HDPE) and graphene nanosheets (GNS)/HDPE) composites with a segregated network structure by alcohol-assisted dispersion and hot-pressing. The electrical properties of the GNS/HDPE and MWCNT/HDPE composites were compared and it was found that the percolation threshold of the GNS/HDPE composites (1 % v/v) was much higher than that of the MWCNT/HDPE composites (0.15 % v/v) while the MWCNT/HDPE composite showed higher electrical conductivity than the GNS/HDPE composite at the same filler content. They concluded that, due to crimp, rolling and aggregation of the GNSs in the HDPE matrix, the two-dimensional GNSs were not as effective as MWCNTs in forming conductive networks. Later, Hu et al. [32] prepared graphene/polyethylene segregated composites using a two-step process. A combination of sonication and mechanical mixing was used to first coat the ultrahigh molecular weight polyethylene (UHMWPE) with graphene oxide (GO) sheets. The excess solvent was removed from the system and then the coated powders were added to a hydrazine solution and stirred at 95 ºC to reduce the GO to graphene. All coated powders were compressively molded and hot pressed to form composite sheets. This two-step process was shown to effectively prevent aggregation, leading to composites exhibiting high electrical conductivity at a very low percolation threshold (0.028 % v/v). In their previous work, the authors demonstrated a simple, inexpensive and commercially viable technique that can be used to disperse conductive sheet-like particles, such as graphene, into a highly organized pattern within polymeric materials [31]. By utilizing capillary interactions between methanol, polystyrene (PS) particles and few-

layer graphene flakes, highly conductive segregated composites were produced. The conducting pathways provided by the graphene located at the particle surfaces through contact of the bounding surfaces allow percolation at a loading of less than 0.01% by volume.

These studies revealed that highly conductive composites can be created when graphene is segregated into organized networks throughout a matrix material. Although the highly segregated networks provide excellent transport properties throughout the composite, they inevitably result in poor mechanical strength, since fracture can occur easily by delamination along the continuous segregated graphene phase. Since most multi-functional materials are required to provide excellent transport properties while maintaining sufficient mechanical strength, alternative methods of distributing graphene need to be developed. Despite recent progresses on the electrical characterization of graphene-based segregated composites, no results have been published yet regarding the combined electro-mechanical behavior of these highly conductive materials. In this work, a novel capillary-driven, particle-level templating technique was utilized to distribute graphite nanoplatelets (GNPs) into specially constructed architectures throughout a polystyrene (PS) matrix to form multi-functional composites with tailored electro-mechanical properties. By precisely controlling the temperature and pressure during a melt compression process, highly conductive composites were formed using very low loadings of graphene particles. To improve the mechanical properties, a new processing technique was developed that uses rotary shear during the compression molding process to gradually evolve the honeycomb graphene network into a concentric band structure. The rearrangement of

the graphene networks allows for a higher degree of conformation and increased number of interactions between the polymer chains, thus providing increased strength in the polymeric phase. The degree of evolution from the honeycomb to the concentric band structure can be precisely determined by the chosen angle of rotation. Two types of composites, organized and shear-modified, were produced to demonstrate the electro-mechanical tailoring of the composite material. An experimental investigation was conducted to understand the effect of graphene content as well as shearing on the mechanical strength and electrical conductivity of the composites. The experimental results show that both the mechanical and electrical properties of the composites can be altered using a very simple technique and the inherent trade-off between electrical versus mechanical performance can be intelligently optimized for a given application by controlling the pre-set angle of rotary shear. The process of shearing one surface of the specimen at elevated temperature causes melting and smearing of the contact surface, thus improving mechanical strength and slightly compromising electrical conductivity.

2. Materials and specimen preparation

2.1 Material

The graphite nanoplatelets used in this study were xGnP^{TM} Nanoplatelets (XG Sciences, USA). These nanoparticles consist of short stacks of graphene layers having a lateral dimension of ~ 25 μm and a thickness of ~ 6 nm. This thickness corresponds to approximately 18 graphene layers at a typical graphite interlayer spacing. It has been proposed that materials of this thickness (> 10 layers) be referred to as exfoliated graphite, or graphite nanoplatelets for scientific classification [8]. The same materials

are sometimes marketed by suppliers as “graphene nanoplatelets”. The polymeric material chosen for this study was polystyrene (Crystal PS 1300, average molecular weight of 121,000 g/mol) purchased from Styrolution, USA. The PS pellets used were elliptical prisms with an average diameter of 2.76 mm and a length of 3.21 mm.

2.2 Particle Templated Composites

A two-step process was utilized to produce the GNP/PS segregated composites [9]. For composites consisting of less than 0.2 % v/v, the desired amount of graphene platelets were measured and added directly to 7 g of dry PS pellets. The GNP spontaneously adheres to the dry polymer particles by physical forces, which may be van der Waals forces or electrostatic attraction associated with surface charges. This coating process works well for GNP loadings below 0.2 % v/v. However, at higher GNP loadings, this dry method leaves behind excess GNP because the charge on the pellets is neutralized after the initial coating.

To provide a means of temporarily attaching larger quantities of the GNP to the surface of the PS, an additional step is implemented during the fabrication procedure as shown in Fig. 1. For GNP loadings greater than 0.2 % v/v, the PS is first soaked in a methanol bath. The excess methanol is drained from the PS pellets. GNP is added, and the mixture is then shaken vigorously, creating a dense coating of graphene on each PS pellet. The methanol temporarily moistens the polymer pellets forming small liquid bridges between the GNP and the pellet surface. The capillary pressure created through these bridges allows the GNPs to stick easily to the surface of the pellets. During the subsequent hot melt pressing, the temperature and mold pressure are precisely controlled allowing the pellets to be consolidated into a

monolith while maintaining boundaries. The methanol evaporates during the molding cycle. In our experiments, a stainless steel mold consisting of a lower base and a plunger was heated to 125 ºC. The graphene flakes coated PS was placed inside the cavity of the lower base and the plunger was placed on top. The temperature of both the plunger and the base mold was maintained for 20 min at which point it was hot-pressed at 45 kN using a hydraulic press. By precisely controlling the temperature and pressure during a melt compression process, highly conductive composites were formed. This method of distributing graphene within a matrix overcomes the need to disperse the sheet-like conducting fillers isotropically within the polymer, and can be scaled up easily.

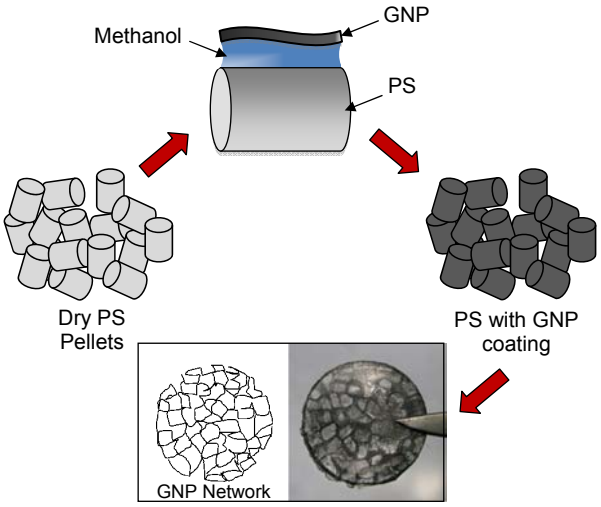

Fig. 1. Capillary-driven particle-level templating technique used to fabricate highly conductive GNP/PS composites.

2.3 Particle Templated Composites with Shear Manipulation

Modified particle-templated composites were fabricated by incorporating a shearing technique during the melt compression process. Following the same coating

process as discussed earlier, the graphene coated pellets were placed inside a modified steel mold, which was equipped with guide pins to ensure that the base remained stationary. The plunger was then placed on top of the material and heated to 160 ºC while the lower base mold was heated to 125 ºC and maintained for 20 min. Next, 20 MPa was applied to the plunger and then rotated to various predetermined angles. Once the desired rotation was achieved, 45 MPa was applied and held for 5 minutes. All shear-modified composites were fabricated with 0.3 % v/v graphene platelets. A schematic of the compression molding process used to produce both types of segregated composites is shown in Fig. 2(a) and Fig.2(b). By applying such a strain in the azimuthal direction on the top surface of the material, as shown in Fig 2(b), a gradient of graphene organization/orientation in the axial direction is formed which results in a composite possessing unique properties.

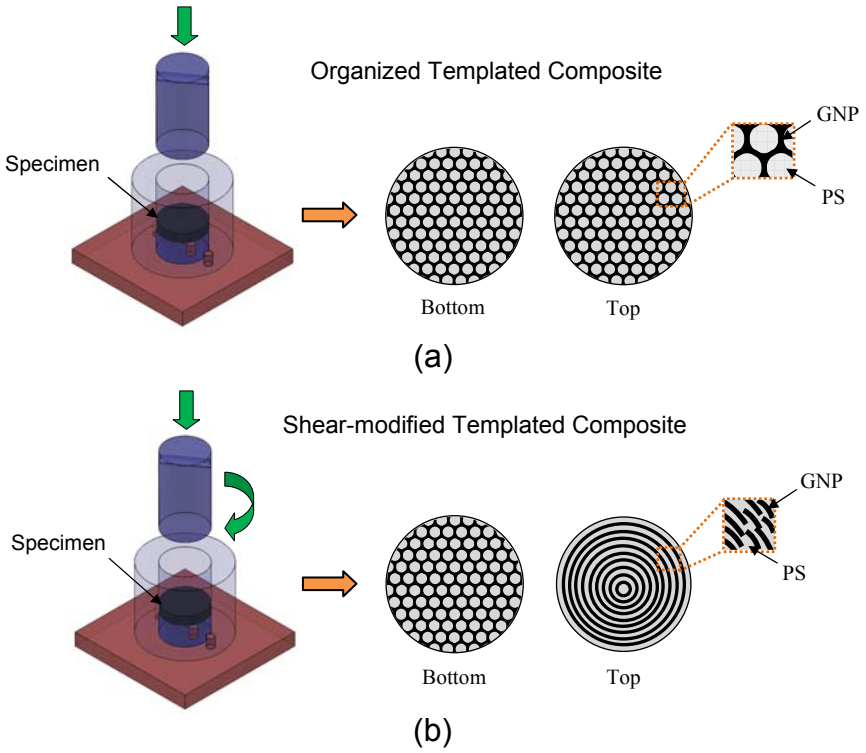

Fig. 2. Schematic of compression molding process to produce (a) organized templated composites and (b) shear-modified templated composites

3. Experimental Procedure

3.1 Electrical Characterization

Electrical conductivity measurements were made on the GNP/PS composites using a volumetric two-point probe measurement technique. The bulk electrical conductivity was measured across the thickness of the sample (perpendicular to pressing). The resistance of the material was experimentally determined by supplying a constant current, ranging from 5 nA to 1 mA, through the specimen while simultaneously measuring the voltage drop across the specimen. A constant current source (Keithley Instruments Model 6221) was used to supply the DC current while two electrometers (Keithley Instruments Model 6514) were used to measure the

voltage drop. The difference between the two voltage readings was measured using a digital multimeter (Keithley Instruments Model 2000 DMM).

3.2 Mechanical Characterization

A series of 3 point bend experiments were carried out to investigate the influence of graphene content on the flexural properties of the composites. A screw-driven testing machine (Instron 3345) was implemented to load the specimens in a three point bending configuration. Specimens were cut into 5 x 6 x 38 mm rectangular prisms. A support span of 30 mm was used and the loading was applied at a rate of 0.1 mm/min.

4. Experimental Results & Discussion

4.1 Particle Templated Composites

As seen in Fig. 1, the composite (with 0.3 % v/v GNP) has a foam-like or honeycomb-like structure in which the dark wall-like structures are GNP while the lighter domains are the PS. Images of a 0.05 % v/v GNP/PS composite exhibiting this segregated structure are shown in Fig. 3.

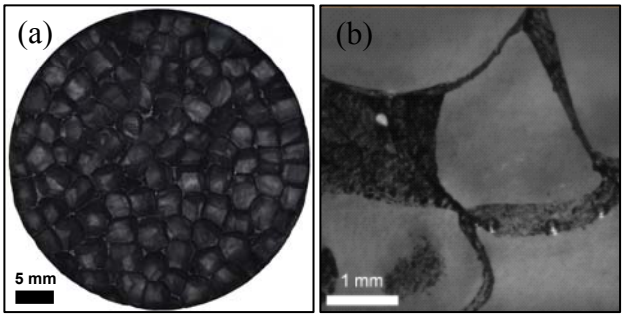

Fig. 3. Optical microscopic images of (a) top surface and (b) cross-section of a 0.05 % v/v GNP/PS composite.

Fig. 4 shows the electrical conductivity as a function of graphene loading. A significant enhancement in electrical conductivity is demonstrated when 0.01 % v/v

GNP was added to the PS. Since the boundaries located between the pellets are maintained, the graphene particles become interconnected throughout the material thus causing a significant increase in conductivity while using very low loadings of graphene. The capillary driven coating process enables more graphene to completely coat the surface of the PS which in turn increases the electrical conductivity of the composite approximately 4-5 orders of magnitude from 0.01 to 0.3 % v/v.

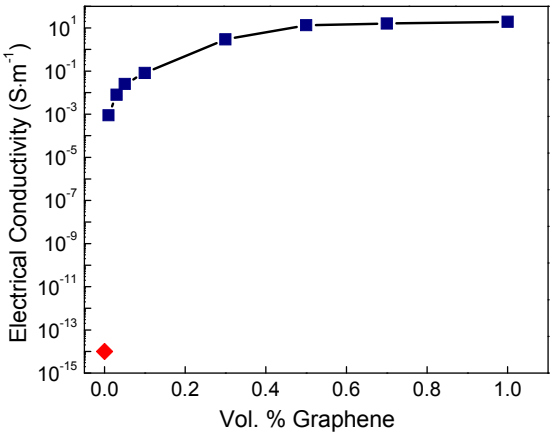

Fig. 4. Electrical conductivity of GNP/polystyrene composite material with organized segregation as a function of graphene content.

A scanning electron microscope (SEM) image showing a section view of a 5 % v/v GNP/PS segregated composite is shown in Fig. 5. It appears that the majority of the GNP flakes are oriented along the PS-PS interface. This alignment of the large graphene sheets enables efficient utilization of the high aspect ratio while also allowing for efficient electron transfer between the graphene particles. These micro-scale interactions further contribute to the exceptional conductivity demonstrated at very low loading fractions.

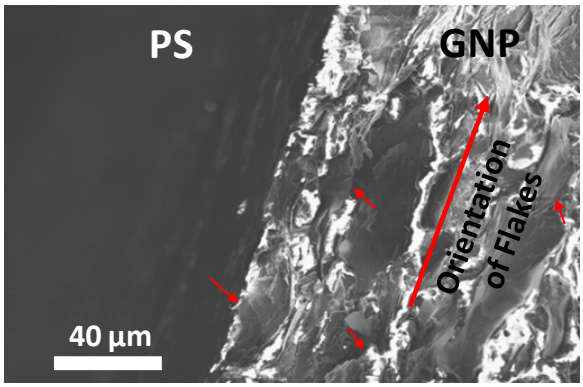

Fig. 5. SEM image of a 5 % v/v GNP/PS segregated composite prepared by the capillary-driven coating process.

While the segregation of the GNPs imparts exceptional transport capabilities, there is an inherent loss in the mechanical strength because of easy fracture by delamination along the continuous graphene honeycomb network. Fig. 6 shows the flexural behavior of the organized GNP/PS composites as a function of graphene loading. Specimens were loaded in two different configurations, parallel and perpendicular to the melt compression, to fully characterize the material in bending. For both loading cases, the flexural strength of the resulting composite decreased significantly with the introduction of GNPs. Since the temperature of the material prior to pressing is maintained at a temperature slightly below the melting temperature of the PS, the interaction between the styrene chains is limited. The GNPs, located at the interfaces of the PS pellets, further inhibit complete tangling of the polymer chains during the melt compression process thus diminishing the flexural strength of the composite. As shown in Fig. 6, the composites also demonstrate anisotropic behavior. This anisotropy of mechanical strength is believed to be a consequence of the melt compression process. Since the softened PS pellets are compressed along the loading

direction during the melt compression process, the PS pellets become elongated in the plane perpendicular to compression. The elongation of the PS pellets in turn causes a directional dependence on the flexural strength of the composite when subjected to bending.

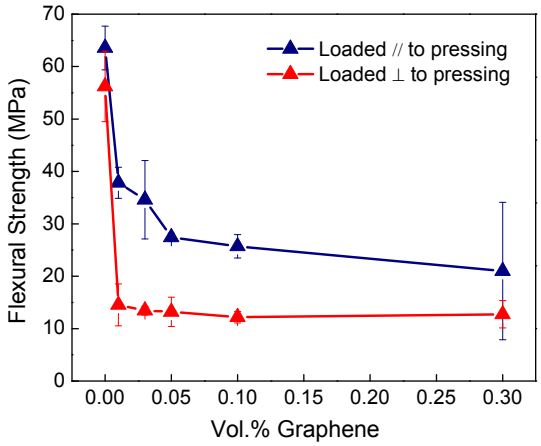

Fig. 6. Effect of graphene content on flexural strength of GNP/PS organized particle templated composites.

The coupled electro-mechanical behavior of the GNP-PS organized particle templated composite, when loaded parallel to the pressing direction, is shown in Fig. 7. The flexural strength and electrical conductivity is normalized with respect to the flexural strength (σ_0) and electrical conductivity (κ_0) of the pristine PS particle templated composite (0 % v/v GNP), respectively. It can be seen that the highly segregated GNP network, although very efficient for electron transfer, causes a significant decrease in flexural strength. While the conducting pathways provided by the graphene, located at the particle interfaces of the PS, allow percolation at a graphene loading less than 0.01 % v/v GNP, they also cause the flexural strength of the composite to decrease by ~ 40 %. As the GNP loading is further increased, the

electrical efficiency of the networks continues to increase while the flexural strength is decreased.

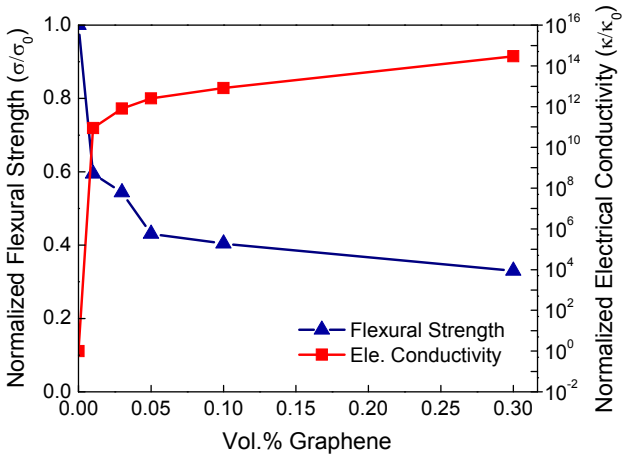

Fig. 7. Electro-mechanical behavior of GNP/PS organized particle templated composites loaded parallel to pressing.

4.2 Shear-modified Particle Templated Composites

Images of a 0.3 % v/v GNP/PS shear modified specimen exhibiting a graphene network that is functionally graded in the axial direction is shown in Fig. 8. The top surface of the composite exhibits a chaotic and disorganized pattern of GNP while the bottom maintains a highly organized segregated structure of GNP.

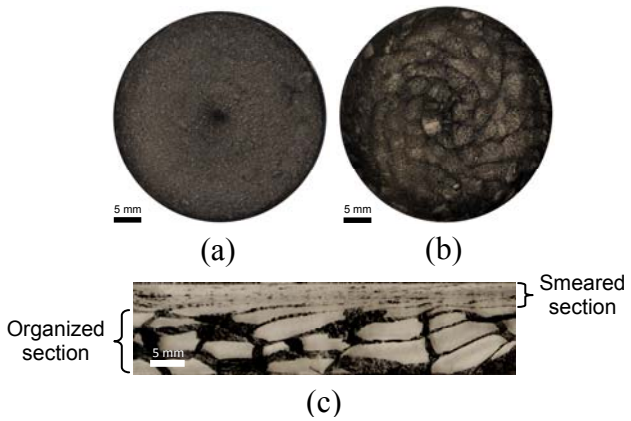

Fig. 8. Optical microscopic images of (a) top smeared surface, (b) bottom organized surface and (c) cross-section of a 0.3 % v/v GNP/PS shear modified composite showing the extent of

The effect of azimuthal strain on the top surface on the electrical conductivity of the shear-modified GNP/PS composite is shown in Fig. 9. The electrical conductivity decreased from ~ 3 $S \cdot m^{-1}$ to ~ $4x10^{-2}$ $S \cdot m^{-1}$ when the plunger was rotated 90° during the compression process. Although, the electrical conductivity decreased by two orders of magnitude, the value of $4x10^{-2}$ $S \cdot m^{-1}$ is still very high and acceptable for many applications. The decrease in electrical conductivity can be attributed to the partial disruption of the GNP networks within the polymer, as shown in Fig. 8 (c). Further rotation of the plunger resulted in only a slight decrease in conductivity.

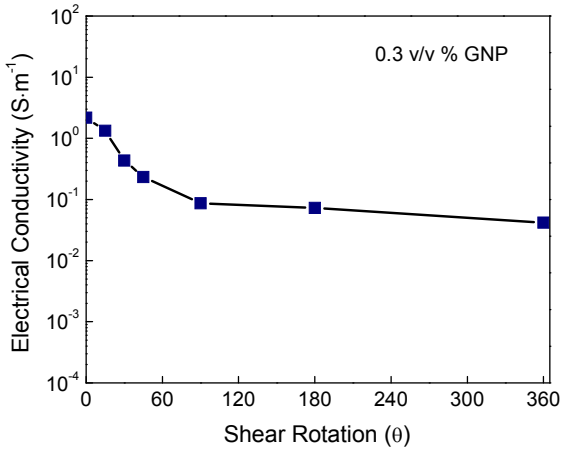

Fig. 9. Electrical conductivity of GNP/PS composite with a shear-modified segregated structure as a function of rotation angle.

Figure 10 shows the electro-mechanical behavior of the shear-modified GNP/PS composites as a function of shear rotation. The flexural strength and electrical conductivity are normalized with respect to the flexural strength (σ_s) and electrical conductivity (κ_s) of the particle templated composite with no shear rotation (0.3 % v/v GNP), respectively. The capillary driven coating process enabled an increase in electrical conductivity of the composite by approximately 14 - 15 orders of magnitude as compared to the pristine PS, owing to the dense coating of GNP on the PS pellets. By applying a shear force to the top surface of the highly segregated material, a gradient of graphene organization/orientation along the sample axis is formed which results in a 600 % increase in flexural strength while only sacrificing ~ 1 - 2 orders of magnitude of conductivity. To further tune the properties of the composite, the extent of disorganization of the GNPs can be controlled by adjusting the preload and/or temperature of the piston during melt compression. This simple, yet commercially viable technique allows for the alteration of both physical and

mechanical properties of composite materials and therefore can be used to intelligently optimize materials for specific target applications.

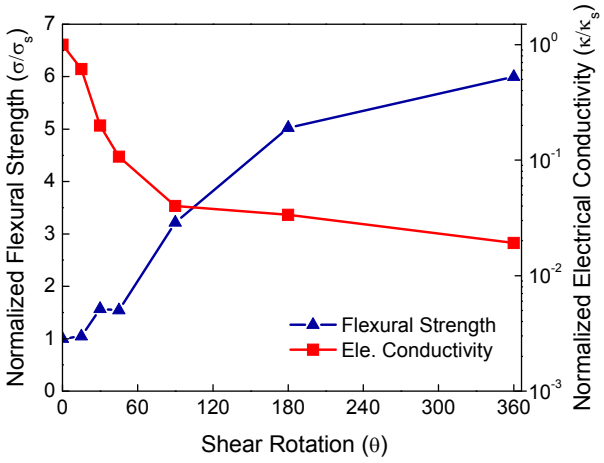

Fig. 10. Electro-mechanical behavior of the shear-modified GNP/PS particle templated composites loaded parallel to pressing.

5. Summary

We demonstrate a simple, inexpensive, and commercially viable technique that can be used to disperse conductive 2D (sheet-like) materials, such as graphene, into specifically constructed hybrid architectures within polymeric materials on either the micro- or macro-scale. Utilizing capillary interactions between polymeric particles and few-layer graphene particles, liquid bridges on the surface of the polymeric material allows for the coating of graphene onto the polymer surfaces. By precisely controlling the temperature and pressure during the melt compression process, highly conductive composites are formed using very low loadings of graphene particles. Since the graphene particles are localized at the boundaries between the polymer matrix particles, the composite exhibited poor mechanical strength. To improve the mechanical properties of the composite, a controlled amount of rotary shear was

applied to the top surface of the material to create a Z-directional gradient of graphene organization/orientation along the sample axis. Results showed that this novel fabrication technique can produce composite materials that possess both excellent transport properties and improved mechanical strength. Furthermore, the properties of the composite can be altered using this very simple technique and the inherent trade-off between electrical and mechanical performance can be optimized for a given application by controlling the pre-set angle of rotary shear.

Acknowledgements

The authors acknowledge the financial support provided by the Rhode Island Science & Technology Advisory Council as well as National Science Foundation (CMMI 1233887) Research Experiences for Undergraduates.

References

[1] Ajayan PM, Tour JM. Materials Science: Nanotube composites. Nature. 2007;447(7148).

[2] Fim FdC, Guterres JM, Basso NRS, Galland GB. Polyethylene/graphite nanocomposites obtained by in situ polymerization. Journal of Polymer Science Part A: Polymer Chemistry. 2009;48(3):692-698.

[3] Heeder N, Shukla A, Chalivendra V, Yang S. Sensitivity and dynamic electrical response of CNT-reinforced nanocomposites. Journal of Materials Science. 2012;47(8):3808-3816.

[4] Heeder NJ, Shukla A, Chalivendra V, Yang S, Park K. Electrical Response of Carbon Nanotube Reinforced Nanocomposites Under Static and Dynamic Loading. Experimental Mechanics. 2012;52(3):315-322.

[5] Li J, Kim J-K, Lung Sham M. Conductive graphite nanoplatelet/epoxy nanocomposites: Effects of exfoliation and UV/ozone treatment of graphite. Scripta Materialia. 2005;53(2):235-240.

[6] Pramoda KP, Hussain H, Koh HM, Tan HR, He CB. Covalent bonded polymer–graphene nanocomposites. Journal of Polymer Science Part A: Polymer Chemistry. 2010;48(19):4262-4267.

[7] Verdejo R, Bernal MM, Romasanta LJ, Lopez-Manchado MA. Graphene filled polymer nanocomposites. Journal of Materials Chemistry. 2010
21(10):3301-3310.

[8] Viculis LM, Mack JJ, Mayer OM, Hahn HT, Kaner RB. Intercalation and exfoliation routes to graphite nanoplatelets. Journal of Materials Chemistry. 2005;15(9):974-978.

[9] Wang L, Hong J, Chen G. Comparison study of graphite nanosheets and carbon black as fillers for high density polyethylene. Polymer Engineering & Science. 2010;50(11):2176-2181.

[10] Cardoso SM, Chalivendra VB, Shukla A, Yang S. Damage detection of rubber toughened nanocomposites in the fracture process zone using carbon nanotubes. Engineering Fracture Mechanics. 2012;96(0):380-391.

[11] Vadlamani VK, Chalivendra V, Shukla A, Yang S. In situ sensing of non-linear deformation and damage in epoxy particulate composites. Smart Materials and Structures. 2012;21(7).

[12] Vadlamani VK, Chalivendra VB, Shukla A, Yang S. Sensing of damage in carbon nanotubes and carbon black-embedded epoxy under tensile loading. Polymer Composites. 2012;33(10):1809-1815.

[13] Chakrabarti MH, Low CTJ, Brandon NP, Yufit V, Hashim MA, Irfan MF, et al. Progress in the electrochemical modification of graphene-based materials and their applications. Electrochimica Acta. 2013;107(0):425-440.

[14] Huang X, Qi X, Boey F, Zhang H. Graphene-based composites. Chemical Society Reviews. 2011;41(2):666-686.

[15] Kim H, Abdala AA, Macosko CW. Graphene/Polymer Nanocomposites. Macromolecules. 2010;43(16):6515-6530.

[16] Li B, Zhong W-H. Review on polymer/graphite nanoplatelet nanocomposites. Journal of Materials Science. 2011;46(17):5595-5614.

[17] Potts JR, Dreyer DR, Bielawski CW, Ruoff RS. Graphene-based polymer nanocomposites. Polymer. 2011;52(1):5-25.

[18] Singh V, Joung D, Zhai L, Das S, Khondaker SI, Seal S. Graphene based materials: Past, present and future. Progress in Materials Science. 2011;56(8):1178-1271.

[19] Stankovich S, Dikin DA, Dommett GHB, Kohlhaas KM, Zimney EJ, Stach EA, et al. Graphene-based composite materials. Nature. 2006;442(7100):282-286.

[20] Jordan J, Jacob KI, Tannenbaum R, Sharaf MA, Jasiuk I. Experimental trends in polymer nanocomposites - a review. Materials Science and Engineering: A. 2005;393(1-2):1-11.

[21] Kalaitzidou K, Fukushima H, Drzal LT. Multifunctional polypropylene composites produced by incorporation of exfoliated graphite nanoplatelets. Carbon. 2007;45(7):1446-1452.

[22] Lu M-D, Yang S-M. Syntheses of polythiophene and titania nanotube composites. Synthetic Metals. 2005;154(1-3):73-76.

[23] Peng H. Aligned Carbon Nanotube/Polymer Composite Films with Robust Flexibility, High Transparency, and Excellent Conductivity. Journal of the American Chemical Society. 2007;130(1):42-43.

[24] Tang Q-Y, Chan Y-C, Wong N-B, Cheung R. Surfactant-assisted processing of polyimide/multiwall carbon nanotube nanocomposites for microelectronics applications. Polymer International. 2010;59(9):1240-1245.

[25] Tibbetts GG, Lake ML, Strong KL, Rice BP. A review of the fabrication and properties of vapor-grown carbon nanofiber/polymer composites. Composites Science and Technology. 2007;67(7-8):1709-1718.

[26] Herrera-Alonso M, Abdala AA, McAllister MJ, Aksay IA, Prud'homme RK. Intercalation and Stitching of Graphite Oxide with Diaminoalkanes. Langmuir. 2007;23(21):10644-10649.

[27] Paredes JI, Villar-Rodil S, MartiÌ nez-Alonso A, TascoÌ n JMD. Graphene Oxide Dispersions in Organic Solvents. Langmuir. 2008;24(19):10560-10564.

[28] Stankovich S, Dikin DA, Piner RD, Kohlhaas KA, Kleinhammes A, Jia Y, et al. Synthesis of graphene-based nanosheets via chemical reduction of exfoliated graphite oxide. Carbon. 2007;45(7):1558-1565.

[29] Stankovich S, Piner RD, Chen X, Wu N, Nguyen ST, Ruoff RS. Stable aqueous dispersions of graphitic nanoplatelets via the reduction of exfoliated graphite oxide in the presence of poly(sodium 4-styrenesulfonate). Journal of Materials Chemistry. 2006;16(2):155-158.

[30] Du J, Zhao L, Zeng Y, Zhang L, Li F, Liu P, et al. Comparison of electrical properties between multi-walled carbon nanotube and graphene nanosheet/high density polyethylene composites with a segregated network structure. Carbon. 2011;49(4):1094-1100.

[31] Heeder N, Yussuf A, Guo F, Chakraborty I, Godfrin M, Hurt R, et al. Highly conductive graphene-based segregated composites prepared by particle templating. Journal of Materials Science. 2013;49(6):2567-2570.

[32] Hu H, Zhang G, Xiao L, Wang H, Zhang Q, Zhao Z. Preparation and electrical conductivity of graphene/ultrahigh molecular weight polyethylene composites with a segregated structure. Carbon. 2012;50(12):4596-4599.

[33] Mamunya Y. Carbon Nanotubes as Conductive Filler in Segregated Polymer Composites - Electrical Properties. In: Yellampalli DS, editor. Carbon Nanotubes-Polymer Nanocomposites: InTech; 2011.

[34] Pang H, Bao Y, Lei J, Tang J-H, Ji X, Zhang W-Q, et al. Segregated Conductive Ultrahigh-Molecular-Weight Polyethylene Composites Containing High-Density Polyethylene as Carrier Polymer of Graphene Nanosheets. Polymer-Plastics Technology and Engineering. 2012;51(14):1483-1486.

[35] Wang B, Li H, Li L, Chen P, Wang Z, Gu Q. Electrostatic adsorption method for preparing electrically conducting ultrahigh molecular weight polyethylene/graphene

nanosheets composites with a segregated network. Composites Science and Technology. 2013;89(0):180-185.

[36] Bianco A, Cheng H-M, Enoki T, Gogotsi Y, Hurt RH, Koratkar N, et al. All in the graphene family - A recommended nomenclature for two-dimensional carbon materials. Carbon. 2013;65(0):1-6.

CHAPTER 6

FLEXIBLE GRAPHENE-POLYMER COMPOSITES WITH TUNABLE PROPERTIES

by

Nicholas Heeder, Abayomi Yussuf, Arijit Bose and Arun Shukla

Under preparation for submission to the Journal Composites Science and Technology

Corresponding Author: Arun Shukla

Dynamic Photo Mechanics Laboratory

Department of Mechanical, Industrial and Systems Engineering

University of Rhode Island

206 Wales Hall, 92 Upper College Rd

Kingston, RI, 02881, USA

Phone: +1-401-874-2283

Email Address: shuklaa@egr.uri.edu

Abstract

Flexible multi-functional composites with tailored electro-mechanical properties were produced using a capillary-driven particle-level templating technique. A fixed-angle rotary shear technique was utilized during the melt compression process to distribute graphite nanoplatelets (GNPs) into specially constructed architectures throughout a styrene-butadiene matrix. An experimental investigation was conducted to understand the effect of GNP loading as well as rotary shear angle on the mechanical strength and electrical conductivity of the composites. The experimental results show that this simple technique can be used to produce flexible composites that possess exceptional conductivity while still maintaining the salient mechanical characteristics the copolymer has to offer.

Keywords: graphene, polymer, flexible composites, segregated composites, tailored composites, electro-mechanical properties, electrical properties, mechanical properties

1. Introduction

Advancements in technology have and continue to drive the evolution of composite materials, making them lighter, stronger and more advanced for use in a vast range of industries [1-3]. In recent decades, polymer nanocomposites have shown tremendous potential in becoming the next generation high performance materials that provide multifunctional capabilities [4-10].

Significant research has shown that, in particular, carbon-based nanocomposites have proven to demonstrate remarkable physical and mechanical properties by incorporating very small amounts of filler material [11-23]. One of the most compelling attributes of polymer nanocomposites is the ability to create a new

class of materials with properties that come both from the filler and the matrix. Having the ability to manipulate the degree and nature of the dispersion is key to the development of these types of novel composites [24]. Many studies have documented enhancement of properties such as stiffness and strength, thermal stability, electrical and thermal conductivities, dielectric performance and gas barrier properties of polymer composites with the incorporation of fillers [25-30].

Although significant research has been performed to develop strategies to effectively incorporate nano-particles into polymers, most techniques rely on solvent based mixing of filler and polymer to disperse particles at the micro- and nano-scale. Due to high cost and the potentially hazardous nature of solvents, such techniques fail to be commercially viable and therefore limit the implementation of this novel technology into many of the potential applications. Despite recent progresses in the development of more advanced polymer composites by graphene reinforcement, a very limited number of commercially viable fabrication techniques have shown efficient incorporation of graphene-based materials into host polymers [31].

As one of the most important thermoplastic elastomers (TPE), styrene/butadiene/styrene block copolymer (SBS) merges good balance of mechanical property along with favorable processability and recyclability, which can be used in various fields, such as modifiers and adhesives [32]. Moreover, SBS can serve as a host polymer with high flexibility to accommodate various conductive fillers to produce electrically conductive composites [33]. SBS electroconductive composites have been successfully prepared using multi-walled carbon nanotubes (MWCNTs) [34], carbon black [35], as well as graphene [32, 36]. Although significant research

has been conducted in producing flexible electroconductive materials, the fabrication techniques used still rely on the use of solvents, thus preventing these types of composites from being manufactured on the commercial scale.

In their previous work [37, 38], the authors developed a simple, inexpensive, and commercially viable technique to effectively disperse conductive 2D (sheet like) materials, such as graphene, into specifically constructed hybrid architectures within polymeric materials. To demonstrate this novel fabrication process, graphite nanoplatelets (GNPs) were distributed into a polystyrene (PS) matrix. Results showed that by applying a fixed angle rotary shear to the material during a melt compression process, a PS/GNP composite that possessed both excellent electrical conductivity and improved flexural strength was produced. Moreover, the properties of the composite can be intelligently optimized for a given application through inherent trade-off between electrical vs. mechanical performance by controlling the pre-set angle of rotary shear. To further this investigation, the fixed-angle rotary shear technique was used to produce flexible composites that exhibit enhanced electro-mechanical behavior. This study experimentally investigates the effect of GNP loading as well as the fixed angle rotary shear on the coupled electro-mechanical behavior of these novel flexible composites when subjected to tensile loading. The experimental results show that the fixed-angle rotary shear technique can be used to produce highly flexible composites that possess exceptional conductivity while still maintaining the salient mechanical characteristics the copolymer has to offer.

2. Experimental Details

2.1 Material

The graphite nanoplatelets used in this study were xGnP^{TM} Nanoplatelets (XG Sciences, USA). These nanoplatelets consist of short stacks of graphene layers having a lateral dimension of ~ 25 μm and a thickness of ~ 6 nm. This thickness corresponds to approximately 18 graphene layers at a typical graphite interlayer spacing. It has been proposed that materials of this thickness (> 10 layers) be referred to as exfoliated graphite, or graphite nanoplatelets [39] for scientific classification. These same materials are sometimes marketed by suppliers as "graphene nanoplatelets". The polymeric material chosen for this study was a styrene/butadiene thermoplastic elastomer (Asaprene T-439) acquired from Asahi Kasei Chemical Corp., Japan. The copolymer contains a total polystyrene weight fraction of 0.45 and came in pellet form (~ 3 mm in diameter).

2.2 Preparation of SBS-GNP Templated Composites

The SBS-GNP templated composites were prepared using the fixed-angle rotary shear technique [37, 38]. This technique, shown in Fig. 1, consists of utilizing capillary interactions between the conductive filler material, such as graphene, and a polymeric material. In this case, the technique is adapted to temporarily attach GNP to the surfaces of the SBS pellets during the melt compression process.

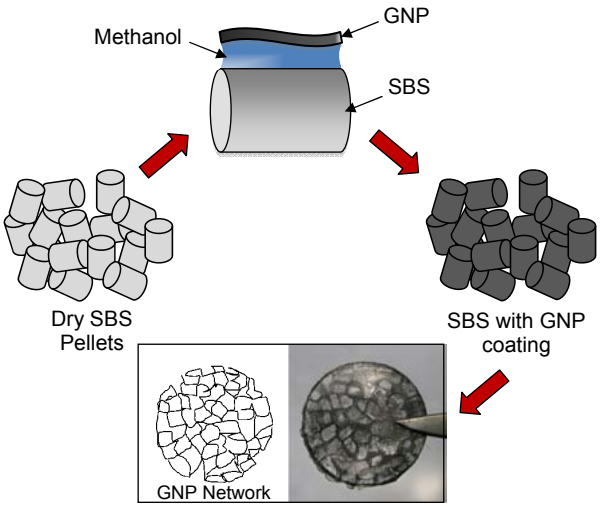

Fig. 1. Capillary-driven particle-level templating technique used to fabricate highly conductive GNP/SBS composites.

The GNP coated SBS pellets were placed into a stainless steel mold consisting of a lower base and a plunger was heated to 140 ºC. The mold was equipped with guide pins to ensure that the base remained stationary. The plunger was then placed on top of the material and heated to 160 ºC and both temperatures were maintained for 20 min. For GNP/SBS composites exhibiting a fully organized segregation of GNP, the material was hot-pressed at 45 kN using a hydraulic press. For GNP/SBS composites exhibiting a functionally graded organization of GNP, the coated pellets were placed inside the mold cavity and pressed to 5 metric tons and rotated to various predetermined angles. Once the desired rotation was achieved, the composite was pressed to 10 metric tons and held for 5 minutes. Finally, the mold is placed into a cooling bath. By applying such a strain in the azimuthal direction on the top surface of the material, a gradient of graphene organization/orientation in the axial direction is formed which results in a composite possessing unique properties. A schematic of the

compression molding process used to produce both types of segregated composites is shown in Fig. 2.

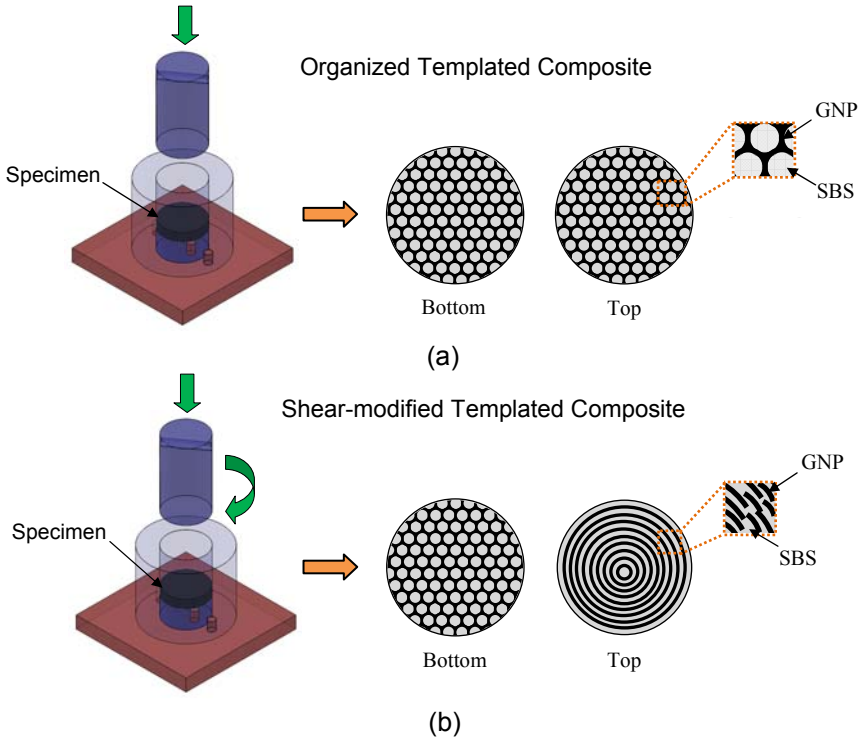

Fig. 2 Schematic of compression molding process to produce (a) organized templated composites and (b) shear-modified templated composites

2.3 Electrical Characterization of SBS/GNP Templated Composites

Electrical conductivity measurements were made on the GNP/PS composites using a volumetric two-point probe measurement technique. The bulk electrical conductivity was measured across the thickness of the sample (perpendicular to pressing). The resistance of the material was experimentally determined by supplying a constant current, ranging from 5 nA to 1 mA, through the specimen while simultaneously measuring the voltage drop across the specimen. A constant current source (Keithley Instruments Model 6221) was used to supply the DC current while

two electrometers (Keithley Instruments Model 6514) were used to measure the voltage drop. The difference between the two voltage readings was measured using a digital multimeter (Keithley Instruments Model 2000 DMM).

2.4 Mechanical Characterization of SBS/GNP Templated Composites

A series of uniaxial tensile experiments were carried out to investigate the influence of graphene content on the tensile properties of the composites. A screw-driven testing machine (Instron 3366) was utilized to load the specimens in uniaxial tension. Specimens were cut into 40 x 12 x 5 mm rectangular prisms and the loading was applied at a rate of 50 mm/min.

3. Experimental Results & Discussion

As seen in Fig. 3, the composite (with 0.3 % v/v GNP) has a foam-like structure in which the dark wall-like structures are GNPs while the lighter domains are the SBS.

Fig. 3 0.3 % v/v GNP/SBS particle template composite with organized GNP structure

3.1 Organized SBS/GNP Templated Composites

Figure 4 shows the electrical conductivity of the GNP/SBS composite with an organized segregated network as a function of graphene loading. A significant enhancement in electrical conductivity is demonstrated when 0.15 % v/v GNP was added to the SBS. Since the boundaries located between the pellets are maintained, the graphene particles become interconnected throughout the material thus causing a significant increase in conductivity. Compared to pristine SBS, the electrical conductivity is increased ~ 9 orders of magnitude with the addition of only 0.15 % v/v. The percolation threshold observed is comparable to the percolation achieved using RGO/HO-SBS [24]. It is important to note that no harsh solvents were needed to fabricate the particle template composites, while still achieving comparable conductivities. Additionally, the melt compression process can easily be scaled up for future commercial application where a solution blending approach cannot.

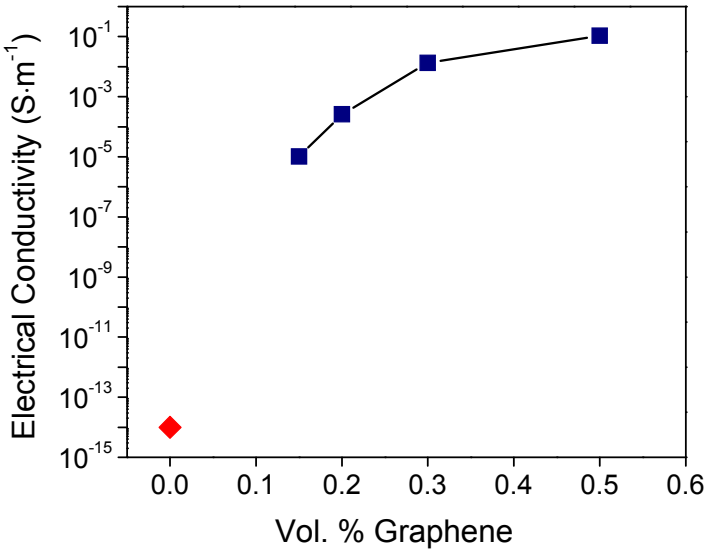

Fig. 4 Electrical conductivity of GNP/SBS composite material as a function of graphene content

While the segregation of the GNPs impart exceptional transport capabilities, there is an inherent loss in mechanical properties because of easy fracture by delamination along the continuous graphene honeycomb network. Fig. 5 shows the tensile behavior of the organized GNP/SBS composites as a function of graphene loading. The elongation at break (EB) of the resulting composites decreased significantly with the introduction of GNP. Since the GNPs reside only at the boundaries of the SBS pellets, limited interaction among the elastomeric pellets occur during the melt compression process. The GNPs inhibit complete tangling of the polymer chains during the melt compression process thus diminishing the tensile properties of the composite.

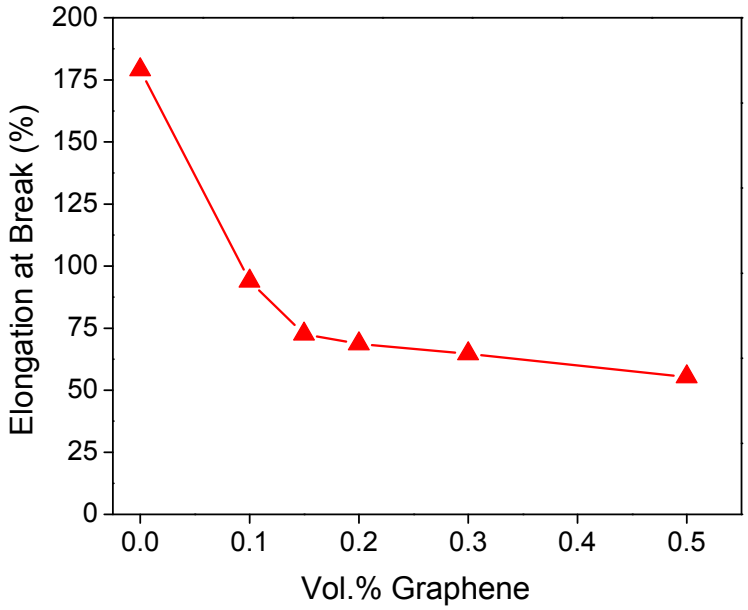

Fig. 5 Effect of GNP content on elongation at break of GNP/SBS particle template composites

The normalized electro-mechanical behavior of the organized GNP/SBS material is shown in Fig. 6. It can be seen that the highly segregated GNP network, although efficient for electron transfer, causes a significant decrease in elongation at

break. While the conducting pathways provided by the graphene, located at the pellet interfaces of the SBS, allow percolation at the graphene loading less than 0.15 % v/v GNP, they also cause the total elongation achieved by the composite to decrease ~ 48 %. As the GNP loading is further increased, the electrical efficiency of the networks continues to increase while the maximum elongation is decreased.

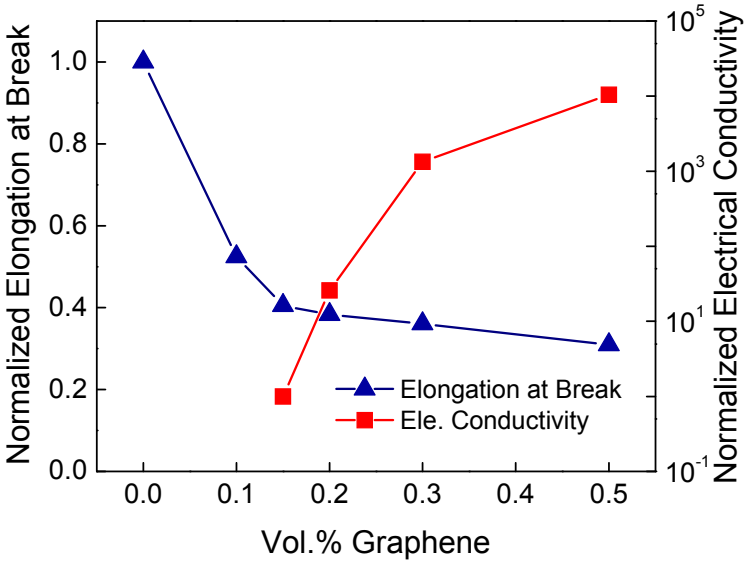

Fig. 6 Electro-mechanical behavior of the organized GNP/SBS template composites loaded parallel to pressing.

3.2 Shear-modified SBS/GNP Templated Composites

The effect of azimuthal strain on the top surface on the electrical conductivity of the shear-modified GNP/SBS composite is shown in Fig. 7. The electrical conductivity decreased from ~ 2 $S \cdot m^{-1}$ to ~ $2x10^{-2}$ $S \cdot m^{-1}$ when the plunger was rotated 15° during the compression process. The decrease in electrical conductivity can be attributed to the partial disruption of the GNP networks within the polymer. Further rotation of the plunger resulted in only a slight decrease in conductivity (~ 2-3 orders of magnitude).

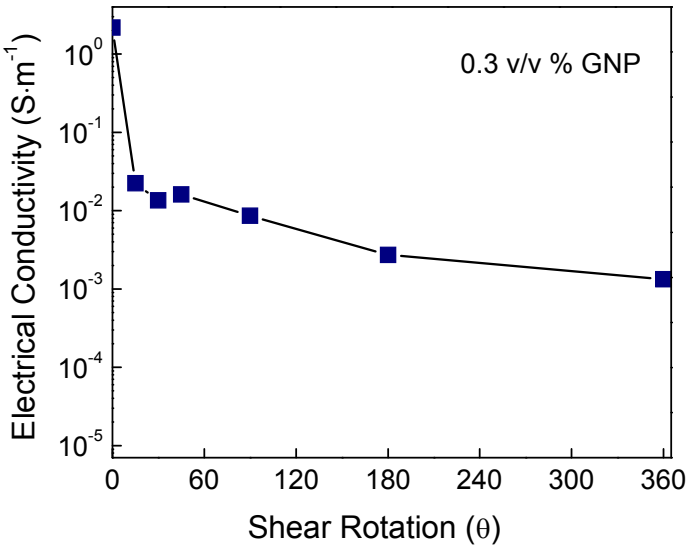

Fig. 7 Electrical conductivity of GNP/SBS composite with a shear-modified segregated structure as a function of rotation angle

While a decrease in electrical properties resulted from the application of shear to the top surface of the material during the melt compression process, a significant increase in the EB is obtained. The effect of the azimuthal strain on the top surface on the ultimate elongation of the GNP/SBS composite is shown in Fig. 8. The results indicate an increase of ~ 270 % in the total elongation before break by rotating the plunger 360°. This enhancement can be attributed to the partial disruption of the highly organized GNP networks. The disruption of the conductive networks provides the SBS polymer chains to have stronger interactions and increased tangling of chains thus resulting in higher strain to failure.

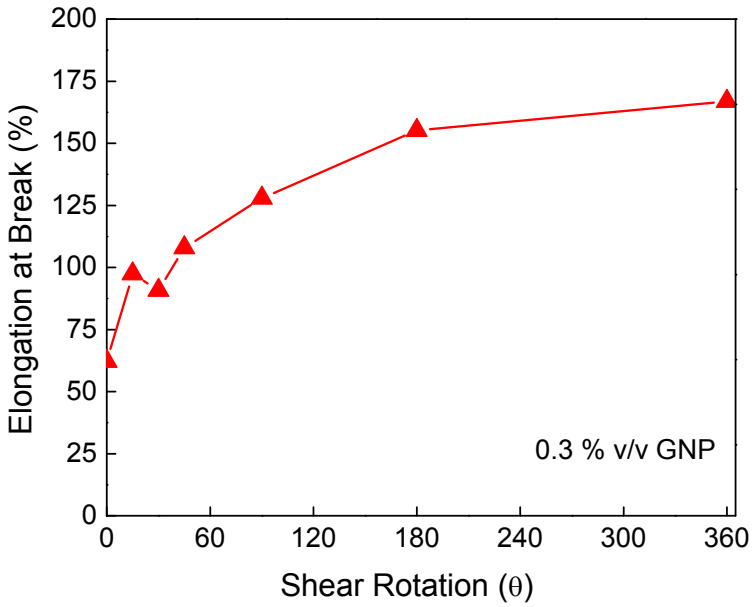

Fig. 8 Effect of shear rotation on the ultimate elongation of GNP/SBS composite with a shear-modified segregated structure

Figure 9 shows the normalized electro-mechanical behavior of the shear modified GNP/SBS composites as a function of shear rotation. Both the EB and electrical conductivity was normalized with respect to the organized 0.3 % v/v GNP composite (0° shear rotation). As discussed previously, the capillary driven coating process enabled an increase in electrical conductivity of the composite by approximately 13 – 14 orders of magnitude as compared to pristine SBS, owing to the dense GNP coating on the SBS pellets. By applying a shear force to the top surface of the highly segregated material, a gradient of GNP organization/orientation along the sample axis is formed which results in a 260 % increase in total strain to failure while only sacrificing ~ 2-3 orders of magnitude of conductivity.

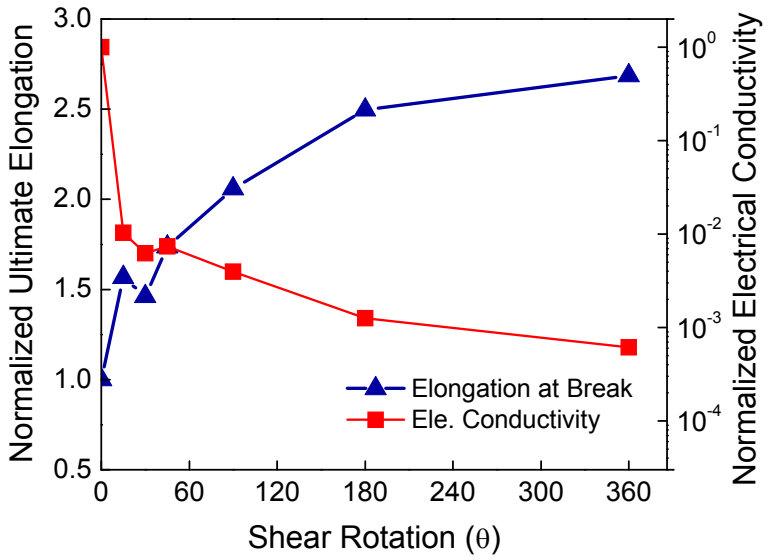

Fig. 9 Electro-mechanical behavior of the shear-modified GNP/SBS template composites loaded parallel to pressing.

4. Conclusions

A fixed-angle rotary shear technique was utilized during the melt compression process to distribute graphite nanoplatelets (GNPs) into specially constructed architectures throughout a styrene-butadiene matrix. An experimental investigation was conducted to understand the effect of GNP loading as well as rotary shear angle on the mechanical strength and electrical conductivity of the composites. The experimental results show that this simple technique can be used to produce highly flexible composites that possess exceptional conductivity while still maintaining the salient mechanical characteristics the copolymer has to offer. By applying a shear force to the top surface of the highly segregated material, a gradient of GNP organization/orientation along the sample axis is formed which results in a 270 % increase in total strain to failure while only sacrificing ~ 2-3 orders of magnitude of conductivity. Using this he properties of this flexible composite can be altered using

this very simple technique and the inherent trade-off between electrical vs. mechanical performance can be intelligently optimized for a given application by controlling the pre-set angle of rotary shear.

Acknowledgements

The authors acknowledge the financial support provided by the Rhode Island Science & Technology Advisory Council as well as Research Experiences for Undergraduates National Science Foundation (CMMI 1233887).

References

[1] H. Kim, A. A. Abdala and C. W. Macosko, Macromolecules 43 (2010) 6515.

[2] J. R. Potts, D. R. Dreyer, C. W. Bielawski and R. S. Ruoff, Polymer 52 (2011) 5.

[3] V. Singh, D. Joung, L. Zhai, S. Das, S. I. Khondaker and S. Seal, Progress in Materials Science 56 (2011) 1178.

[4] P. M. Ajayan and J. M. Tour, Nature 447 (2007).

[5] F. d. C. Fim, J. M. Guterres, N. R. S. Basso and G. B. Galland, Journal of Polymer Science Part A: Polymer Chemistry 48 (2009) 692.

[6] J. Li, J.-K. Kim and M. Lung Sham, Scripta Materialia 53 (2005) 235.

[7] K. P. Pramoda, H. Hussain, H. M. Koh, H. R. Tan and C. B. He, Journal of Polymer Science Part A: Polymer Chemistry 48 (2010) 4262.

[8] R. Verdejo, M. M. Bernal, L. J. Romasanta and M. A. Lopez-Manchado, Journal of Materials Chemistry 21 (2010) 3301.

[9] L. M. Viculis, J. J. Mack, O. M. Mayer, H. T. Hahn and R. B. Kaner, Journal of Materials Chemistry 15 (2005) 974.

[10] L. Wang, J. Hong and G. Chen, Polymer Engineering & Science 50 (2010) 2176.

[11] S. M. Cardoso, V. B. Chalivendra, A. Shukla and S. Yang, Engineering Fracture Mechanics 96 (2012) 380.

[12] M. Fang, K. Wang, H. Lu, Y. Yang and S. Nutt, Journal of Materials Chemistry 19 (2009) 7098.

[13] G. Goncalves, P. A. A. P. Marques, A. Barros-Timmons, I. Bdkin, M. K. Singh, N. Emami and J. Gracio, Journal of Materials Chemistry 20 (2010) 9927.

[14] N. Heeder, A. Shukla, V. Chalivendra and S. Yang, Journal of Materials Science 47 (2012) 3808.

[15] N. J. Heeder, A. Shukla, V. Chalivendra, S. Yang and K. Park, Experimental Mechanics 52 (2012) 315.

[16] U. Khan, P. May, A. O'Neill and J. N. Coleman, Carbon 48 (2011) 4035.

[17] H. Kim and C. W. Macosko, Macromolecules 41 (2008) 3317.

[18] J. Liang, Y. Huang, L. Zhang, Y. Wang, Y. Ma, T. Guo and Y. Chen, Advanced Functional Materials 19 (2009) 2297.

[19] T. Rath and Y. Li, Composites Part A: Applied Science and Manufacturing 42 (2011) 1995.

[20] V. K. Vadlamani, V. Chalivendra, A. Shukla and S. Yang, Smart Materials and Structures 21 (2012).

[21] V. K. Vadlamani, V. B. Chalivendra, A. Shukla and S. Yang, Polymer Composites 33 (2012) 1809.

[22] S. Vadukumpully, J. Paul, N. Mahanta and S. Valiyaveettil, Carbon 49 (2011) 198.

[23] S. Yang, W. Lin, Y. Huang, H. Tien, J. Wang, C. Ma, S. Li and Y. Wang, Carbon 49 (2011) 793.

[24] S. Stankovich, D. A. Dikin, G. H. B. Dommett, K. M. Kohlhaas, E. J. Zimney, E. A. Stach, R. D. Piner, S. T. Nguyen and R. S. Ruoff, Nature 442 (2006) 282.

[25] J. Jordan, K. I. Jacob, R. Tannenbaum, M. A. Sharaf and I. Jasiuk, Materials Science and Engineering: A 393 (2005) 1.

[26] K. Kalaitzidou, H. Fukushima and L. T. Drzal, Carbon 45 (2007) 1446.

[27] M.-D. Lu and S.-M. Yang, Synthetic Metals 154 (2005) 73.

[28] H. Peng, Journal of the American Chemical Society 130 (2007) 42.

[29] Q.-Y. Tang, Y.-C. Chan, N.-B. Wong and R. Cheung, Polymer International 59 (2010) 1240.

[30] G. G. Tibbetts, M. L. Lake, K. L. Strong and B. P. Rice, Composites Science and Technology 67 (2007) 1709.

[31] O. Hayden, K. Nielsch, T. Hasan, V. Scardaci, P. H. Tan, F. Bonaccorso, A. G. Rozhin, Z. Sun and A. C. Ferrari, in "Molecular- and Nano-Tubes" (Springer US, 2011) p. 279.

[32] Y. Xiong, Y. Xie, F. Zhang, E. Ou, Z. Jiang, L. Ke, D. Hu and W. Xu, Materials Science and Engineering: B 177 (2012) 1163.

[33] W. Tang, B. Liu, Z. Liu, J. Tang and H. Yuan, Journal of Applied Polymer Science 123 (2011) 1032.

[34] L. G. Pedroni, M. A. Soto-Oviedo, J. M. Rosolen, M. I. Felisberti and A. F. Nogueira, Journal of Applied Polymer Science 112 (2009) 3241.

[35] M. E. Leyva, G. M. O. Barra, A. C. F. Moreira, B. G. Soares and D. Khastgir, Journal of Polymer Science Part B: Polymer Physics 41 (2003) 2983.

[36] Y.-T. Liu, X.-M. Xie and X.-Y. Ye, Carbon 49 (2011) 3529.

[37] Heeder N, Yussuf A, Chakraborty I, Godfrin M, Hurt R, Tripathi A, et al. Fixed-Angle Rotary Shear as a New Method for Tailoring Electro-Mechanical Properties of Templated Graphene-Polymer Composites. Journal of Composites Science and Technology. 2014; (under review).

[38] Heeder N, Yussuf A, Guo F, Chakraborty I, Godfrin M, Hurt R, et al. Highly conductive graphene-based segregated composites prepared by particle templating. Journal of Materials Science. 2013;49(6):2567-2570.

[39] A. Bianco, H.-M. Cheng, T. Enoki, Y. Gogotsi, R. H. Hurt, N. Koratkar, T. Kyotani, M. Monthioux, C. R. Park, J. M. D. Tascon and J. Zhang, Carbon 65 (2013) 1.

CHAPTER 7

CONCLUSIONS AND FUTURE WORK

1. Conclusions

The first part of the research conducted experimentally investigated the dynamic electro-mechanical behavior of multifunctional composites when subjected to static and dynamic mechanical loadings. When properly dispersed within a polymeric matrix, conductive nanofillers such as CNTs and graphene can be assembled into a three-dimensional internal sensory network. These highly intricate electrical networks can be utilized to detect important information such as material deformation as well as various forms of damage. The main objective of this investigation was to characterize the electro-mechanical behavior of multifunctional composites when compressively deforming under low and high strain rates. Two types of multifunctional materials were investigated: carbon nanotube/epoxy and graphene/polystyrene composites. The knowledge obtained from this study will further the development of novel "smart" materials that could be used in many applications where compressive loading may be present.

The second part of the research focused on the development of novel strategies to effectively incorporate graphene into polymeric host materials. To further the development of more advanced multifunctional materials, novel techniques were developed that overcame many of the major limitations and issues associated with incorporating two-dimensional conductive filler materials into polymers matricies. Moreover, the techniques developed allow for the fabrication of multifunctional composites with tunable properties.

The specific deliverables of the project can be summarized as follows:

(1) The electrical resistance of the CNT-reinforced epoxy composites was highly affected by material strain and deformation mechanisms induced by the applied loading. The electrical response observed during SHPB loading demonstrated a similar response as previously observed during both quasi-static and drop weight loadings, where the bulk electrical resistance decreased during compression and then increased as damage initiated and propagated. The bulk electrical resistance of these nanocomposites decreased ~ 85% during SHPB experiments.

(2) The change in electrical conductivity of the material due to the CNT arrangement for small strains was determined using a Taylor expansion model to better characterize the electrical response demonstrated by the material.

(3) It was observed that the changes in CNT networks within the nanocomposite contributed approximately 64% to the overall resistance change of the material while only 36% was due to dimensional changes. This phenomenon differs from a typical strain gage measurement where the change in electrical resistance is based primarily on the dimensional changes rather than the change in material conductivity.

(4) The sensitivity of the CNT/epoxy composite, or the rate of increase in electrical conductivity as a function of strain, increased as the material became closer to yield for both quasi-static and dynamic loading. However, the rate of change of conductivity as a function of strain is higher during quasi-static loading than dynamic loading. It can be postulated that the difference between the two curves is due to an increase in matrix stiffness occurring over a very brief period of time in

SHPB loading. This phenomenon may cause a slight delay in the change in electrical conductivity based on the time it takes for the internal networks to rearrange.

(5) A modified split Hopkinson (Kolsky) pressure bar apparatus, capable of simultaneous mechanical and electrical characterization, was developed and implemented to investigate the dynamic electro-mechanical response of the graphene/polystyrene composites.

(6) The real-time damage was correlated to both stress-strain and percent change in resistance profiles. Due to a high concentration of graphene particles, relative aggregations of the graphene were inevitably formed which resulted in inadequate load transfer between the graphene particles and the polystyrene matrix. Consequently, a significant decrease in mechanical properties under both static and dynamic loading conditions with the presence of graphene was observed. The bulk electrical resistance of the composite increased significantly due to the brittle nature of the PS matrix as well as the presence of relative agglomerations of graphene platelets which resulted in micro-crack formations.

(7) A simple, inexpensive and commercially viable technique that can be used to disperse conductive sheet-like particles, such as graphene, into a highly organized pattern within polymeric materials on either the micro- or macro-scale was developed. Utilizing capillary interactions between polymeric particles and few-layer graphene particles, liquid bridges on the surface of a polymeric material allows for coating of graphene onto the polymer surfaces. By precisely controlling

the temperature and pressure during the melt compression process, highly conductive composites were formed using very low loadings of graphene particles.

(8) A modified capillary-driven particle level templating technique was developed that can be used to distribute conductive 2D (sheet-like) materials, such as graphene, into specifically constructed hybrid architectures within polymeric materials on either the micro- or macro-scale. Utilizing capillary interactions between polymeric particles and few-layer graphene particles, liquid bridges on the surface of the polymeric material allows for the coating of graphene onto the polymer surfaces. By precisely controlling the temperature and pressure during the melt compression process, highly conductive composites were formed using very low loadings of graphene particles. Since the graphene particles were localized at the boundaries between the polymer matrix particles, the composite exhibited poor mechanical strength. To improve the mechanical properties of the composite, a controlled amount of rotary shear was applied to the top surface of the material to create a Z-directional gradient of graphene organization/orientation along the sample axis. Results showed that this novel fabrication technique can produce composite materials that possess both excellent transport properties and improved mechanical strength. Furthermore, the properties of the composite can be altered using this very simple technique and the inherent trade-off between electrical vs. mechanical performance can be intelligently optimized for a target application by controlling the pre-set angle of rotary shear.

(9) Highly flexible composites that possess exceptional conductivity while still maintaining the salient mechanical characteristics were successfully fabricated

using a modified fixed-angle rotary shear technique. Moreover, the properties of this flexible composite can be altered using this very simple technique and the inherent trade-off between electrical vs. mechanical performance can be intelligently optimized for a given application by controlling the pre-set angle of rotary shear.

2. Future Work

The current research is a step forward in understanding the electro-mechanical response of tailored carbon-based multifunctional materials under dynamic loading. It elucidates a more comprehensive understanding on the dynamic behavior of such materials when subjected to high-intensity loadings as well as fruitful insight towards more efficient fabrication methods to create composites with multiple functionalities. Different materials, ranging from carbon nanotube reinforced epoxy, graphene reinforced polystyrene and graphene reinforced styrene-butadiene-styrene were studied. The proposed future projects are as follows,

(1) The dynamic electro-mechanical response of carbon nanotube-based epoxy was investigated using only composites containing 0.2 wt.% CNTs. There is a need to conduct a parametric study of CNT/epoxy composites to investigate the effect of CNT loading on the electrical sensitivity of the composite. For composites containing volume fractions of CNTs less than, equal to, and greater than the respective percolation threshold, it is postulated that significantly different electrical sensitivities will be evident when subjected to various types of mechanical loading. Various types of loading schemes (compression, tension,

flexure, torsion, etc.) can be implemented to further understand the change in transport properties of CNT-reinforced composites when subjected to deformation.

(2) Prior to investigating the behavior of a material under various loading conditions, it is imperative to understand the material under static conditions. While producing the electro-conductive GNP/PS composites for the dynamic studies, interesting behaviors were observed when different material fabrication parameters were altered. For example, when smaller GNPs (< ~ 2μm) were incorporated into the PS matrix instead of the 25 μm GNPs a significantly different electrical behavior was observed. It is postulated that the change in behavior is an effect of joule heating within the composite. Further investigation would provide a more complete understanding of the electrical behavior of the solvent casted composites and may also be beneficial for obtaining more information related to the electro-mechanical behavior of other multi-functional composites.

(3) Using the fixed-angle rotary shear technique that was developed, conductive 2D (sheet-like) materials, such as graphene, can be distributed into specifically constructed hybrid architectures within polymeric materials on either the micro- or macro-scale. The resulting composites can be tailored using this very simple technique and the inherent trade-off between electrical and mechanical performance can be intelligently optimized for a given application. More work is needed to fully understand the change in transport properties of this material under both static and dynamic loading conditions. These physical and mechanical properties of these functionally graded composites can be altered using a number of parameters (i.e. polymer type, polymer pellet size, filler type, filler size, angle

of rotary shear, etc.) to specifically tailor the composite for a target application. Understanding the static and dynamic electro-mechanical response would be highly beneficial to further the development of novel, more robust sensing devices.

(4) Since the capillary-driven particle templating technique was successful in producing highly conductive composites using polymeric pellets, this process could be extended to coat fibers / yarns. The coated fibers / yarns can then be woven into highly intricate structures throughout a polymer thus producing a novel multifunctional composite. Examples of smart fiber reinforced composites are schematically represented in Fig. 1. The rectangular specimen, shown in Fig 1.(a), has conductive fibers intricately woven into a three dimensional network throughout the polymer. Fig. 1(b) shows a hollow cylindrical fiber reinforced specimen with the conductive fibers weaved throughout the thickness of the tube. The investigation would include using certain chemical or mechanical processes to enhance and/or optimize the coating process. These novel composites would possess unique properties that may be useful for many future applications. The electro-mechanical behavior could also be investigated when the composites are subjected to various types of loading schemes (i.e. compression, tension, flexure, torsion, blast loading).

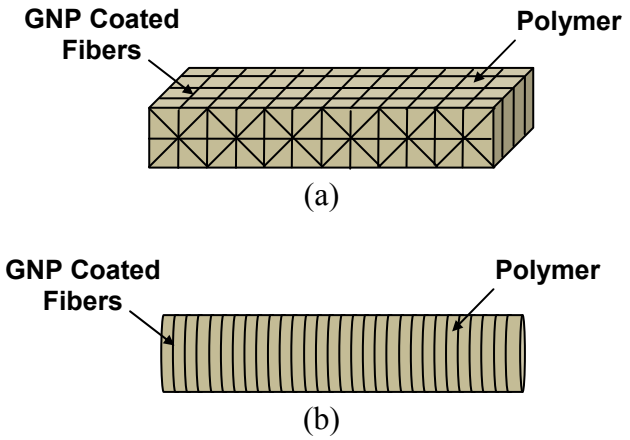

Fig. 1 Schematic of smart fiber reinforced composite

(5) The electro-mechanical behavior of CNT/epoxy and GNP/PS was studied under dynamic compressive loading using an SHPB apparatus. These investigations revealed fundamental information about the electrical behavior of such composites when subjected to compressive loading. Using this information, these novel sensors could be incorporated into structures optimized for energy absorption applications, thus creating a novel smart sandwich structure. Figure 2 shows a schematic of a smart composite structure that could be used in a blast application. The electro-conductive polymeric sensing material can be sandwiched between two stiff facesheets ($E_{composite} << E_{facesheet}$). A shock tube apparatus could be used to generate a controlled shock wave directed at the sandwich structure while the electrical resistance of the composites could be monitored. Along with high-speed photography, a 3-D digital image correlation could be implemented to obtain the real-time in-plane strains and out-of-plane displacements of the structure. The change in electrical resistance could be correlated to deformation. Once the fundamental physics and electro-mechanical behaviors are understood, the smart

sandwich structure could be optimized by tailoring the resistance (CNT concentration) as well as the stiffness (polymeric material) so that the optimal sensitivity could be achieved.

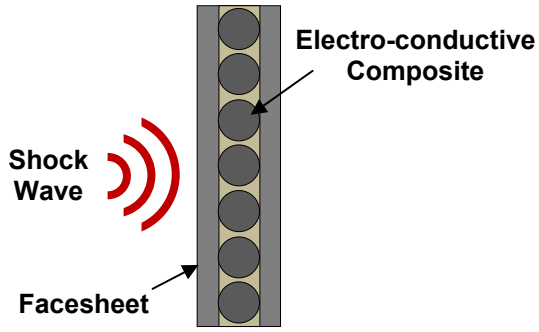

Fig. 2 Schematic of a smart structure for energy absorption application

APPENDICES

APPENDIX A: DETAILS OF MATERIALS

Multi-walled Carbon Nanotubes

Acquired from *Nano-Lab*, Waltham MA (www.nano-lab.com)

Catalog No. PD30L5-20

Description: Multiwall CNTs, Hollow Structure

Purity > 95%, residuals may include iron, sulfur

OD: 30 ± 15 nm

Length: 5 – 20 microns

SSA: 200 – 400 m^2/g

Graphite Nanoplatelets

Acquired from *XG Science*s, Lansing, MI (www.xgsciences.com)

Catalog No. xGnP-M-25

Description: xGnP Graphene Nanoplatelets: Grade M

Thickness: ~ 6 nm

Surface Area: 120 – 150 m^2/g

Particle Diameter: 25 microns

Epoxy

Acquired from *Buehler*, IL (www.buehler.com)

Catalog No. 203440032 (Resin), 203442064 (Hardener)

Description: Epothin 2 Epoxy System

Clear, very low viscosity

9 hr cure time at room temperature

< 30 °C Peak Temperature

~ 78 Shore D Hardness

Polystryene

Acquired from *Styrolution*, Frankfurt, Germany (www.styrolution.com)

Catalog No. PS 1300

Description: Crystal PS 1300

Processing Temp.: 180 °C– 280 °C

Tensile Stress at Yield, 23 °C: 49 MPa

Elongation, Failure: 2 %

Flexural Strength: 100 Mpa

Flexural Modulus: 3 GPa

Styrene-Butadiene-Styrene (SBS)

Acquired from *AKelastomer*, Japan (www.akelastomer.com)

Catalog No. Asaprene T439

Description: Asaprene T-439

Molding Temp.: 160 °C– 220 °C

Tensile Strength: 6 MPa

Elongation: 880 %

Stryrene/Butadiene Weight Ratio: 45/55

APPENDIX B: DETAILED FABRICATION PROCEDURE FOR PRODUCING CNT/EPOXY COMPOSITES

Materials

Matrix: Epothin Epoxy (Buehler Inc.)

Filler: Multi-wall carbon nanotubes (Nanolab, purity >95%, diameter: 30 ± 15 nm, length: 5 to 20 μm)

Procedure:

1. Pour 70 g of Epothin Resin (Part A: 20-8140-032) into a 250 mL copper beaker.
2. Measure out desired amount of CNTs to add to the Part A based on the total mass of polymer (97.3 g) and add to Part A.
3. Place beaker in shear mixer (Ika Werke RW 16 Basic) outfitted with a 3-blade propeller stirrer (R1381 Propella stirrer) and set to 600 RPM for 30 minutes.
4. Following shear mixing, the ultrasonication process is applied for one hour on pulse mode, 4.5 on 9 s off, with 100 kHz (Sonics & Materials Inc. VCX750).
5. The mixture is then placed inside of the vacuum chamber and vacuumed for ~ 1 h, ensuring that all air is completely removed from the Part A/CNT solution.
6. Next, 27.3 g of Part B is slowly mixed gently into the Part A/CNT mixture and then placed back into the vacuum chamber for 5 min.
7. Finally, the CNT/epoxy solution was slowly poured into pre-manufactured wax mold, as shown in Fig. 1, and allowed to cure for 3 days under ambient conditions.

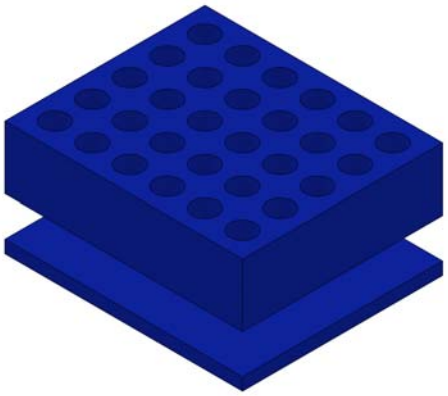

Fig. 1. Wax mold for CNT/Epoxy quasi static specimens

APPENDIX C: DETAILS OF SOLVENT CASTING PROCEDURE FOR PRODUCING GNP/PS COMPOSITES

Materials

Matrix: Crystal Polystyrene 1300 (Styrolution Inc.)

Filler: xGnP Nanoplatelets M-25 (XG Sciences, Inc.)

Part I: Dispersion of Nanoplatelets

1. Polystyrene homopolymer and graphene nanoplatelets will be dried in a vacuum oven at 25°C to remove any residual moisture.

2. In a small covered glass beaker, 7 g of PS pellets is added to 42 mL of dimethyl formamide (DMF) and placed on a magnetic stirring plate until fully dissolved.

3. In a separate beaker, the desired amount of graphene will be allowed to swell in DMF. The ratio of graphene to DMF should be kept close to ~0.1 g graphene per 100 mL DMF.

4. xGnP / DMF solution will be sonicated for 1 h at 28 kHz (Pulse mode 30 sec on/ 15 off, amplitude: 20 %)

5. The two solutions are then combined and stirred for 2 hrs.

6. Next, the solution is dropped into a large volume of vigorously stirred methanol to coagulate the PS nanocomposites.

7. The composite is then filtered and dried in an oven at ~80 °C for ~ 25 hrs.

8. Finally, the PS-G nanocomposites are compression melted using a hot press

Melt Compression Procedure

A schematic of the stainless steel mold fabricated is shown in Fig. 1. The mold consists of a base plate, lower insert, outer shell, die, piston and a cartridge heater. It is

important to note for proper melt compression, sufficient material must be first accumulated (i.e. ~ 5 batches = ~ 4 specimens).

1. Break the dried PS-FLG composite into small pieces, then fill specimen die.

2. Place the mold (with no piston) on top of hot plate.

3. Insert thermocouple into auxiliary hole in outer ring and bring temperature of the mold to ~110 °C and maintain.

4. As the composite softens, manually compress using an aluminum rod. Continue this procedure until no more material can fit inside the cavities.

5. Finally, add extra composite material on top of the specimen die to allow for sufficient compression.

6. Place piston on top and heat to ~110 °C using the cartridge heater.

7. Once both the base mold and piston reach ~110 °C, maintain temperature for 20 minutes.

8. Remove all thermocouples and cartridge heater and place on hydraulic press.

9. Press to 15 US tons and hold for 5 min. (While doing this fill sink up with cold water for use as a cold bath)

10. After 5 minutes, submerge the entire mold into the cold bath.

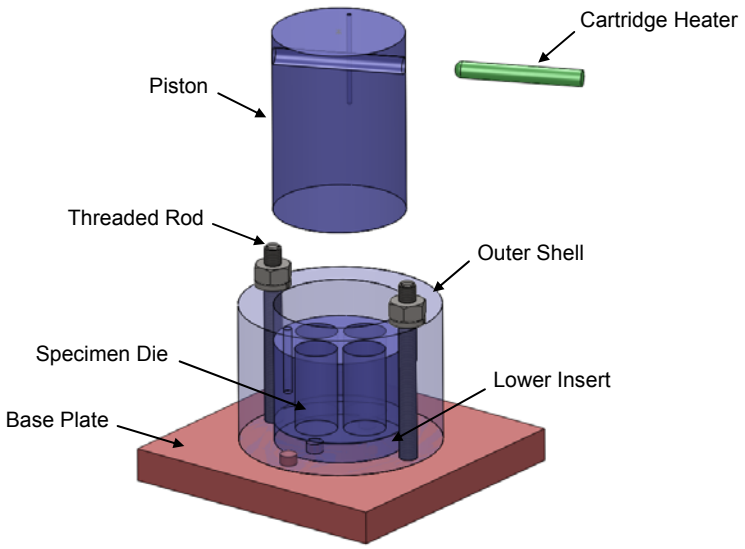

Fig. 1 Compression molding apparatus for SHPB specimens

APPENDIX D: DETAILS OF CAPILLARY DRIVEN-PARTICLE TEMPLATING PROCEDURE FOR GNP/PS COMPOSITES

Materials: **Matrix**: Crystal Polystyrene 1300 (Styrolution Inc.)

Filler: xGnP Nanoplatelets M-25 (XG Sciences, Inc.)

I. Organized GNP/PS Particle Templated Composites

1. Measure out 10 g of PS and place into a glass vile.
2. Measure out desired amount of GNP and add to the PS.
3. Shake vigorously to allow for complete coating of PS pellets
4. For GNP loadings ≥ 0.1 % v/v, add (10) droplets of methanol to PS/GNP mixture, and shake until all FLG is adsorbed to the surfaces of the PS.
5. Place coated pellets into mold, and place on hot plate.
6. Set hot plate to 540°C and small cartridge on 5 V.
7. When base mold reaches 125°C, shut off hot plate completely. When piston reaches 160°C, lower voltage and maintain temperature between 140-160°C for 20 minutes.
8. Press to 10 metric tons and maintain pressure for 20 seconds. Release, then cool.

II. Shear-modified GNP/PS Particle Templated Composites

1. Follow steps (1-7).
2. Place ball bearing (sandwiched between two brass plates) on top of piston and press to 5 metric tons.
3. Rotate piston to desired angle, and press to 10 metric tons. Hold pressure for 5 min.

4. Submerge entire mold into cold bath.

A schematic of the stainless steel mold fabricated is shown in Fig. 1. The mold consists of a base plate, lower insert, outer shell, piston and a cartridge heater.

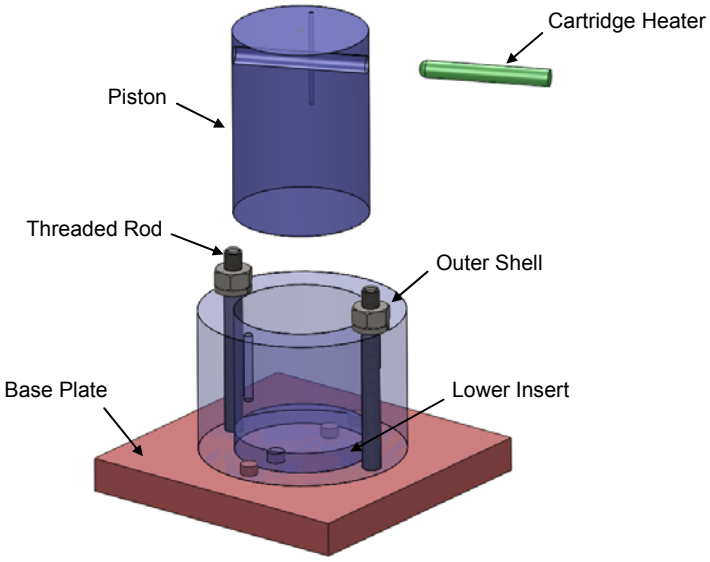

Fig. 1 Compression molding apparatus for particle template composites

APPENDIX E: DETAILS OF CAPILLARY DRIVEN-PARTICLE TEMPLATING PROCEDURE FOR GNP/SBS COMPOSITES

Materials: **Matrix**: Asaprene T_429 SBS (Asahi Kasei Chemicals Corp.)

Filler: xGnP Nanoplatelets M-25 (XG Sciences, Inc.)

I. Organized GNP/SBS Particle Templated Composites

1. Measure out 7 g of SBS and place into a glass vile.
2. Measure out desired amount of GNP and add to the SBS.
3. Shake vigorously to allow for complete coating of PS pellets
4. For GNP loadings ≥ 0.1 % v/v, add (10) droplets of methanol to SBS/GNP mixture, and shake until all GNP is adsorbed to the surfaces of the SBS.
5. Place coated pellets into mold, and place on hot plate.
6. Set hot plate to 540°C and small cartridge on 5 V.
7. When base mold reaches 125°C, shut off hot plate completely. When piston reaches 160°C, lower voltage and maintain temperature between 140-160°C for 20 minutes.
8. Press to 10 metric tons and maintain pressure for 20 seconds. Release, then cool.

II. Shear-modified GNP/SBS Particle Templated Composites

1. Follow steps (1-7).
2. Place ball bearing (sandwiched between two brass plates) on top of piston and press to 5 metric tons.
3. Rotate piston to desired angle, and press to 10 metric tons. Hold pressure for 5 minutes.
4. Submerge entire mold into cold bath.

A schematic of the stainless steel mold fabricated is shown in Fig. 1. The mold consists of a base plate, lower insert, outer shell, piston and a cartridge heater.

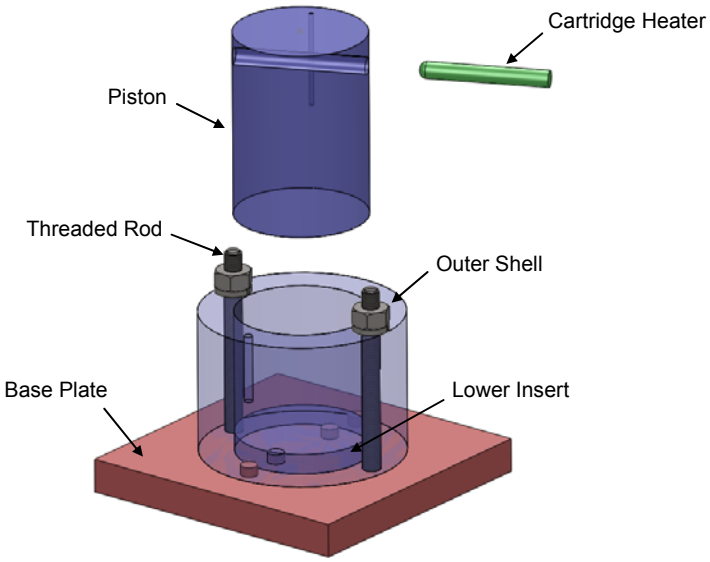

Fig. 1 Compression molding apparatus for particle template composites

APPENDIX F: PRELIMINARY STUDIES ON THE ELECTRICAL BEHAVIOR OF GNP/PS PREPARED BY SOLVENT CASTING

Prior to studying the electrical response of the GNP/PS composites under load, it was essential to understand the electrical behavior of these composites under static conditions. In order to obtain an electro-conductive composite, a conductive filler material must be properly dispersed throughout the polymer. The level of dispersion directly correlates with the resulting composite properties. For this reason, two separate studies were carried out to determine (1) which size of graphene is best to use and (2) which solvent will better disperse the GNP in polystyrene.

< 2μm vs. 25 μm xGnP Nanoplatelets

Two types of graphite nanoplatelets (GNPs), < ~ 2μm and 25 μm in diameter, were studied to determine which would provide a higher electrical efficiency. Briefly, 5 g of PS was first dissolved in 30 mL of chloroform ($CHCl_3$). The desired amount of graphene platelets were dispersed in a separate $CHCl_3$ solution (~ 0.1 g graphene per 100 mL $CHCl_3$) using ultrasonication. The graphene / $CHCl_3$ solution was sonicated for 1.5 h at 20 kHz on pulse mode, 30 s on 10 s off using a Sonics & Materials Inc. VCX750 probe sonicator. The graphene / $CHCl_3$ suspension was then added to the PS / $CHCl_3$ solution and mechanically stirred for ~ 2 h. Since the nanoplatelets tend to agglomerate during slow solvent evaporation, the solution was dropped into a large volume of methanol to coagulate the graphene-PS composites. The resulting composite was then filtered and dried in an oven at ~ 80 ºC for ~ 18 h. Finally, the dried graphene-PS composites were hot-pressed into disks having a diameter of 45

mm and a thickness of ~ 2-3 mm. using a heated steel mold (~ 190 ºC) and a hydraulic press.

To evaluate the dispersion of the graphene nanoplatelets inside the polystyrene matrix, each disk was sliced into approximately 12 rectangular prisms, as shown in Fig. 1. A two-point probe measurement technique was utilized to measure the conductivity of the material. A schematic representation of the measuring technique is shown in Fig. 2. Silver paint was used to reduce contact resistance between the specimen and measurement device. Currents ranging from 1 nA to 1 mA was passed through the sample to obtain the resulting resistance measurements.

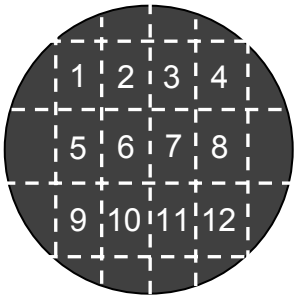

Fig. 1. Schematic of composite slicing for electrical characterization

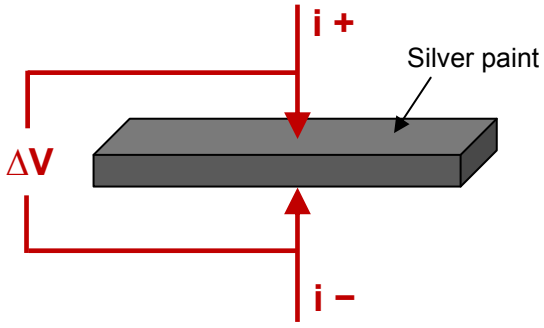

Fig. 2. Two point probe measurement technique

Figure 3 shows the typical electrical behavior of a 5 vol.% xGnP (25 μm)/PS composite prepared using solvent casting. It can be seen that the resistance remains constant for all currents supplied. This response is typical for a material acting as a conductor.

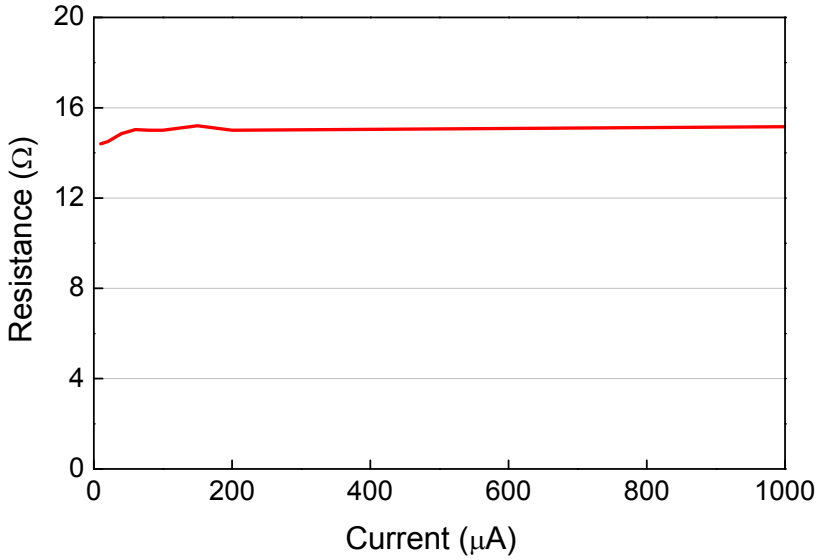

Fig. 3. Electrical resistance (through-thickness) of a 5 vol.% xGnP (25 μm)/PS composite (low resistance)

Figure 4 shows the typical electrical behavior of a 5 vol.% xGnP (< ~2 μm)/PS composite prepared using the same solvent casting method. Unlike the composite with the larger xGnP particles, the resistance of the composite containing the small xGnP particles decreases as the current increases. This behavior is analogous to the electrical behavior of a semiconductor when different temperatures are applied. For a typical semiconductor, the material resistivity drastically increases as the temperature → 0. The behavior observed in the 5 vol.% xGnP (<~2 μm)/PS is postulated to be a result of joule heating occurring inside the material.

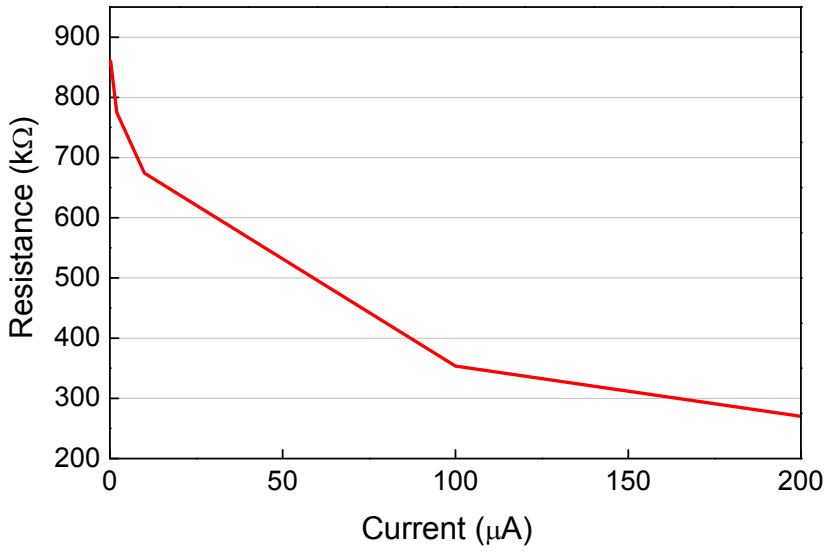

Fig. 4. Electrical resistance (through-thickness) of a 5 vol.% xGnP (~2 μm)/PS composite (high resistance)

A separate study was conducted to further investigate the non-linear behavior observed for composites exhibiting higher electrical resistances (kΩ to MΩ range). Moreover, it is evident that the larger xGnP particles (25 μm) provided better conductivity in the final composite than the smaller particles (<~2μm). For this reason alone, the 25 μm xGnP particles were used as the conductive additive for all composites produced in these studies.

Chloroform vs. Dimethylformamide (DMF)

A small investigation was performed to study the effect of different solvents on the dispersion of the graphene nanoplatelets (GNPs) inside the polystyrene (PS) matrix. Two types of solvents were used to disperse the GNPs, namely, dimethylformamide (DMF) and Cholorform ($CHCl_3$). Figure 5 and 6 show the electrical behavior of the GNP/PS composites produced using $CHCl_3$ and DMF respectively. To evaluate the dispersion of the GNPs inside the PS matrix and to

obtain an estimate of material conductivity, each composite disk was sliced into approximately 12 rectangular prisms, as shown in Fig. 1. When $CHCl_3$ was used as a solvent, only (7) out of (20) specimens exhibited a resistance that was measureable (<52 GΩ). On the other hand, (23) out of (23) specimens that were made using DMF were all conductive. For this reason, DMF was chosen over $CHCl_3$ as the solvent of choice to use in the composite fabrication.

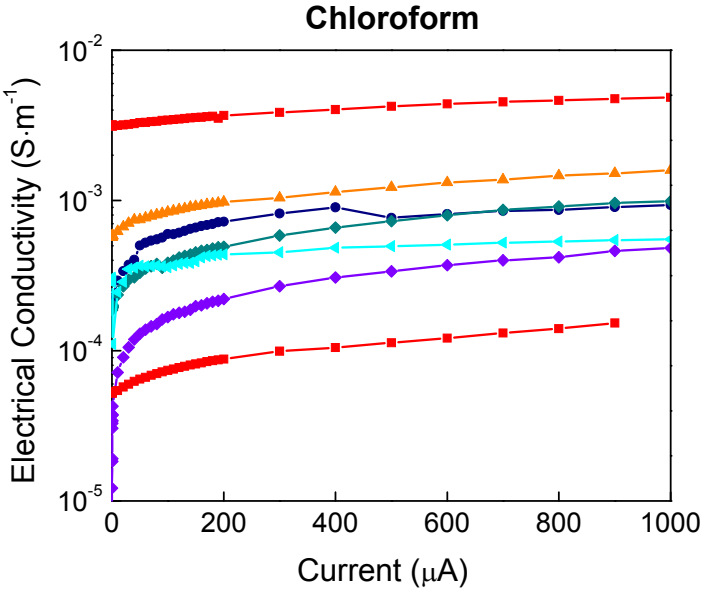

Fig. 5. Electrical behavior of 5 vol.% xGnP (25 μm)/PS composite prepared by the solvent mixing approach in which $CHCl_3$ was used as a solvent

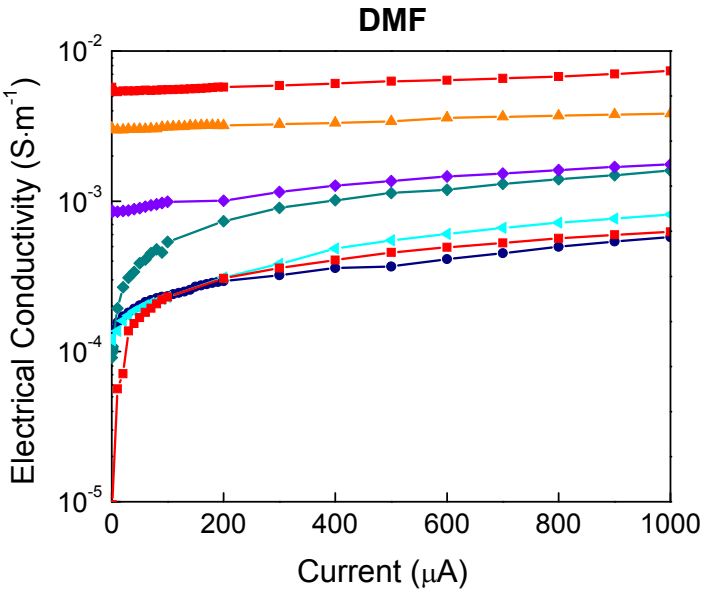

Fig. 6. Electrical behavior of 5 vol.% xGnP (25 μm)/PS composite prepared by the solvent mixing approach in which DMF was used as a solvent

Joule Heating Investigation

Joule heating, or ohmic heating or resistive heating, is the process by which the passage of an electric current through a conductor releases heat. As seen in Fig. 4, composites exhibiting higher resistances appear to behave similarly to how semiconductors perform for different temperature ranges. Figure 7 further demonstrates the material resistivity effect on the electrical behavior of the resulting composite. For low resistance samples, the resistance remains constant which is analogous to how a conductor behaves electrically. On the other hand, if the resistance is high, the resistivity of the material appears to decreases when the magnitude of current increases.

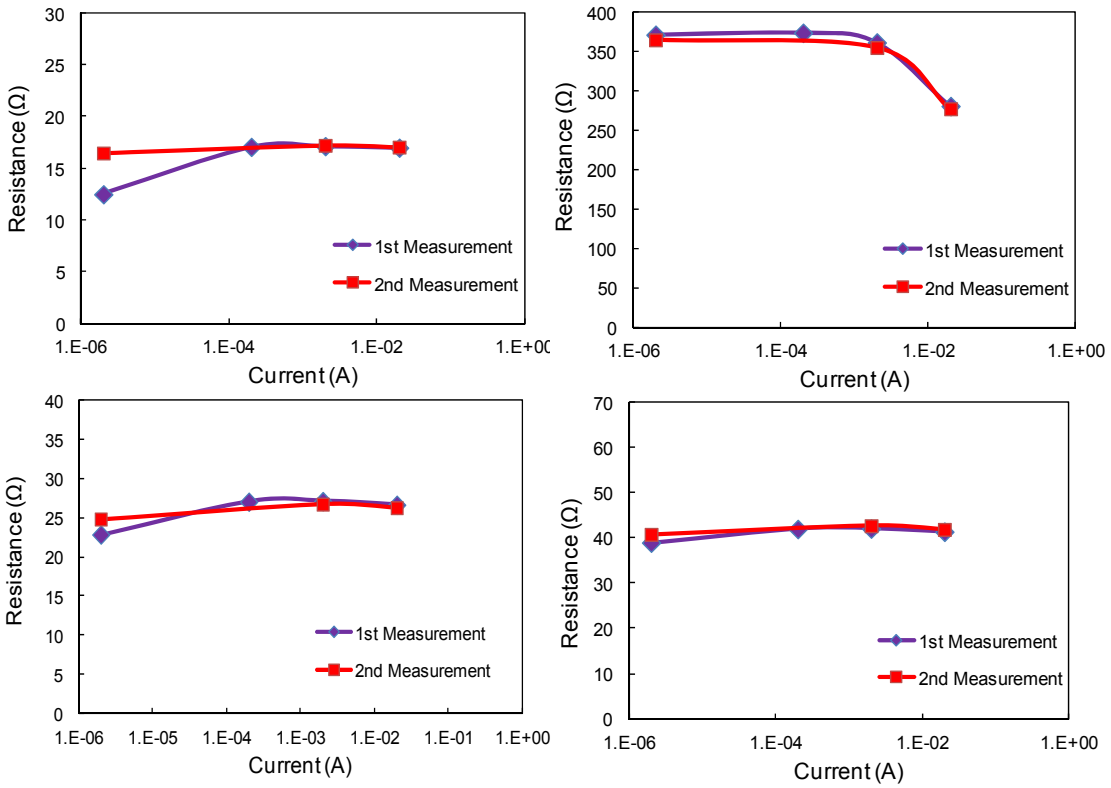

Fig. 7. Electrical behavior of 2 vol.% GNP/PS (25μm) fabricated using the solvent casting method

To further understand the electrical behavior demonstrated by the GNP/PS composites, a series of experiments were carried out to study the influence of the current magnitude and the resistivity of the material for a long period of time. Different magnitudes of current were supplied to the GNP/PS composites and the voltage drop across each specimen was recorded for 60 seconds. Fig. 8 shows the electrical behavior of a 2 vol.% GNP (25 μm)/PS composite for different supplied currents. The resistance of the composite appears to remain constant (~15 kΩ) for all currents magnitudes supplied. However, when 2 mA of current was supplied, the voltage did decrease slightly as time increased thus showing further evidence of joule

heating. On the contrary, for a composite of lower resistance (40 Ω) , the resistance remains constant for all currents supplied, as shown in Fig. 9. Further studies were carried out and sufficient evidence was found to support the theory that joule heating of the GNP/PS composites that had electrical resistances in either the kilo-ohm or mega-ohm range was occurring.

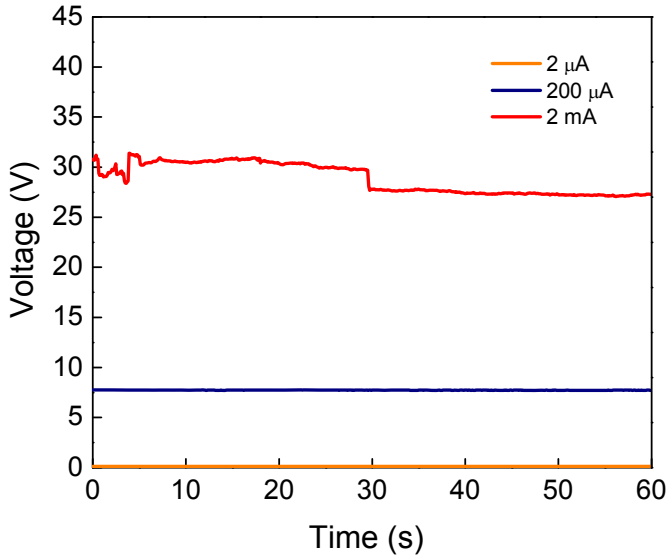

Fig. 8. Electrical behavior as a function of time of a 2 vol.% xGnP (25 μm)/PS composite prepared by the solvent mixing approach in which DMF was used as a solvent.

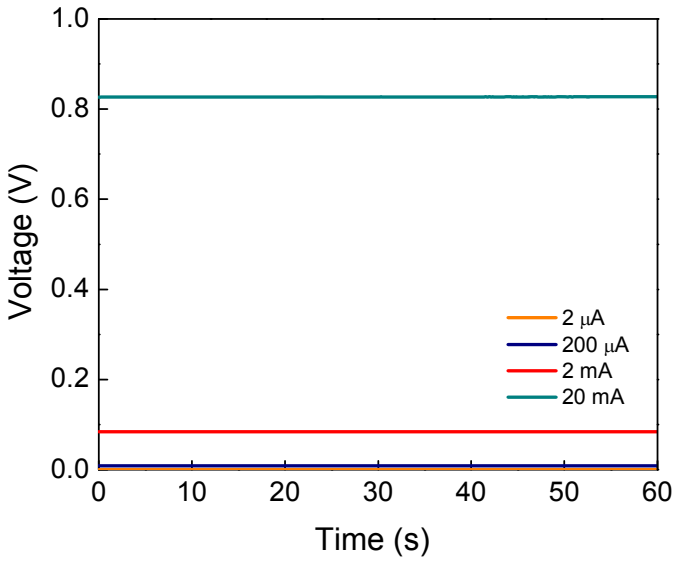

Fig. 9. Electrical behavior as a function of time of a 2 vol.% xGnP (25 μm)/PS composite prepared by the solvent mixing approach in which DMF was used as a solvent.

APPENDIX G: ELECTRICAL BEHAVIOR OF GNP/PS PARTICLE TEMPLATED COMPOSITES

Electrical conductivity measurements were made on the GNP/PS composites using a volumetric two-point probe measurement technique. Electrical conductivity was measured across the thickness of the sample. The resistance of the material was experimentally determined by supplying a constant current through the specimen while simultaneously measuring the voltage drop across the sample. A constant current source was used to supply the DC current through the specimen (Keithley Instruments Model 6221) while two electrometers (Keithley Instruments Model 6514) were used to measure the voltage drop across. The difference between the two voltage readings was measured using a digital multimeter (Keithley Instruments Model 2000 DMM). Figure 1 shows the electrical conductivity as a function of graphene content. A significant enhancement in electrical conductivity is demonstrated when 0.1 % v/v GNP was added to the PS. Since the boundaries located between the pellets are maintained, the GNPs are condensed and become interconnected throughout the material thus causing a significant increase in conductivity while using very low loadings of graphene. When 0.3 % v/v graphene is coated onto the PS, the electrical conductivity of the composite increases approximately 4-5 orders of magnitude higher than 0.1 % v/v graphene.

According to the classical percolation theory, the electrical conductivity of the composite can be described as

$$\sigma = \sigma_0 \left(\varphi - \varphi_c \right)^t \tag{5}$$

where σ is the electrical conductivity of the composite, σ_o is a scaling factor, φ is the volume fraction of the conductive filler, φ_c is the volume fraction filler at percolation, and t is a critical exponent which is related to system dimensionality. The conductivity data was fitted by plotting log σ vs log $(\varphi-\varphi_c)$ and incrementally varying φc until the best fit was achieved. The best fit produced $\varphi_c \sim 0.085$ % v/v and $t \sim 2.75$. For monodispersed, randomly oriented disk shaped particles within an insulating matrix, the theoretical percolation threshold based exclusively on geometry is 0.01 % v/v [Kim et al. 2010]. Based on the obtained results, the fabrication technique demonstrated provides the means to produce highly conductive composite materials using very small loadings of graphene. Typically, reported values of t in literature ~ 1.1-1.3 for two-dimensional conductive systems and 1.6-2.0 for three-dimensional conductive systems. The slightly higher measured critical exponent may be attributed to the extreme geometry and orientation of the graphene particles within the boundaries [Cai et al, 2005]. Kogut and Straley (1979) first showed that t could be larger than 2.0 if the low conductance bonds in the percolation network had a very wide distribution. This distribution can be attributed to a large range of effective geometrical factors in a continuous homogeneous conducting phase [Kogut et al, 1979]. During the melt compression process, the graphene particles are templated over the polymer pellets, and forced into a conducting network through the sample. Due to the anisotropic conductivity of graphene, the orientation of the graphene sheets will have a significant effect on the electron transport through the conductive networks.

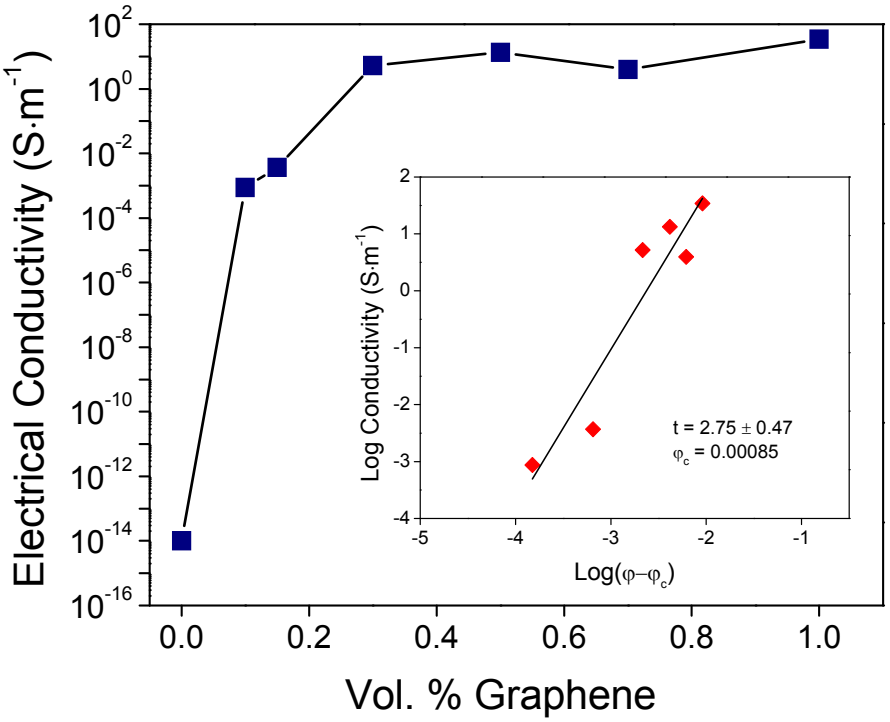

Fig. 1. Electrical conductivity of GNP/PS composite material as a function of graphene content. The insert shows the log-log plot of electrical conductivity with φ-φ_c for $\varphi>\varphi_c$

Effect of Particle Size on GNP – Polystyrene Particle Templated Composites

A small study was conducted to investigate the effect of the polymer particle size on the electrical behavior of the composites. Two different particle sizes were experimentally tested. The standard pellet size consisted of PS pellets having an average size between 2.23 mm – 3.18 mm while the crushed pellet size consists of pellet sizes ranging from 590 µm – 1400 µm. To obtain the smaller pellets, an ordinary coffee grinder was used and the crushed material was assorted according to size using a set of sieves. Again, for GNP loadings less than 0.1 % v/v, the dry

electrostatic adsorption technique was sufficient to coat the PS pellets. For loadings greater than and equal to 0.1 % v/v, the capillary-driven particle templating technique was used.

A volumetric two-point probe measurement technique was implemented to evaluate the material conductivity, as shown in Fig. 2. The conductivity measurements were made in the direction perpendicular to the molding direction.

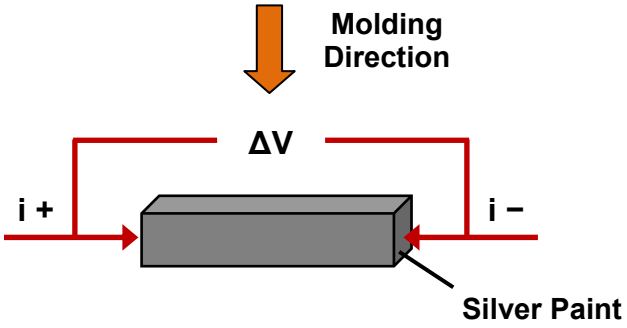

Fig. 2. Schematic of electrical measurement technique to obtain the bulk electrical conductivity.

Figure 3 shows the particle size effect on the electrical behavior of the GNP/PS composites. Both the standard and crushed particle composites exhibited excellent electrical conductivity. However, the standard size particles exhibited a percolation threshold at a volume fraction less than 0.1 while the crushed particles showed a percolation to occur below 0.3 % v/v. As the GNP content was further increased from 0.5 % v/v to 1 % v/v, the conductivity remained unchanged and showed similar magnitude for both particle sizes. The variation in the percolation threshold for these composites may be attributed to the particle size difference but may also be attributed to the non uniform coating of GNP on the crushed pellets. When handling the smaller

pellets, the capillary driven coating technique must be carefully executed so that the small polymeric particles do not stick to other polymeric particle via capillary forces. It is important to note that careful attention must be paid to using a critical amount of methanol, no more and no less, as well as the mixing procedure used.

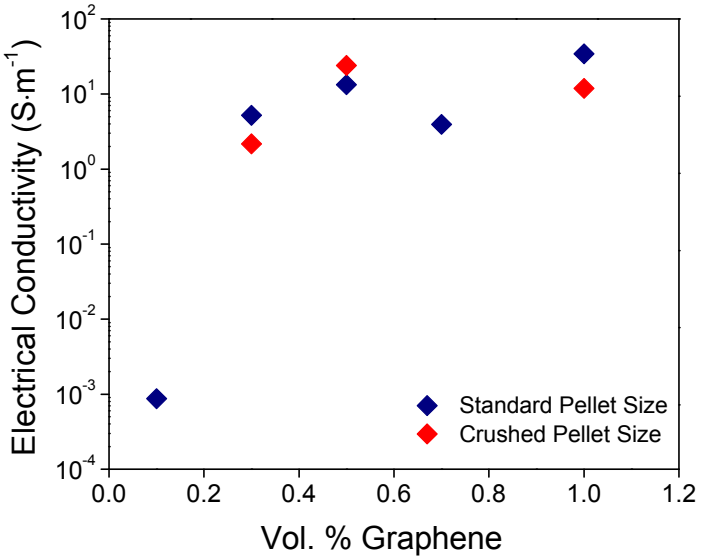

Fig 3. Particle size effect on the electrical behavior of GNP/PS particle templated composites

APPENDIX H: ELECTRICAL BEHAVIOR OF CARBON BLACK – POLYSTYRENE PARTICLE TEMPLATED COMPOSITES

A brief study was performed to investigate the electrical behavior of the particle templated composites using carbon black (CB) as a filler material. The CB used was acquired from Cabot Corp (LITX 50, Cas No. 1333-86-4). The average particle size of was ~ 50 nm. The polymeric material chosen for this study was polystyrene (Crystal PS 1300, average molecular weight of 121,000 g/mol) purchased from Styrolution, USA. The PS pellets (~ 2 mm) used were elliptical prisms with a total surface area of 1.03 ± 0.01 cm2. All CB/PS particle templated composites were fabricated using the same capillary driven-particle templated procedure used to produce the GNP/PS composites. The electrical behavior of the CB/PS and GNP/PS is shown in Fig. 1. Similar to the GNP/PS, it can be observed that the capillary driven fabrication procedure was successful in creating highly conductive CB/PS also. The percolation threshold was < 0.05 % v/v carbon black for the CB/PS composites. This value is slightly higher than the GNP/PS composites (< 0.01 % v/v GNP). Furthermore, the electrical conductivity at 0.5 % v/v filler for CB/PS was ~ 2-3 orders of magnitude less than GNP/PS. This difference can be attributed to the variation in particle shape size since the CB particles were ~ 50 nm whereas the GNP sheets were ~ 25 microns in length.

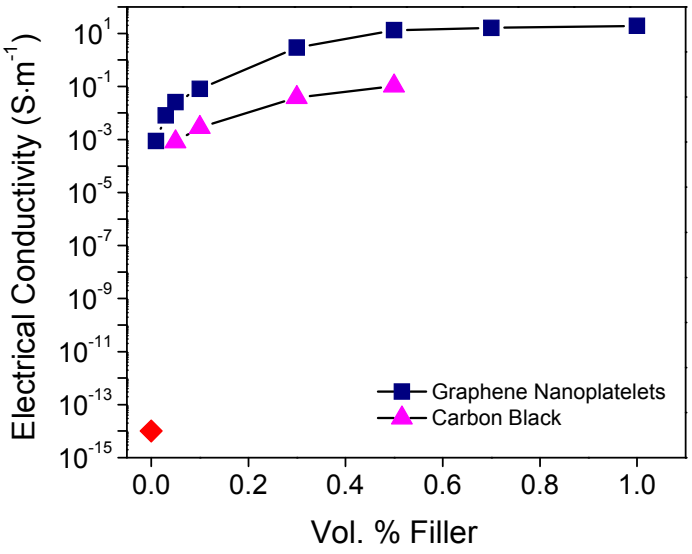

Fig 1. Comparison of the electrical behavior of CB/PS and GNP/PS particle template composites

APPENDIX I: ELECTRICAL CHARACTERIZATION EQUIPMENT

SPECIFICATIONS

Keithley Model 6220 DC Current Source

SOURCE SPECIFICATIONS

Range (+5% over range)	Accuracy (1 Year) 23°C±5°C ±(%rdg. + amps)	Programming Resolution	Temperature Coefficient/°C 0°-18°C& 28°-50°C	Typical Noise (peak-peak) /RMS[3,4,5] 0.1Hz-10Hz	Settling Time[1,2] (1% of final value)
2nA	0.4% + 2pA	100fA	0.02% + 200fA	400/80fA	100µs
20nA	0.3% + 10pA	1pA	0.02% + 200fA	4/0.8pA	100µs
200nA	0.3% + 100pA	10pA	0.02% + 2pA	20/4pA	100µs
2µA	0.1% + 1nA	100pA	0.01% + 20pA	200/40pA	100µs
20µA	0.05% + 10nA	1nA	0.005% + 200pA	2/0.4nA	100µs
200µA	0.05% + 100nA	10nA	0.005% + 2nA	20/4nA	100µs
2mA	0.05% + 1µA	100nA	0.005% + 20nA	200/40nA	100µs
20mA	0.05% + 10µA	1µA	0.005% + 200nA	2/0.4µA	100µs
100mA	0.1% + 50µA	10µA	0.01% + 2µA	10/2µA	100µs

ADDITIONAL SOURCE SPECIFICATIONS

OUTPUT RESISTANCE: $>10^{14}\Omega$. (2nA/20nA range)

OUTPUT CAPACITANCE: <10pF, <100pF Filter ON. (2nA/20nA range)

LOAD IMPEDANCE: Stable into 100µH typical.

CURRENT REGULATION: Line: <0.01% of range. **Load:** <0.01% of range.

VOLTAGE LIMIT (Compliance): Bipolar voltage limit set with single value. 0.1V to 105V in 0.01V programmable steps. Accuracy for 0.1V to 20V: 0.1% +20mV, accuracy for 20V to 105V: 0.1% + 100mV

MAX. OUTPUT POWER: 11W, four quadrant source or sink operation.

GUARD OUTPUT:

Maximum Load Capacitance: 10nF.

Maximum Load Current: 1mA for rated accuracy.

Accuracy: ±1mV for output currents <2mA. (excluding output lead voltage drop).

PROGRAM MEMORY: (offers point-by-point control and triggering, e.g. Sweeps)

Number of Locations: 64K.

EXTERNAL TRIGGER: TTL-compatible EXTERNAL TRIGGER INPUT and OUTPUT.

Max Trigger Rate: 1000/s.

6220 – 2182 MEASUREMENT FUNCTIONS

DUT RESISTANCE: Up to 1GΩ (1 nSiemen).

DELTA MODE RESISTANCE MEASUREMENTS and DIFFERENTIAL CONDUCTANCE: Controls Keithley Model 2182A Nanovoltmeter at up to 24Hz reversal rate (2182 at up to 12Hz).

Source Notes

1 Settling times are specified into a resistive load, with a maximum resistance equal to 2V / $I_{fullscale\ of\ range}$. See manual for other load conditions.
2 Settling times to 0.1% of final value are typically <2x of 1% settling times.
3 Noise current into <100Ω.
4 RMS Noise 10Hz-20MHz (2nA – 20mA Range) Less than 1mVrms, 5mVp-p (into 50Ω load).
5 Typical values are non-warranted, apply at 23°C, represent the 50th percentile, and are provided solely as useful information.

Keithley Model 6221 DC/AC Current Source

SOURCE SPECIFICATIONS

Range (+5% over range)	Accuracy (1 Year) 23°C±5°C ±(%rdg. + amps)	Programming Resolution	Temperature Coefficient/°C 0°-18°C& 28°-50°C	Typical Noise (peak-peak) /RMS[3,5] 0.1Hz-10Hz	Typical Noise (peak-peak) /RMS[3,4,5] 10Hz-(BW)	Output Response Bandwidth (BW) into Short	Settling Time[1,2] (1% of final value)	
							Output Resp. Fast (Typical[5])	Output Resp. Slow (Max)
2nA	0.4% + 2pA	100fA	0.02% + 200fA	400/80fA	250/50pA	10kHz	90µs	100µs
20nA	0.3% + 10pA	1pA	0.02% + 200fA	4/0.8pA	250/50pA	10kHz	90µs	100µs
200nA	0.3% + 100pA	10pA	0.02% + 2pA	20/4pA	2.5/0.5nA	100kHz	30µs	100µs
2µA	0.1% + 1nA	100pA	0.01% + 20pA	200/40pA	25/5.0nA	1MHz	4µs	100µs
20µA	0.05% + 10nA	1nA	0.005% + 200pA	2/0.4nA	500/100nA	1MHz	2µs	100µs
200µA	0.05% + 100nA	10nA	0.005% + 2nA	20/4nA	1.0/0.2µA	1MHz	2µs	100µs
2mA	0.05% + 1µA	100nA	0.005% + 20nA	200/40nA	5.0/1µA	1MHz	2µs	100µs
20mA	0.05% + 10µA	1µA	0.005% + 200nA	2/0.4µA	20/4.0µA	1MHz	2µs	100µs
100mA	0.1% + 50µA	10µA	0.01% + 2µA	10/2µA	100/20µA	1MHz	3µs	100µs

ADDITIONAL SOURCE SPECIFICATIONS

OUTPUT RESISTANCE: $>10^{14}\Omega$. (2nA/20nA range)

OUTPUT CAPACITANCE: <10pF, <100pF Filter ON. (2nA/20nA range)

LOAD IMPEDANCE: Stable into 10µH typical, 100µH with Output Response SLOW.

CURRENT REGULATION: Line: <0.01% of range. **Load:** <0.01% of range.

VOLTAGE LIMIT (Compliance): Bipolar voltage limit set with single value. 0.1V to 105V in 0.01V programmable steps. Accuracy for 0.1V to 20V: 0.1% +20mV, accuracy for 20V to 105V: 0.1% + 100mV

MAX. OUTPUT POWER: 11W, four quadrant source or sink operation.

GUARD OUTPUT:

Maximum Load Capacitance: 10nF.

Maximum Load Current: 1mA for rated accuracy.

Accuracy: ±1mV for output currents <2mA (excluding output lead voltage drop).

PROGRAM MEMORY: (offers point-by-point control and triggering, e.g. Sweeps)

Number of Locations: 64K.

EXTERNAL TRIGGER: TTL-compatible EXTERNAL TRIGGER INPUT and OUTPUT.

Max Trigger Rate: 1000/s.

Source Notes

1. Settling times are specified into a resistive load, with a maximum resistance equal to 2V / $I_{fullscale\ of\ range}$. See manual for other load conditions.
2. Settling times to 0.1% of final value are typically <2x of 1% settling times.
3. Noise current into <100Ω.
4. RMS Noise 10Hz-20MHz (2nA – 20mA Range) Less than 1mVrms, 5mVp-p (into 50Ω load).
5. Typical values are non-warranted, apply at 23°C, represent the 50th percentile, and are provided solely as useful information.

Keithley Model 6514 Electrometer

VOLTS

RANGE	5½ DIGIT RESOLUTION	ACCURACY (1 Year)[1] 18°–28°C ±(%rdg+counts)	TEMPERATURE COEFFICIENT 0°–18°C & 28°–50°C ±(%rdg+counts)/°C
2 V	10 µV	0.025 + 4	0.003 + 2
20 V	100 µV	0.025 + 3	0.002 + 1
200 V	1mV	0.06 + 3	0.002 + 1

Note:
[1] When properly zeroed, 5½-digit. Rate: Slow (100ms integration time).

NMRR: 60dB on 2V, 20V, >55dB on 200V, at 50Hz or 60Hz ±0.1%.

CMRR: >120dB at DC, 50Hz or 60Hz.

INPUT IMPEDANCE: >200TΩ in parallel with 20pF, < 2pF guarded (10MΩ with zero check on).

SMALL SIGNAL BANDWIDTH AT PREAMP OUTPUT: Typically 100kHz (–3dB).

AMPS

RANGE	5½ DIGIT RESOLUTION	ACCURACY (1 Year)[1] 18°–28°C ±(%rdg+counts)	TEMPERATURE COEFFICIENT 0°–18°C & 28°–50°C ±(%rdg+counts)/°C
20 pA	100 aA[2]	1 + 30	0.1 + 5
200 pA	1 fA[2]	1 + 5	0.1 + 1
2 nA	10 fA	0.2 + 30	0.1 + 2
20 nA	100 fA	0.2 + 5	0.03 + 1
200 nA	1 pA	0.2 + 5	0.03 + 1
2 µA	10 pA	0.1 + 10	0.005 + 2
20 µA	100 pA	0.1 + 5	0.005 + 1
200 µA	1 nA	0.1 + 5	0.005 + 1
2 mA	10 nA	0.1 + 10	0.008 + 2
20 mA	100 nA	0.1 + 5	0.008 + 1

Notes:
[1] When properly zeroed, 5½-digit. Rate: Slow (100ms integration time).
[2] aA = 10^{-18}A, fA=10^{-15}A.

INPUT BIAS CURRENT: <3fA at T_{CAL} (user adjustable). Temperature coefficient = 0.5fA/°C.

INPUT BIAS CURRENT NOISE: <750aA p-p (capped input), 0.1Hz to 10Hz bandwidth, damping on. Digital filter = 40 readings.

INPUT VOLTAGE BURDEN at T_{CAL} ±1°C (user adjustable):
<20µV on 20pA, 2nA, 20nA, 2µA, 20µA ranges.
<100µV on 200pA, 200nA, 200µA ranges.
<2mV on 2mA range.
<4mV on 20mA range.

TEMPERATURE COEFFICIENT OF INPUT VOLTAGE BURDEN: <10µV/°C on pA, nA, µA ranges.

PREAMP SETTLING TIME (to 10% of final value): 2.5s typical on pA ranges, damping off, 3s typical on pA ranges damping on, 15ms on nA ranges, 5ms on µA and mA ranges.

NMRR: >95dB on pA, 60dB on nA, µA, and mA ranges at 50Hz or 60Hz ±0.1%. Digital Filter = 40.

OHMS

RANGE	5½-DIGIT RESOLUTION	ACCURACY (1Year)[1] 18°–28°C ±(% rdg+counts)	TEMPERATURE COEFFICIENT 0°–18°C & 28°–50°C ±(% rdg+counts)/°C	TEST CURRENT (nominal)
2 kΩ	10 mΩ	0.20+ 10	0.01 + 2	0.9 mA
20 kΩ	100 mΩ	0.15+ 3	0.01 + 1	0.9 mA
200 kΩ	1 Ω	0.25+ 3	0.01 + 1	0.9 mA
2 MΩ	10 Ω	0.25+ 4	0.02 + 2	0.9 µA
20 MΩ	100 Ω	0.25+ 3	0.02 + 1	0.9 µA
200 MΩ	1 kΩ	0.30+ 3	0.02 + 1	0.9 µA
2 GΩ	10 kΩ	1.5 + 4	0.04 + 2	0.9 nA
20 GΩ	100 kΩ	1.5 + 3	0.04 + 1	0.9 nA
200 GΩ	1 MΩ	1.5 + 3	0.04 + 1	0.9 nA

[1] When properly zeroed, 5½ digit. Rate: Slow (100ms integration time).

MAXIMUM OPEN CIRCUIT VOLTAGE: 250VDC.

PREAMP SETTLING TIME (To 10% of final reading with <100pF input capacitance): 2kΩ through 200kΩ: 2ms; 20MΩ through 200MΩ: 90ms. 2GΩ through 200GΩ: 1s.

COULOMBS

RANGE	6½ DIGIT RESOLUTION	ACCURACY (1 Year)[1,2] 18°–28°C ±(%rdg+counts)	TEMPERATURE COEFFICIENT 0°–18°C & 28°–50°C ±(%rdg+counts)/°C
20 nC	10 fC	0.4 + 50	0.04 + 10
200 nC	100 fC	0.4 + 50	0.04 + 10
2 µC	1 pC	1 + 50	0.05 + 10
20 µC	10 pC	1 + 50	0.05 + 10

Notes:
[1] Charge acquisition time must be <1000s, derate 2% for each additional 10,000s.
[2] When properly zeroed, 6½ digit. Rate: Slow (100ms integration time).

INPUT BIAS CURRENT: <4fA at T_{CAL}. Temperature coefficient = 0.5fA/°C.

Keithley Model DMM 2000 Digital Multimeter

DC CHARACTERISTICS

CONDITIONS: MED (1 PLC)[1] or SLOW (10 PLC) or MED (1 PLC) with filter of 10

ACCURACY: ±(ppm of reading + ppm of range) (ppm = parts per million) (e.g., 10ppm = 0.001%)

FUNCTION	RANGE	RESOLUTION	TEST CURRENT OR BURDEN VOLTAGE (±5%)	INPUT RESISTANCE	24 HOUR[14] 23°C ± 1°	90 DAY 23°C ± 5°	1 YEAR 23°C ± 5°	TEMPERATURE COEFFICIENT 0°–18°C & 28°–50°C
Voltage	100.0000 mV	0.1 µV		> 10 GΩ	30 + 30	40 + 35	50 + 35	2 + 6
	1.000000 V	1.0 µV		> 10 GΩ	15 + 6	25 + 7	30 + 7	2 + 1
	10.00000 V	10 µV		> 10 GΩ	15 + 4	20 + 5	30 + 5	2 + 1
	100.0000 V	100 µV		10 MΩ ±1%	15 + 6	30 + 6	45 + 6	5 + 1
	1000.000 V[9]	1 mV		10 MΩ ±1%	20 + 6	35 + 6	45 + 6	5 + 1
Resistance[15]	100.0000 Ω	100 µΩ	1 mA		30 + 30	80 + 40	100 + 40	8 + 6
	1.000000 kΩ	1 mΩ	1 mA		20 + 6	80 + 10	100 + 10	8 + 1
	10.00000 kΩ	10 mΩ	100 µA		20 + 6	80 + 10	100 + 10	8 + 1
	100.0000 kΩ	100 mΩ	10 µA		20 + 6	80 + 10	100 + 10	8 + 1
	1.000000 MΩ[16]	1 Ω	10 µA		20 + 6	80 + 10	100 + 10	8 + 1
	10.00000 MΩ[11,16]	10 Ω	700 nA // 10MΩ		150 + 6	200 + 10	400 + 10	95 + 1
	100.0000 MΩ[11,16]	100 Ω	700 nA // 10MΩ		800 + 30	1500 + 30	1500 + 30	900 + 1
Current	10.00000 mA	10 nA	< 0.15 V		60 + 30	300 + 80	500 + 80	50 + 5
	100.0000 mA	100 nA	< 0.03 V		100 + 300	300 + 800	500 + 800	50 + 50
	1.000000 A	1 µA	< 0.3 V		200 + 30	500 + 80	800 + 80	50 + 5
	3.00000 A	10 µA	< 1 V		1000 + 15	1200 + 40	1200 + 40	50 + 5
Continuity 2W	1 kΩ	100 mΩ	1 mA		40 + 100	100 + 100	120 + 100	8 + 1
Diode Test	3.00000 V	10 µV	1 mA		20 + 6	30 + 7	40 + 7	8 + 1
	10.00000 V	10 µV	100 µA		20 + 6	30 + 7	40 + 7	8 + 1
	10.00000 V	10 µV	10 µA		20 + 6	30 + 7	40 + 7	8 + 1

DC OPERATING CHARACTERISTICS[2]

FUNCTION	DIGITS	READINGS/s	PLCs[8]
DCV (all ranges),	6½[3,4]	5	10
DCI (all ranges), and	6½[3,7]	30	1
Ohms (<10M range)	6½[3,5]	50	1
	5½[3,5]	270	0.1
	5½[5]	500	0.1
	5½[5]	1000	0.04
	4½[5]	2000	0.01

DC SYSTEM SPEEDS[2,6]

RANGE CHANGE[3]: 50/s.

FUNCTION CHANGE[3]: 45/s.

AUTORANGE TIME[3,10]: <30 ms.

ASCII READINGS TO RS-232 (19.2K BAUD): 55/s.

MAX. INTERNAL TRIGGER RATE: 2000/s.

MAX. EXTERNAL TRIGGER RATE: 500/s.

DC GENERAL

LINEARITY OF 10VDC RANGE: ±(2ppm of reading + 1ppm of range).

DCV, Ω, TEMPERATURE, CONTINUITY, DIODE TEST INPUT PROTECTION: 1000V, all ranges.

MAXIMUM 4WΩ LEAD RESISTANCE: 10% of range per lead for 100Ω and 1kΩ ranges; 1kΩ per lead for all other ranges.

DC CURRENT INPUT PROTECTION: 3A, 250V fuse.

SHUNT RESISTOR: 0.1Ω for 3A, 1A and 100mA ranges. 10Ω for 10mA range.

CONTINUITY THRESHOLD: Adjustable 1Ω to 1000Ω.

AUTOZERO OFF ERROR: Add ±(2ppm of range error + 5µV) for <10 minutes and ±1°C change.

OVERRANGE: 120% of range except on 1000V, 3A and Diode.

SPEED AND NOISE REJECTION

RATE	READINGS/S	DIGITS	RMS NOISE 10V RANGE	NMRR[12]	CMRR[13]
10 PLC	5	6½	< 1.5 µV	60 dB	140 dB
1 PLC	50	6½	< 4 µV	60 dB	140 dB
0.1 PLC	500	5½	< 22 µV	—	80 dB
0.01 PLC	2000	4½	< 150 µV	—	80 dB

DC Notes

1. Add the following to "ppm of range" uncertainty:1V and 100V, 2ppm; 100mV, 15ppm; 100Ω, 15ppm; 1K-1MΩ, 2ppm; 10mA and 1A, 10ppm; 100mA, 40ppm.
2. Speeds are for 60 Hz operation using factory default operating conditions (*RST). Autorange off, Display off, Trigger delay = 0.
3. Speeds include measurement and binary data transfer out the GPIB.
4. Auto zero off.
5. Sample count = 1024, auto zero off.
6. Auto zero off, NPLC = 0.01.
7. Ohms = 24 readings/second.
8. 1 PLC = 16.67ms @ 60Hz, 20ms @ 50Hz/400Hz. The frequency is automatically determined at power up.
9. For signal levels >500V, add 0.02ppm/V uncertainty for the portion exceeding 500V.
10. Add 120ms for ohms.
11. Must have 10% matching of lead resistance in Input HI and LO.
12. For line frequency ±0.1%.
13. For 1kΩ unbalance in LO lead.
14. Relative to calibration accuracy.
15. Specifications are for 4-wire ohms. For 2-wire ohms, add 1Ω additional uncertainty.
16. For rear inputs, add the following to Temperature Coefficient "ppm of reading" uncertainty: 10MΩ 70ppm. 100MΩ 385ppm. Operating environment specified for 0° to 50°C and 50% RH at 35°C.

APPENDIX J: TRIGGER SETUP FOR DROP TOWER-HIGH SPEED CAMERA SETUP

Trigger Setup

National Semiconductor

February 1988

CD4009M/CD4009C Hex Buffers (Inverting)
CD4010M/CD4010C Hex Buffers (Non-Inverting)

General Description

These hex buffers are monolithic complementary MOS (CMOS) integrated circuits. The N- and P-channel enhancement mode transistors provide a symmetrical circuit with output swings essentially equal to the supply voltage. This results in high noise immunity over a wide supply voltage range. No DC power other than that caused by leakage current is consumed during static conditions. All inputs are protected against static discharge. These gates may be used as hex buffers, CMOS to DTL or TTL interface or as CMOS current drivers. Conversion ranges are from 3V to 15V providing $V_{CC} \leq V_{DD}$.

Features

■ Wide supply voltage range	3.0V to 15V
■ Low power	100 nW (typ.)
■ High noise immunity	0.45 V_{DD} (typ.)
■ High current sinking capability	8 mA (min.) at V_O = 0.5V and V_{DD} = 10V

Applications

- Automotive
- Data terminals
- Instrumentation
- Medical electronics
- Alarm system
- Industrial controls
- Remote metering
- Computers

Schematic and Connection Diagrams

Dual-In-Line Package

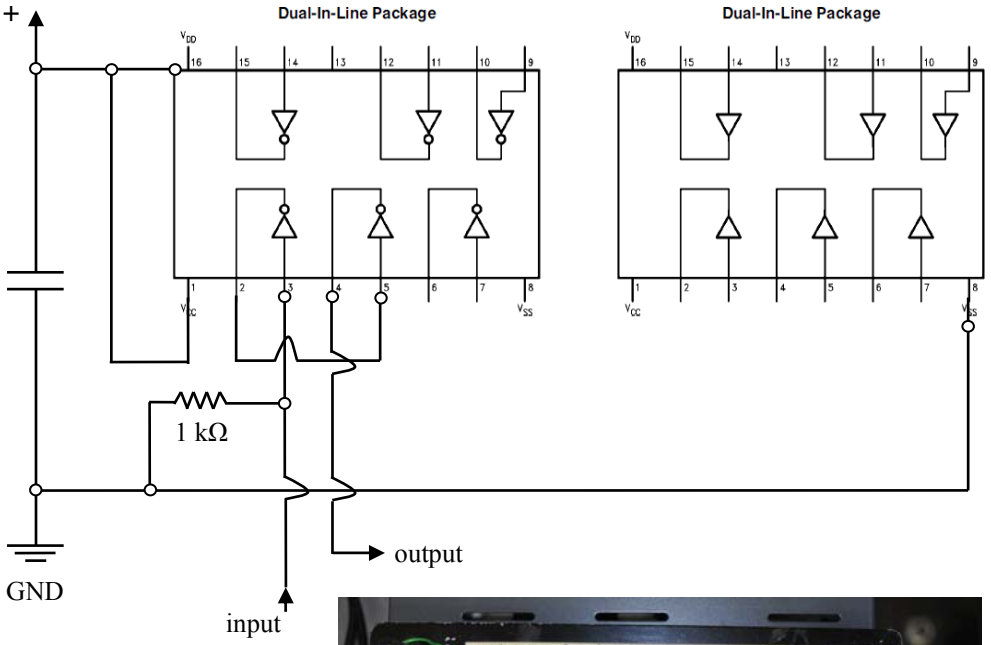

Dual-In-Line Package

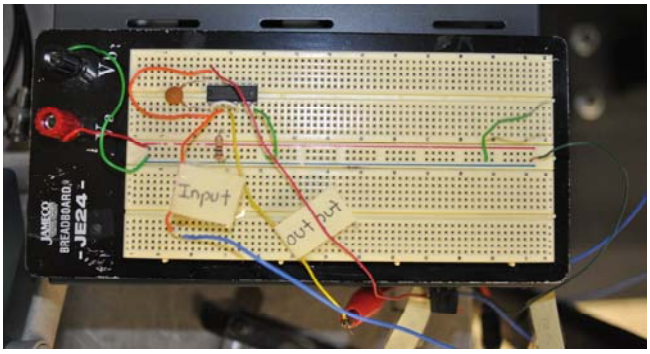

APPENDIX K: STANDARD OPERATING PROCEDURES (SOP)

SHPB

Specimen preparation:

1. The specimen dimensions should follow the below relation:

$$\frac{L}{D} = \sqrt{\frac{3\upsilon}{4}}$$

where L is the length, D is the diameter and υ is the Poisson's ratio of the specimen.

2. Make sure the faces of the specimen are parallel and flat (use step collet while machining metal specimens to get parallel faces). The diameter of the specimen after the test should be smaller than the diameter of the pressure bars.

Selecting the bar:

1. Determine the impedance (ρcA) of the specimen.

where ρ is the density, c $\left(c = \sqrt{\frac{E}{\rho}} \right)$ is the wave speed and A is the area.

2. Then select the pressure bars (steel or Aluminum) closer to the impedance of the specimen. We also have different diameters for the pressure bars.

Note: The basic thumb rule is that we use steel bars for the harder materials (metals etc..) and Aluminum bars for the softer materials (polymers, foams etc..).

3. After the pressure bars are selected, make sure the end faces of the bars are flat and parallel.
4. Align the pressure bars and striker on the mounting frame.

Experimental procedure:

(a) Give all required connections. Connections include: Connect the BNC cables from the amplifier to the oscilloscope. Check the right channels and connect them. Make sure the amplifier (2310A) and oscilloscope are grounded. Do not change any settings on the amplifier. The amplifier has been calibrated for 350 ohms strain gages. Please refer to manual if you we

wish to make any changes and let everyone in the lab know before you make any changes. Turn ON the amplifier and oscilloscope.

(a) The excitation voltage and gain are set to 10V and 100 respectively. Turn the reset switch ON for all the four channels.

(b) Check the resistance on the strain gauges and they should read around 350 ohms.

(c) Set the voltage levels, trigger position, data duration time (2ms-4ms), for all the four channels in Oscilloscope. These values depend on the experiments.

(d) Balance the Wheatstone bridge for all the four channels by turning the reset button.

(e) Check whether the bars are well aligned or not, and also the projectile should be well aligned to the impact end of the incident bar.

(f) Then make sure that the bars are moving freely, if not apply WD-40 lubricant and adjust the screws of the clamps.

(g) Clean the interfaces of the bar and the projectile with Kim wipes and ethyl alcohol.

(h) Push the projectile to the end of the barrel of gas gun assembly with a flexible poly rod.

(i) Measure the dimensions of both specimen and pulse shaper. Dimensions include: diameter and thickness.

(j) Select the striker depending on the strain rate you are trying to get. You can vary strain rate by using different pressures and different striker bars. Make sure the pulses are not getting overlapped. If the pulses are getting overlapped, use the shorter striker bar. (Thumb rule: The longer the striker, the lower the strain rate. The higher the pressure, the higher the strain rate).

(k) Lubricate both faces of the test specimen with Molybdenum disulfide lubricant and sandwich the specimen between the bars and align the specimen with respect to bar center.

(l) Place the pulse shaper at the impact end of the incident bar with a thin layer of KY jelly grease (if you are using lead pulse shaper) and align it with respect to bar center. We generally use clay and lead pulse shapers. These give us very good results for harder materials, but for the softer materials, you can try different pulse shapers. These include paper, copper etc.

(m) Release the nitrogen gas from the gas tank into the gas gun chamber until the required pressure level is achieved.

(n) Arm the oscillation to capture the strain gage voltage signals and make sure the arm holds until you release the projectile. If the arm is not holding, adjust trigger levels. (Note: if you are getting high noise in your signals more than 20mv, turn off the tube lights before the experiment).

(o) Once again, ensure that the specimen is well aligned between the bars and verify the status of the trigger hold before pressing the solenoid valve release button.

(p) Press solenoid valve control box button to release the projectile.

(q) Save captured voltage pulses onto a USB drive for further analysis of the data.

(r) A MATLAB program is written to read the data from the pulses and analyze the pulses using the one-dimensional wave theory stress and strain equations. After the experiments are performed, the pulses are used along with the MATLAB program to determine the equilibrium and true stress-strain plots of the specimen.

(s) After the experiment is completed, turn off the cylinder and make sure all the left over nitrogen gas in the gas chamber is released.

(t) After the data is transferred from the oscilloscope to USB drive, verify that in your computer and turn off the amplifier and oscilloscope.

Analyzing the results:

1. There are two MATLAB codes to analyze the data. 1. Verify_Equilibrium and 2. Steel/aluminum_SHPB. Use the appropriate codes to analyze the data. Depending on the bars you used, the respective code has to be used.

2. Make sure the code has the right properties and dimensions of the pressure bars you used. These include diameter, wave speed, and diameter.
3. If we use hollow tubes, make sure you have the right dimensions in the code. For solid bars, dimensions for the hollow tube should be zero.
4. First run the verify equilibrium code. Make sure the data you get from the oscilloscope has the following names for the four channels. TEK00000, TEK00001, TEK00002,and TEK00003. The code recognizes these names. Make sure the codes and the data are in the same folder.
5. TEK00000 and TEK00001 represent incident and reflected pulses (channel 1 and channel2). TEK00002 and TEK00003 represent the transmitted pulse (channel 3 and channel 4). The code averages channel 1 and channel 2. And channel 3 and channel 4.
6. The code converts the voltage output to microstrains and balances.
7. Default values for filtering are given in the code. For incident and reflected pulse, default value of 0.2 (fn=0.2) is used and for transmitted pulse, a value of 0.05 (fn=0.05) is used. Depending on the noise you get, change the values of fn. The value of 'fn' ranges from 0.001 to 0.99. Higher value of 'fn' means, the pulses were not filtered. Decrease the value of 'fn' if you would like to filter more. You can use different values for incident and transmitted pulses.
8. When you run the code, you get two figures. Figure 1 gives the incident and reflected pulses. Figure 2 gives the transmitted pulse.

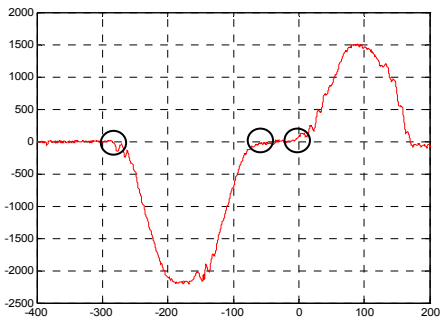

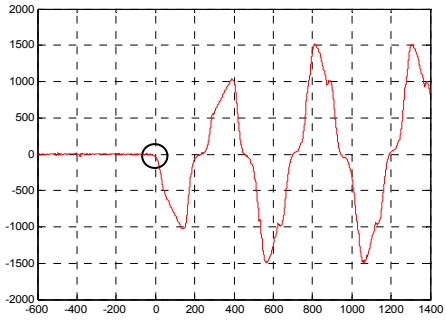

9. Note the incident starting time, incident end time, reflected starting time and transmitted starting time as shown in the above figures. You can zoom the

pulses by pressing ‘zoom in’ button at the top to get the right times. Then go to MATLAB main window and press ‘ENTER’.

10. Input the values you found out and press ‘ENTER’.
11. Now you will get 3 more Figures. Figure 3 shows the incident, reflected and transmitted pulses. Figure 4 shows the incident, reflected and transmitted pulses you picked on before. Figure 5 shows the force ratio. Front face represents the forces calculated on the incident and reflected pulses. Back face represents the force calculated on the transmitted pulse. Ideally, these two fronts and back face should match perfectly.
12. Various factors decide the equilibrium. These include type of material tested, strain rate etc..
13. Make sure the incident and reflected pulses start at the same time on Figure 4. On the first trial, you might end up something as below

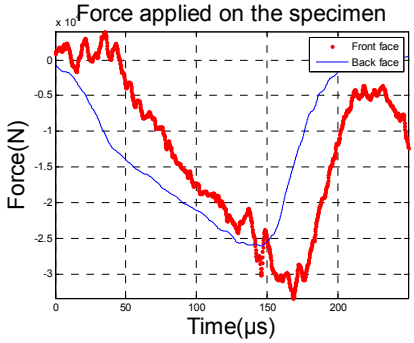

14. Go back to the times you found for the incident, reflected and transmitted pulses. Never change the times of reflected and transmitted pulses. Shift the incident pulse to either side and try for different values until you get decent equilibrium. For the case shown above, by shifting the time of the incident pulse, the below equilibrium was obtained.

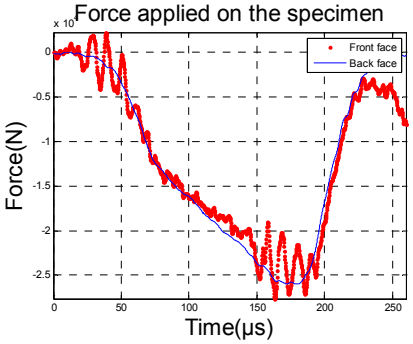

15. Save this Figure in to the respective folder. Also save the new times of the pulses.
16. Now open the SHPB code and make sure you have the same value for filter as in the verify_equilibrium code.
17. Enter the specimen thickness and diameter in inches.
18. Again, you get two figures. Figure 1 gives the incident and reflected pulses. Figure 2 gives the transmitted pulse.
19. Go to main 'MATLAB' window and enter the final times here.
20. You get Eng. stress strain curve (Figure 3) and True stress-strain curve (Figure 4).
21. Follow the directions of the Figure 4.
22. Pick two points to calculate the slope. You can pick at the initial elastic region of the true stress-strain curve.
23. You will end up with Figure 5. Pick two points at the linear region as shown below.

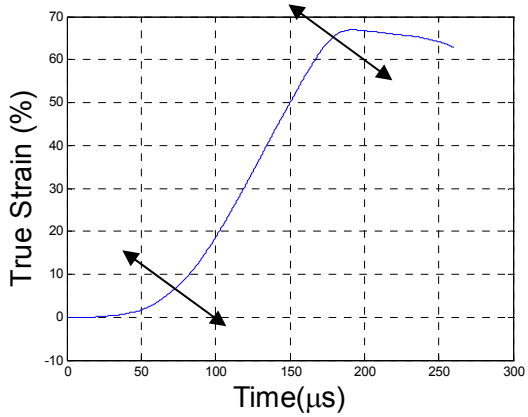

24. Go to MATLAB main window and you can see the strain rate. Note down this value. Next you will end up with final figure (Figure 6). This is eng. strain rate vs. time.
25. Be careful when you pick up the strain rate points. Consider the following points
    a. Make sure the region you pick is in the equilibrium.

b. For foam materials, you might not get very good equilibrium and constant strain rate. So calculate the strain rate over the entire loading duration.

Tensile SHPB:

Procedure:

1. The specimen dimensions are given below. These dimensions vary with the material tested. For metals, the below dimensions can be used. To perform experiments at lower strain rate, increase the gage diameter (D) to 0.2". For plastics, use gage length of 0.2" and gage diameter of 0.2".

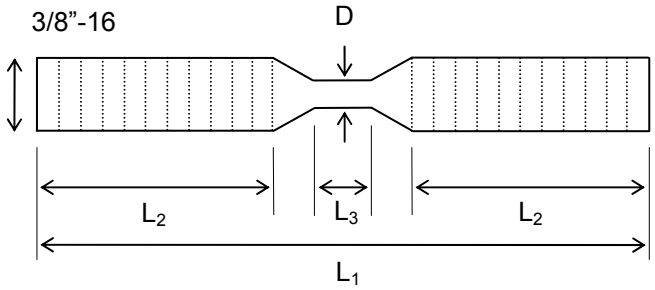

D (Diameter) = 0.15"

L_1 = 1.5"

L_2 = 0.56"

2. Selecting the bar is same as explained before.
3. Experimental procedure is also similar to the above. Here, you place the pulse shaper on the flange. You can use paper, clay or lead.
4. Different striker bars can be used to perform experiments at different strain rates. Make sure the striker bar slides freely on the bars.
5. The specimen will be threaded at both ends to the pressure bars. There is no need to use the lubricant.
6. The connections remain the same as explained before. You can use the same amplifier and oscilloscope, and same settings.
7. The MATLAB codes have been modified and use the appropriate code to perform your analysis. The steps to run the code is same as explained for compression SHPB.

Electro-mechanical SHPB:

1. To ensure proper electrical measurements, both the incident and transmitter bar must be completely isolated from any external fixtures. To do this, nylon bushings are used to hold both bars rather than brass.
2. Lead wires should be securely attached to each bar to provide a means of supplying a DC current flow through the specimen during loading.
3. Apply a conductive lubricant (i.e. AI Technology Inc. ELGR8501) to the specimen faces to minimize contact resistance as well as frictional forces at the specimen-bar interfaces.
4. A pulse shaper must be carefully chosen to provide good force equilibrium conditions while still ensuring complete isolation between the striker bar and incident bar throughout the experiment. An example of a pulse shaper used is 1 layer of electrical tape and clay (~ 2 mm thick).
5. The voltage across the specimen can be measured one of two ways. Additional lead wires can be attached to the incident and transmitter bar. This approach provides a better volumetric measurement and has less risk of having the measurement probes disturbed/damaged during the experiment. The other option is to implement the concentric ring method where two very small concentric rings are machined into the surface of the specimen, filled with silver paint and lead wires are attached. This method is more accurate in the sense that the contact resistance between the bar and specimen is avoided. However, validation experiments were completed to ensure very minimal difference between the two measurement techniques.
6. A constant current source with high frequency response (Keithley Instruments Model 6221) was used to supply the constant DC current flow under the high rate deformation while the voltage drop between the two inner probes was measured by a differential amplifier (Tektonix ADA 400A) and recorded by a digital oscilloscope (Tektronix TDS 3014).
7. It is important to note that proper strain gage selection is critical in preventing any electrical interference in strain measurements while conducting these types of experiments. The particular strain gages chosen (Micro-Measurements C2A-

13-250LW-350) consists of an encapsulated gage mounted on a thin high-performance laminated polyimide film backing. The polyimide film backing provides a layer of insulation between the actual gage and the bar surface and therefore prevents any voltage interference. A series of experiments were performed with and without supplying current through the bars, validating that the strain gages bonded to the bars remain unaffected.

8. **Compression SHPB at elevated temperatures:**

1. The tungsten carbide inserts will be used. The specimen will be sandwiched between these inserts.
2. The diameter of the specimen should be smaller than the inserts. The below figure shows the set up.

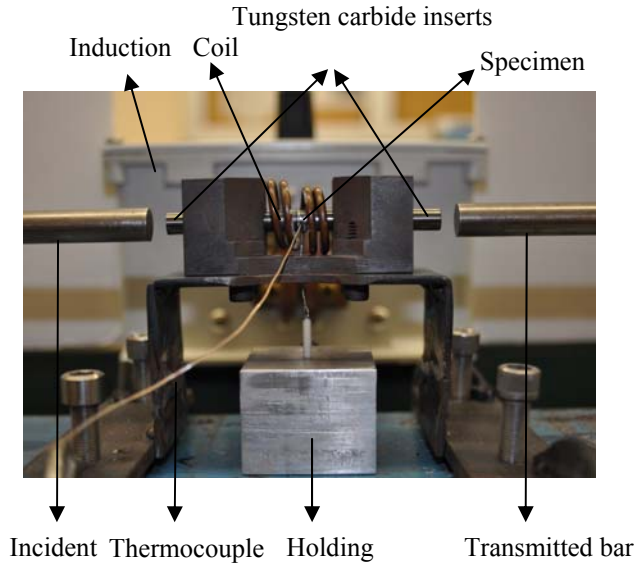

3. For experiments at elevated temperatures, the SHPB apparatus in conjunction with the induction coil heating system will be utilized as shown in Fig. 2.
4. A special fixture is used to load the specimen.
5. The inserts were used to eliminate the temperature gradient in the bars and thus protect the strain gages mounted on them.
6. The impedance of the inserts was matched with the bars; hence they do not disturb the stress wave profiles in the bar. The impedance matching requires the diameter of these tungsten carbide inserts to be smaller than the main

pressure bars. This is the reason for the specimen diameter for high temperature testing being smaller than that for room temperature testing.

7. By varying the power, higher temperatures can be achieved.
8. The induction coil heating system has a power control box, remote to start and stop, a cooling unit and cooling supply (blue box) to reserve water. Make sure the blue box has sufficient distilled water. The copper coils are connected to the cooling unit and it is places around the inserts.
9. First turn ON the blue box, then the power supply. The power supply needs the larger output in the DPML lab.
10. Make sure the wheel on the cooling unit is pinning smoothly and fast. If not, do not do the experiment. Increase the power supply, to heat the specimen.
11. When the regulator is turned ON, it should give a click sound after around 30s. If it does not, turn it off and try again. If the problem persists, turn off the regulator and the problem can be determined.
12. Turning ON the power supply regulator, it will read 'cycle continuous' on the remote (smallest one), which is desired.
13. The system should already be set to manual power output again, which will allow to control the power. If it is not set, you can do by using the switch located to the immediate right of the dial on the regulator.
14. Make sure the dial on the regulator is zero, so there will be no immediate power output.
15. Now press 'start' button on the remote (small one that reads the diaplay).
16. The bars were kept apart initially, later the specimen and carbide inserts were heated in isolation to the desired temperature (usually about 20-50°C higher than the test temperature) and soon after the bars were brought manually into contact with the specimen. The temperature of the specimen was monitored using a 0.127mm chromel-alumel thermocouple, which was spot welded onto the specimen.

17. In most of the experiments, it takes less than two minutes to heat the specimen to the required temperature and it takes less than 10 seconds to bring the pressure bars into contact with the tungsten inserts and fire the gun.
18. Once the temperature is reached, hit ‘stop’ on the display and turn off the regulator and the induction heater. Now trigger the oscilloscope. If you trigger the oscilloscope before, due to magnetic fields from the induction heater, you will see lot of noise.
19. Allow the cooling unit to run for some time son that it reaches room temperature.
20. All other experimental procedure, data capturing, and analyzing the results remain the same as explained in compression SHPB section.

Note:

1. Always make sure the yield strength of the material you are testing is never beyond the yield strength pressure bars.
2. For testing ceramics of high strength, we need to use inserts so as to protect the bars from plastic deformation.

APPENDIX L: SAFETY GUIDELINES FOR EXPERIMENTAL EQUIPMENT

SHPB

1. Never perform experiment without the help of other students
    a. For ease of conducting a safe and efficient experiment
2. Make sure proper precautions are made prior to experiment
    a. Wear safety glasses at al l times
    b. Long sleeve shirts and shoes should be worn, no open toe shoes or sandals
    c. Make sure all wires and gauges are adhered correctly and prepared properly
3. Make sure proper bars are being used depending upon specific materials being tested (steel or aluminum bars)
    a. Solid-Solid Bar (hard materials)
    b. Solid-Hollow Bar (soft materials)
    c. Hollow-Hollow (real soft materials)
4. **DO NOT PRESSURIZE GUN UNTIL YOU ARE ABOUT TO FIRE**
    a. Do not put fingers between bars, i.e. striker and incident bar or incident and transmitter bar when SHPB is pressurized
    b. Do not stand in front of muzzle or try to load striker bar when pressurized
    c. Do not leave bar unattended after pressurized
    d. If adjustments are needed, vent the pressure beforehand
5. Conduct yourself in a mature and responsible manner at all times in the laboratory
6. Make sure to yell “firing” when experiment is about to be run and SHPB is being pressurized, keep outside doors closed so no one walks in
7. Make sure everyone in the lab, helping or not with the experiment, is aware an experiment will be taking place

Safety Hazards Associated with Handling Liquid Nitrogen:

1. The extremely low temperature of the liquid can cause **severe frostbite or eye damage** upon contact. Items in contact with liquid nitrogen become extremely cold. Touching these items may result in torn flesh. Many substances become brittle upon contact with liquid nitrogen and may shatter when cold (such as common glass and large solid plastics), sending pieces of the material flying.

2. On vaporization it expands by a factor of 700; one liter of liquid nitrogen becomes 24.6 cubic feet of nitrogen gas. This can cause **explosion** of a sealed container. This release of nitrogen can also displace oxygen in the room and cause **asphyxiation** without warning.

3. Because the boiling point of oxygen is above that of nitrogen, oxygen can condense from the air into the liquid nitrogen. If dewars and insulated flasks containing liquid nitrogen are left uncovered for an extended period of time, liquid oxygen can build up to levels which may cause **violent reactions** with organic materials (i.e. a severe clothing fire could result).

Personal Protective Equipment (PPE) Required When Handling Liquid Nitrogen:

1. **Safety goggles (unvented)** – Required at all times.

2. **Face shield** – Required when pouring or filling.

3. **Insulating gloves** (gloves should be loose fitting, so they can be thrown off if liquid pours inside them, or they should be elastic cuff insulated gloves). – Required when pouring or filling.

4. **A lab coat or long sleeves** is required to minimize skin contact. Also, trousers should be worn on the outside of boots or work shoes to prevent shoes filling in the event of a spillage. – Required when pouring or filling.

Rules and Precautions for Handling Liquid Nitrogen:

1. You must have Department approval prior to handling liquid nitrogen.

2. Always wear PPE when handling liquid nitrogen.

3. Use liquid nitrogen only in well ventilated places. Never dispose of liquid nitrogen by pouring it on the floor. It could displace enough oxygen to cause suffocation. Nitrogen is colorless and odorless – the cloud that forms when you pour liquid nitrogen is condensed water vapor from the air, not nitrogen gas.

4. Do not allow any liquid nitrogen to touch any part of your body or become trapped in clothing near the skin.

5. Do not touch any item that has been immersed in liquid nitrogen until it has warmed to room temperature.

6. Do not store liquid nitrogen in any container with a tight fitting lid. A tightly sealed container will build up pressure as the liquid boils and may explode after a short time. Use only approved unsealed containers. Do not store liquid nitrogen for long periods in an uncovered container. Use only fittings that have been designed specifically for use with cryogenic liquids as non-specialized equipment may crack or fail. Do not transport liquid nitrogen in wide-mouthed glass dewars or dewars not protected with safety tape.

7. Never dip a hollow tube into liquid nitrogen; it may spurt liquid.

8. **Never ride in an elevator with liquid nitrogen!** When using passenger elevators, use an elevator key to prevent the door from being opened by unauthorized persons. If a key is not available, then station a person at each floor to ensure no one enters.

9. Note that outside of normal working hours (M-F, 8:00 a.m. – 5:00 p.m.), no one is allowed to transfer liquid nitrogen from the Dow loading dock area without a second person present. Failure of a container or a large spillage could result in asphyxiation at a time when you are unlikely to be found or able to get assistance.

10. Always fill warm dewars slowly to reduce temperature shock effects and to minimize splashing.

11. Always make sure that containers of liquid nitrogen are suitably vented and unlikely to block due to ice formation.

12. Do not fill cylinders and dewars to more than 80% of capacity, since expansion of gases during warming may cause excessive pressure buildup.

APPENDIX M: MATLAB CODES

Data Retrieval Code for Voltage – Time Data From Quasi-static Experiments

```
% This program can be used to extract the time and voltage data recorded
% using the quasi-static electrical measurement system.  The time and
% voltage data are saved within a .lvm file. First, change the .lvm file to a .m
% file then place in same directory as this code.
%
clc;
clear all;
s = load('DataFPP.m');
n = 0; m = 0;
t = length(s);
for i = 1:t
   if mod(i,2)== 0;
      n= n+1;
      x(n) = s(i,2);
   else
      m = m+1;
      y(m) = s(i,2);
   end
end
T = [x', y'];
```

Spline Code for Data Analysis with Drop Weight Tower and SHPB Experiments (without Strain Data)

```
% This program can be used to spline the load and resistance data obtained
% during a drop weight tower so that the two data sets can be plotted
% against each other due to the difference in frequency response.
%
clear all;
close all;
clc;
 load resistance.txt
load force.txt

time_period=min([resistance(length(resistance(:,1)),1),force(length(force(:,1)),1)]);

n0=input('how many time step you want? (integer) ');

dt=time_period/n0;
```

```
for i=1:n0
   t(i,1)=(i-1)*dt;
end

res_modified(:,1)=t;
res_modified(:,2)=spline(resistance(:,1),resistance(:,2),t);

Figure(1)
plot(resistance(:,1),resistance(:,2),'r'); hold on;
plot(res_modified(:,1),res_modified(:,2),'b'); hold on;
title('resistance')
grid on;
xlabel('time (s)')

force_modified(:,1)=t;
force_modified(:,2)=spline(force(:,1),force(:,2),t);

Figure(2)
plot(force(:,1),force(:,2),'r'); hold on;
plot(force_modified(:,1),force_modified(:,2),'b'); hold on;
title('force')
grid on;
xlabel('time (s)')


save modifed_resistance.txt res_modified /ascii
save modifed_force.txt force_modified /ascii
```

(with strain data)

```
% This program can be used to spline the load, strain and resistance data obtained
% during a drop weight tower so that the two data sets can be plotted
% against eachother due to the difference in frequency response.
%
clear all;
close all;
clc;

load resistance.txt
load force.txt
load strain.txt

time_period=min([resistance(length(resistance(:,1)),1),force(length(force(:,1)),1),strai
n(length(strain(:,1)),1)]);
```

```
n0=input('how many time step you want? (integer) ');

dt=time_period/n0;

for i=1:n0
   t(i,1)=(i-1)*dt;
end

res_modified(:,1)=t;
res_modified(:,2)=spline(resistance(:,1),resistance(:,2),t);

Figure(1)
plot(resistance(:,1),resistance(:,2),'r'); hold on;
plot(res_modified(:,1),res_modified(:,2),'b'); hold on;
title('resistance')
grid on;
xlabel('time (s)')

force_modified(:,1)=t;
force_modified(:,2)=spline(force(:,1),force(:,2),t);

Figure(2)
plot(force(:,1),force(:,2),'r'); hold on;
plot(force_modified(:,1),force_modified(:,2),'b'); hold on;
title('force')
grid on;
xlabel('time (s)')

strain_modified(:,1)=t;
strain_modified(:,2)=spline(strain(:,1),strain(:,2),t);

Figure(3)
plot(strain(:,1),strain(:,2),'r'); hold on;
plot(strain_modified(:,1),strain_modified(:,2),'b'); hold on;
title('strain')
grid on;
xlabel('time (s)')


save modifed_resistance.txt res_modified /ascii
save modifed_force.txt force_modified /ascii
save modifed_strain.txt strain_modified /ascii
```

Measurement Code to Obtain Strain Data using High Speed Photography (Drop Weight Tower)

```
%%%%%%%%%%%%%%%%%%%%%%%%%%%%%%%%
% This program is for calculating the strain demonstrated by the specimen during
% a drop weight experiment
%%%%%%%%%%%%%%%%%%%%%%%%%%%%%%%%
clear all;
close all;
clc;
format long;

disp('%%%%%%%%%%%%%%%%%%%%%%%%%%%%%%%%');
disp('This program is for calculating the energy that bends the specimen during a shock tube experiment.');
disp('Please follow the instruction.');
disp('%%%%%%%%%%%%%%%%%%%%%%%%%%%%%%%%');
disp(' ');

% disp('%%%%%%%%%%%%%%%%%%%%%%%%%%%%%%%%');
% disp('First Step: load the reflection pressure profile.');
% disp(' ');
% disp('The reflection pressure profile should have following form:');
% disp('0.00001  124');
% disp('0.00002  160');
% disp('0.00003  215');
% disp('0.00004  260');
% disp('0.00005  302');
% disp('The first column is time. And second column is pressure.');
% disp('You need to input the unit of time and pressure. Please check the unit carefully.');
% disp('Please follow the instruction.');
% disp(' ');
%
% disp('Now please input the filename of the reflect pressure profile with specimen (without extension):');
% reflect_name=input('(For example: ref_sp) ','s');
% disp('Now please input the extension of the reflect pressure profile with specimen:');
% reflect_extension=input('(for example: dat) ','s');
% eval(['load ',reflect_name,'.',reflect_extension,';'])
% disp(' ');
%
% disp('We have following time unit:');
% disp('1. second');
```

```
% disp('2. millisecond');
% disp('3. microsecond');
% unit_judge=true;
% time_unit=0; % this number can be any integer except 1, 2 and 3.
% while unit_judge==true
%     time_unit=input('Please choose the unit you use (input the No. before the unit):');
%     if time_unit==1
%         disp(' ');
%         disp('The time unit you use is second;');
%         eval(['ref_sp(:,1)=',reflect_name,'(:,1);'])
%         unit_judge=false;
%     elseif time_unit==2
%         disp(' ');
%         disp('The time unit you use is millisecond;');
%         eval(['ref_sp(:,1)=',reflect_name,'(:,1)./1000;'])
%         unit_judge=false;
%     elseif time_unit==3
%         disp(' ');
%         disp('The time unit you use is microsecond;');
%         eval(['ref_sp(:,1)=',reflect_name,'(:,1)./1000000;'])
%         unit_judge=false;
%     else
%         disp('Wrong input. Please choose again.');
%         unit_judge=true;
%     end
% end
% disp(' ');
%
% disp('We have following pressure unit:');
% disp('1. psi');
% disp('2. MPa');
% disp('3. Pa');
% unit_judge=true;
% pressure_unit=0; % this number can be any integer except 1, 2 and 3.
% while unit_judge==true
%       pressure_unit=input('Please choose the unit you use (input the No. before the
unit):');
%     if pressure_unit==1
%         disp(' ');
%         disp('The pressure unit you use is psi;');
%         eval(['ref_sp(:,2)=',reflect_name,'(:,2);'])
%         unit_judge=false;
%     elseif pressure_unit==2
%         disp(' ');
%         disp('The pressure unit you use is MPa;');
```

```
%        eval(['ref_sp(:,2)=',reflect_name,'(:,2).*1000000./6894.7;'])
%        unit_judge=false;
%    elseif pressure_unit==3
%        disp(' ');
%        disp('The pressure unit you use is Pa;');
%        eval(['ref_sp(:,2)=',reflect_name,'(:,2)./6894.7;'])
%        unit_judge=false;
%    else
%        disp('Wrong input. Please choose again.');
%        unit_judge=true;
%    end
% end
% disp(' ');
%
% disp('The pressure data has been resaved into variable ref_sp.');
% disp('There are two columns in ref_sp. The first column is time and unit is s
(second).');
% disp('The second column is pressure and unit is psi.');
% disp('First Step end');
% disp('%%%%%%%%%%%%%%%%%%%%%%%%%%%%%%%%%%%%%%%%%%%%%%%%%%%%%%%%');
% disp(' ');
%

disp('%%%%%%%%%%%%%%%%%%%%%%%%%%%%%%%%%%%%%%%%%%%%%%%%%%%%%%%%');
disp('First Step: load the time series of the images.');
disp(' ');

disp('You have three ways to load the time series of the images.');
disp('1. The time between two frames is same.');
disp('   You can input total number of frames and time between two frames.')
disp('   The code will generate the time series automatically.');
disp(' ');

disp('2. The time between two frames is not same.');
disp('    You can input total number of frames and input time between two frames
frame by frame.')
disp(' ');

disp('3. The time between two frames is not same.');
disp('   And you have saved the time series into one data file.')
disp('   Then you can just load that time series data file.');
disp(' ');

time_series_judge=true;
time_series=0; % this number can be any integer except 1, 2 and 3.
```

```
while time_series_judge==true
   time_series=input('Please choose which method you want to use (input the No. before the method):');
   if time_series==1
      frames=input('Please input the total number of frames for calculating(integer): '); % the number of images for calculating
      frame_time=input('Please input the time between two frames (unit: microsecond): ')/1000000;
      for i=1:frames
         t_frame(i,1)=(i-1)*frame_time;
      end
      time_series_judge=false;
   elseif time_series==2
      frames=input('Please input the total number of frames for calculating(integer): '); % the number of images for calculating
      sum_time=0;
      for i=1:frames
         disp('recent frame is')
         i
         disp('frame.')
         disp('Please input 0 when i=1;');
         sum_time=input('Please input the time between this frame and one frame before(unit: \mus): ')/1000000+sum_time;
         t_frame(i,1)=sum_time;
      end
      time_series_judge=false;
   elseif time_series==3
      time_series_name=input('Please input the filename of the time serise (without extension):','s')
      time_series_extension=input('Please input the extension of the time serise:','s')
      eval(['load ',time_series_name,'.',time_series_extension,';'])
      eval(['t_frame=',time_series_name,';'])
      time_series_judge=false;
   else
      disp('Wrong input. Please choose again.');
      time_series_judge=true;
   end
end
disp(' ');

disp('Second Step end');
disp('%%%%%%%%%%%%%%%%%%%%%%%%%%%%%%%%%%%%%%%%%%%%%%%%%%%%%%%%');
disp(' ' );
```

```
disp('%%%%%%%%%%%%%%%%%%%%%%%%%%%%%');
disp('Third Step: length calculation.');
disp(' ');
disp('you can choose any image for length calculation.');
disp('you need to know one real scale in the image.');
disp('For example, ');
disp('the span of the supports is 6 inches');
disp('the outer diameter of the shock tube is 5 inches');
disp('Please follow the instruction.');
disp(' ');

disp('Please enter image filename for length calibration:');
I=input('(for example: calibration.jpg) ','s');
Judge1='n';
while Judge1=='n'
   % load the jpg file
   imshow(I);
   hold on

   xlabel('Length Calculation')
   title('Please pick first point for calibration');
   [xc(1),yc(1)] = ginput(1);
   title('Please pick second point for calibration');
   [xc(2),yc(2)] = ginput(1);
   title('Please pick third point for calibration');
   [xc(3),yc(3)] = ginput(1);
   title('Please pick fourth point for calibration');
   [xc(4),yc(4)] = ginput(1);
   title('Please pick fifth point for calibration');
   [xc(5),yc(5)] = ginput(1);
   title('Please pick sixth point for calibration');
   [xc(6),yc(6)] = ginput(1);

   title('Please go to the matlab main window and input the real distance');
   % average point between two calibration points
   X(1) = abs(xc(1)-xc(2));
   X(2) = abs(xc(3)-xc(4));
   X(3) = abs(xc(5)-xc(6));
   measured = mean(X);

   % determin the middle position of the shock tube
   xm(1)=(xc(1)+xc(2))/2;
   xm(2)=(xc(3)+xc(4))/2;
   xm(3)=(xc(5)+xc(6))/2;
   midx=mean(xm);
```

```
    % real distance between two calibration points. unit: m
    true = input('Please input the real distance between two points you choose (in): ')*0.0254;

    % The transfor from the pixes to distance
    scale = measured/true;

    xlabel('')
    title('Length Calculation End');

    Judge1=input('Is calibration OK? (y/n)','s');

    close all;
end

disp('Third Step end');
disp('%%%%%%%%%%%%%%%%%%%%%%%%%%%%%%%%%%%%');
disp(' ' );

disp('%%%%%%%%%%%%%%%%%%%%%%%%%%%%%%%%%%%%');
disp('Fourth Step: real measurement.');
disp(' ');
disp('you need to measure the deformation shape of front face for every image.');
disp('For each image, you need to choose seven points on the front face.');
disp('There will be a symmetric line on the image.');
disp('It is better to choose these points symmetric to this line.');
disp('Please follow the instruction.');
disp(' ');

% origin_t=input('Original thickness of specimen (in): ')*0.0254;

for i = 1:frames

    disp(' ');
    if i==1
        disp('Please enter the first image filename for measurement:');
        I=input('(for example: measure_image.jpg) ','s');
    else
        I=input('Please enter next image filename for measurement: ','s');
    end

    % Simulate the Front Surface Shape with Cubic Spline interpolation method
    Judge2='n';
    while Judge2=='n'
```

```
    imshow(I);
    hold on;
    xlabel('displacement measurement');

%       x1=linspace(0,1200);
%       y1=linspace(midy,midy);
%       plot(x1,y1,'c-.')

%       if i==1
%       else
%          plot(xx(:,(i-1)),yy(:,(i-1)),'y','linewidth',0.25), hold on;
%          legend('symmetric line','previous shape');
%       end

    % choose seven points for the surface shape fit
    title('Please pick the first point for displacement calculation');
    [x(1,i),y(1,i)] = ginput(1);
    plot(x(1,i),y(1,i),'go'),hold on;

    title('Please pick the second point for displacement calculation');
    [x(2,i),y(2,i)] = ginput(1);
    plot(x(2,i),y(2,i),'go'),hold on;

    title('Please pick the third point for displacement calculation');
    [x(3,i),y(3,i)] = ginput(1);
    plot(x(3,i),y(3,i),'go'),hold on;

    title('Please pick the fourth point for displacement calculation');
    [x(4,i),y(4,i)] = ginput(1);
    plot(x(4,i),y(4,i),'go'),hold on;

    title('Please pick the fifth point for displacement calculation');
    [x(5,i),y(5,i)] = ginput(1);
    plot(x(5,i),y(5,i),'go'),hold on;

    title('Please pick the sixth point for displacement calculation');
    [x(6,i),y(6,i)] = ginput(1);
    plot(x(6,i),y(6,i),'go'),hold on;

%       title('Please pick the seventh point for displacement calculation');
%       [x(7,i),y(7,i)] = ginput(1);
%       plot(x(7,i),y(7,i),'go'),hold on;

%       d=Tube_d*scale; % the pixes scale of the diameter of shock tube
%       dD=d/100;
```

```
%       for m=1:101
%          yy(m,i)=midy-(d/2)+(m-1)*dD; % the range of shock applied
%       end
%       xx(:,i)=spline(y(:,i),x(:,i),yy(:,i));   % cubic spline data interpolation
%       plot(xx(:,i),yy(:,i),'r'), hold on;
%
%       title('Press any key to continue');
%       pause;

      Y(1) = abs(y(2,i)-y(1,i));
      Y(2) = abs(y(4,i)-y(3,i));
      Y(3) = abs(y(6,i)-y(5,i));
      measured = mean(Y)/scale;

      if i==1
         origin_t= measured;
      end

      Strain(i,1)=t_frame(i,1);
      Strain(i,2)=(origin_t-measured)/origin_t;

      Judge2=input('Is the measurement OK? (y/n)','s');

      close all;
   end
end

% % calculate the surface position of every frame
% xf=xx(:,1);
% yf=yy(:,1);
%
% for i = 1:frames
%    for j=1:101
%       xd(j,i)=(xx(j,i)-xf(i))/scale;
%    end
% end
%
% % calculate the deflection for every points of every frame
% for j=1:101;
%    for i=1:frames
%       xdd(j,i)=abs(xd(j,i)-xd(j,1));
%    end
% end

% Figure(2)
```

```
% for i=1:frames;
%     plot(-xdd(:,i),yy(:,i)/scale,'k'),hold on
%     plot(-xdd(:,2),yy(:,1)/scale,'k--'),hold on
%     plot(-xdd(:,3),yy(:,1)/scale,'r'),hold on
%     plot(-xdd(:,4),yy(:,1)/scale,'r--'),hold on
%     plot(-xdd(:,5),yy(:,1)/scale,'g'),hold on
%     plot(-xdd(:,6),yy(:,1)/scale,'g--'),hold on
%     plot(-xdd(:,7),yy(:,1)/scale,'b'),hold on
%     plot(-xdd(:,8),yy(:,1)/scale,'b--'),hold on
%     plot(-xdd(:,9),yy(:,1)/scale,'m'),hold on
% end
% plot(-xdd(:,10),yy(:,1)/scale,'m--'),hold on
% plot(-xdd(:,11),yy(:,1)/scale,'y'),hold on
% plot(-xdd(:,12),yy(:,1)/scale,'c'),hold on
% plot(-xdd(:,13),yy(:,1)/scale,'c--'),hold on
% xlabel('unit: m');
% ylabel('unit: m');
% title('Deflection Sketch');
% axis tight

% choose the biggest time to normalize data
% n0=length(ref_sp(:,1));
% for i=1:n0
%     t(i,1)=ref_sp(i,1);
%     ref(i,1)=ref_sp(i,2);
%     if (ref_sp(i,1)>=t_frame(frames,1))
%         break;
%     end
% end
%
% % normalize the time for deflection data
% for j=1:101
%     De(:,j)=spline(t_frame,xdd(j,:),t);
% end
%
% Figure(3)
% plot(t,De(:,51),'r','linewidth',3),hold on
% ylabel('Deflection (m)');
% xlabel('Time (s)');
% grid on;
% title('Maxi Deflection-Time Curve(Middle Point)');
%
% % calculate the energy increase between every two closed frame
% n0=length(t);
% egy(1)=0;
```

```
% delta_d=(Tube_d*0.99)/99;
% for i=2:n0
%     A(i)=0;
%     for j=1:100
%                                     B(j)=((ref_sp(i,2)+ref_sp(i-1,2))*6894.7)*(De(i,j)-De(i-
1,j))*delta_d*(sqrt((Tube_d/2)^2-((Tube_d/2)-j*delta_d)^2)+sqrt((Tube_d/2)^2-
((Tube_d/2)-(j-1)*delta_d)^2))/2;
%         A(i)=B(j)+A(i);
%     end
%     egy(i)=A(i);
% end
%
% % calculate the energy increase between every frame and initial frame
% for i=1:n0
%     A1=0;
%     for j=1:i
%         B1=egy(j);
%         A1=A1+B1;
%     end
%     energy(i,1)=A1;
% end
%
% DFLE(:,1)=t;
% DFLE(:,2)=energy(:,1);
%
% Figure(4),plot(t,energy(:,1),'r','linewidth',3);
% xlabel('Time (s)');
% ylabel('Energy (J)');
% % axis tight;
% grid on;
%
% Figure(5),plot(De(:,50),energy(:,1),'r','linewidth',3);
% xlabel('Deflection (m)');
% ylabel('Energy (J)');
% grid on;

Figure(1)
plot(Strain(:,1),Strain(:,2),'r','linewidth',3), hold on
xlabel('Time (\mus)')
ylabel('Strain')
grid on;

filename=input('Please input the filename you want to save final data into: ','s');

save strain.mat;
```

```
eval(['save ',filename,'_Strain.DAT',' Strain',' /ascii'])

clc
```

(split Hopkinson pressure bar)

```
%%%%%%%%%%%%%%%%%%%%%%%%%%%%%%%%%%%%%%%%%%%%
% This program is for calculating the strain demonstrated by the specimen during
% a SHPB compression experiment
%%%%%%%%%%%%%%%%%%%%%%%%%%%%%%%%%%%%%%%%%%%%
clear all;
close all;
clc;
format long;

disp('%%%%%%%%%%%%%%%%%%%%%%%%%%%%%%%%%%%%%%%%%%%%');
disp('This program is for calculating the energy that bends the specimen during a shock tube experiment.');
disp('Please follow the instruction.');
disp('%%%%%%%%%%%%%%%%%%%%%%%%%%%%%%%%%%%%%%%%%%%%');
disp(' ');

% disp('%%%%%%%%%%%%%%%%%%%%%%%%%%%%%%%%%%%%%%%%%%%%');
% disp('First Step: load the reflection pressure profile.');
% disp(' ');
% disp('The reflection pressure profile should have following form:');
% disp('0.00001  124');
% disp('0.00002  160');
% disp('0.00003  215');
% disp('0.00004  260');
% disp('0.00005  302');
% disp('The first column is time. And second column is pressure.');
% disp('You need to input the unit of time and pressure. Please check the unit carefully.');
% disp('Please follow the instruction.');
% disp(' ');
%
% disp('Now please input the filename of the reflect pressure profile with specimen (without extension):');
% reflect_name=input('(For example: ref_sp) ','s');
% disp('Now please input the extension of the reflect pressure profile with specimen:');
% reflect_extension=input('(for example: dat) ','s');
% eval(['load ',reflect_name,'.',reflect_extension,';'])
% disp(' ');
%
```

```
% disp('We have following time unit:');
% disp('1. second');
% disp('2. millisecond');
% disp('3. microsecond');
% unit_judge=true;
% time_unit=0; % this number can be any integer except 1, 2 and 3.
% while unit_judge==true
%     time_unit=input('Please choose the unit you use (input the No. before the unit):');
%     if time_unit==1
%         disp(' ');
%         disp('The time unit you use is second;');
%         eval(['ref_sp(:,1)=',reflect_name,'(:,1);'])
%         unit_judge=false;
%     elseif time_unit==2
%         disp(' ');
%         disp('The time unit you use is millisecond;');
%         eval(['ref_sp(:,1)=',reflect_name,'(:,1)./1000;'])
%         unit_judge=false;
%     elseif time_unit==3
%         disp(' ');
%         disp('The time unit you use is microsecond;');
%         eval(['ref_sp(:,1)=',reflect_name,'(:,1)./1000000;'])
%         unit_judge=false;
%     else
%         disp('Wrong input. Please choose again.');
%         unit_judge=true;
%     end
% end
% disp(' ');
%
% disp('We have following pressure unit:');
% disp('1. psi');
% disp('2. MPa');
% disp('3. Pa');
% unit_judge=true;
% pressure_unit=0; % this number can be any integer except 1, 2 and 3.
% while unit_judge==true
%       pressure_unit=input('Please choose the unit you use (input the No. before the
unit):');
%     if pressure_unit==1
%         disp(' ');
%         disp('The pressure unit you use is psi;');
%         eval(['ref_sp(:,2)=',reflect_name,'(:,2);'])
%         unit_judge=false;
%     elseif pressure_unit==2
```

```
%        disp(' ');
%        disp('The pressure unit you use is MPa;');
%        eval(['ref_sp(:,2)=',reflect_name,'(:,2).*1000000./6894.7;'])
%        unit_judge=false;
%    elseif pressure_unit==3
%        disp(' ');
%        disp('The pressure unit you use is Pa;');
%        eval(['ref_sp(:,2)=',reflect_name,'(:,2)./6894.7;'])
%        unit_judge=false;
%    else
%        disp('Wrong input. Please choose again.');
%        unit_judge=true;
%    end
% end
% disp(' ');
%
% disp('The pressure data has been resaved into variable ref_sp.');
% disp('There are two columns in ref_sp. The first column is time and unit is s
(second).');
% disp('The second column is pressure and unit is psi.');
% disp('First Step end');
% disp('%%%%%%%%%%%%%%%%%%%%%%%%%%%%%%%%%%%%%%%%%%%%%%%%%%%%%%%%');
% disp(' ');
%

disp('%%%%%%%%%%%%%%%%%%%%%%%%%%%%%%%%%%%%%%%%%%%%%%%%%%%%%%%%');
disp('First Step: load the time series of the images.');
disp(' ');

disp('You have three ways to load the time series of the images.');
disp('1. The time between two frames is same.');
disp('   You can input total number of frames and time between two frames.')
disp('   The code will generate the time series automatically.');
disp(' ');

disp('2. The time between two frames is not same.');
disp('    You can input total number of frames and input time between two frames
frame by frame.')
disp(' ');

disp('3. The time between two frames is not same.');
disp('   And you have saved the time series into one data file.')
disp('   Then you can just load that time series data file.');
disp(' ');
```

```
time_series_judge=true;
time_series=0; % this number can be any integer except 1, 2 and 3.
while time_series_judge==true
   time_series=input('Please choose which method you want to use (input the No. before the method):');
   if time_series==1
      frames=input('Please input the total number of frames for calculating(integer): '); % the number of images for calculating
      frame_time=input('Please input the time between two frames (unit: microsecond): ')/1000000;
      for i=1:frames
         t_frame(i,1)=(i-1)*frame_time;
      end
      time_series_judge=false;
   elseif time_series==2
      frames=input('Please input the total number of frames for calculating(integer): '); % the number of images for calculating
      sum_time=0;
      for i=1:frames
         disp('recent frame is')
         i
         disp('frame.')
         disp('Please input 0 when i=1;');
         sum_time=input('Please input the time between this frame and one frame before(unit: \mus): ')/1000000+sum_time;
         t_frame(i,1)=sum_time;
      end
      time_series_judge=false;
   elseif time_series==3
      time_series_name=input('Please input the filename of the time serise (without extension):','s')
      time_series_extension=input('Please input the extension of the time serise:','s')
      eval(['load ',time_series_name,'.',time_series_extension,';'])
      eval(['t_frame=',time_series_name,';'])
      time_series_judge=false;
   else
      disp('Wrong input. Please choose again.');
      time_series_judge=true;
   end
end
disp(' ');

disp('Second Step end');
disp('%%%%%%%%%%%%%%%%%%%%%%%%%%%%%%%%%%%');
disp(' ' );
```

```
disp('%%%%%%%%%%%%%%%%%%%%%%%%%%%%%%%%%%%');
disp('Third Step: length calculation.');
disp(' ');
disp('you can choose any image for length calculation.');
disp('you need to know one real scale in the image.');
disp('For example, ');
disp('the span of the supports is 6 inches');
disp('the outer diameter of the shock tube is 5 inches');
disp('Please follow the instruction.');
disp(' ');

disp('Please enter image filename for length calibration:');
I=input('(for example: calibration.jpg) ','s');
Judge1='n';
while Judge1=='n'
   % load the jpg file
   imshow(I);
   hold on

   xlabel('Length Calculation')
   title('Please pick first point for calibration');
   [xc(1),yc(1)] = ginput(1);
   title('Please pick second point for calibration');
   [xc(2),yc(2)] = ginput(1);
   title('Please pick third point for calibration');
   [xc(3),yc(3)] = ginput(1);
   title('Please pick fourth point for calibration');
   [xc(4),yc(4)] = ginput(1);
   title('Please pick fifth point for calibration');
   [xc(5),yc(5)] = ginput(1);
   title('Please pick sixth point for calibration');
   [xc(6),yc(6)] = ginput(1);

   title('Please go to the matlab main window and input the real distance');
   % average point between two calibration points
   Y(1) = abs(yc(1)-yc(2));
   Y(2) = abs(yc(3)-yc(4));
   Y(3) = abs(yc(5)-yc(6));
   measured = mean(Y);

   % determin the middle position of the shock tube
   ym(1)=(yc(1)+yc(2))/2;
   ym(2)=(yc(3)+yc(4))/2;
```

```
   ym(3)=(yc(5)+yc(6))/2;
   midy=mean(ym);

   % real distance between two calibration points. unit: m
   true = input('Please input the real distance between two points you choose (in):
')*0.0254;

   % The transfor from the pixes to distance
   scale = measured/true;

   xlabel('')
   title('Length Calculation End');

   Judge1=input('Is calibration OK? (y/n)','s');

   close all;
end

disp('Third Step end');
disp('%%%%%%%%%%%%%%%%%%%%%%%%%%%%%%%%');
disp(' ' );

disp('%%%%%%%%%%%%%%%%%%%%%%%%%%%%%%%%');
disp('Fourth Step: real measurement.');
disp(' ');
disp('you need to measure the deformation shape of front face for every image.');
disp('For each image, you need to choose seven points on the front face.');
disp('There will be a symmetric line on the image.');
disp('It is better to choose these points symmetric to this line.');
disp('Please follow the instruction.');
disp(' ');

origin_t=input('Original thickness of specimen (in): ')*0.0254;

for i = 1:frames

   disp(' ');
   if i==1
      disp('Please enter the first image filename for measurement:');
      I=input('(for example: measure_image.jpg) ','s');
   else
      I=input('Please enter next image filename for measurement: ','s');
   end

   % Simulate the Front Surface Shape with Cubic Spline interpolation method
```

```
   Judge2='n';
   while Judge2=='n'
      imshow(I);
      hold on;
      xlabel('displacement measurement');

%        x1=linspace(0,1200);
%        y1=linspace(midy,midy);
%        plot(x1,y1,'c-.')

%        if i==1
%        else
%           plot(xx(:,(i-1)),yy(:,(i-1)),'y','linewidth',0.25), hold on;
%           legend('symmetric line','previous shape');
%        end

        % choose seven points for the surface shape fit
        title('Please pick the first point for displacement calculation');
        [x(1,i),y(1,i)] = ginput(1);
        plot(x(1,i),y(1,i),'go'),hold on;

        title('Please pick the second point for displacement calculation');
        [x(2,i),y(2,i)] = ginput(1);
        plot(x(2,i),y(2,i),'go'),hold on;

        title('Please pick the third point for displacement calculation');
        [x(3,i),y(3,i)] = ginput(1);
        plot(x(3,i),y(3,i),'go'),hold on;

        title('Please pick the fourth point for displacement calculation');
        [x(4,i),y(4,i)] = ginput(1);
        plot(x(4,i),y(4,i),'go'),hold on;

        title('Please pick the fifth point for displacement calculation');
        [x(5,i),y(5,i)] = ginput(1);
        plot(x(5,i),y(5,i),'go'),hold on;

        title('Please pick the sixth point for displacement calculation');
        [x(6,i),y(6,i)] = ginput(1);
        plot(x(6,i),y(6,i),'go'),hold on;

%        title('Please pick the seventh point for displacement calculation');
%        [x(7,i),y(7,i)] = ginput(1);
%        plot(x(7,i),y(7,i),'go'),hold on;
```

```
%       d=Tube_d*scale; % the pixes scale of the diameter of shock tube
%       dD=d/100;
%       for m=1:101
%          yy(m,i)=midy-(d/2)+(m-1)*dD; % the range of shock applied
%       end
%       xx(:,i)=spline(y(:,i),x(:,i),yy(:,i));   % cubic spline data interpolation
%       plot(xx(:,i),yy(:,i),'r'), hold on;
%
%       title('Press any key to continue');
%       pause;

      X(1) = abs(x(2,i)-x(1,i));
      X(2) = abs(x(4,i)-x(3,i));
      X(3) = abs(x(6,i)-x(5,i));
      measured = mean(X)/scale;

      Strain(i,1)=t_frame(i,1);
      Strain(i,2)=(origin_t-measured)/origin_t;

      Judge2=input('Is the measurement OK? (y/n)','s');

      close all;
   end
end

% % calculate the surface position of every frame
% xf=xx(:,1);
% yf=yy(:,1);
%
% for i = 1:frames
%    for j=1:101
%       xd(j,i)=(xx(j,i)-xf(i))/scale;
%    end
% end
%
% % calculate the deflection for every points of every frame
% for j=1:101;
%    for i=1:frames
%       xdd(j,i)=abs(xd(j,i)-xd(j,1));
%    end
% end

% Figure(2)
% for i=1:frames;
%    plot(-xdd(:,i),yy(:,i)/scale,'k'),hold on
```

```
%     plot(-xdd(:,2),yy(:,1)/scale,'k--'),hold on
%     plot(-xdd(:,3),yy(:,1)/scale,'r'),hold on
%     plot(-xdd(:,4),yy(:,1)/scale,'r--'),hold on
%     plot(-xdd(:,5),yy(:,1)/scale,'g'),hold on
%     plot(-xdd(:,6),yy(:,1)/scale,'g--'),hold on
%     plot(-xdd(:,7),yy(:,1)/scale,'b'),hold on
%     plot(-xdd(:,8),yy(:,1)/scale,'b--'),hold on
%     plot(-xdd(:,9),yy(:,1)/scale,'m'),hold on
% end
% plot(-xdd(:,10),yy(:,1)/scale,'m--'),hold on
% plot(-xdd(:,11),yy(:,1)/scale,'y'),hold on
% plot(-xdd(:,12),yy(:,1)/scale,'c'),hold on
% plot(-xdd(:,13),yy(:,1)/scale,'c--'),hold on
% xlabel('unit: m');
% ylabel('unit: m');
% title('Deflection Sketch');
% axis tight

% choose the biggest time to normalize data
% n0=length(ref_sp(:,1));
% for i=1:n0
%     t(i,1)=ref_sp(i,1);
%     ref(i,1)=ref_sp(i,2);
%     if (ref_sp(i,1)>=t_frame(frames,1))
%         break;
%     end
% end
%
% % normalize the time for deflection data
% for j=1:101
%     De(:,j)=spline(t_frame,xdd(j,:),t);
% end
%
% Figure(3)
% plot(t,De(:,51),'r','linewidth',3),hold on
% ylabel('Deflection (m)');
% xlabel('Time (s)');
% grid on;
% title('Maxi Deflection-Time Curve(Middle Point)');
%
% % calculate the energy increase between every two closed frame
% n0=length(t);
% egy(1)=0;
% delta_d=(Tube_d*0.99)/99;
% for i=2:n0
```

```
%     A(i)=0;
%     for j=1:100
%                                       B(j)=((ref_sp(i,2)+ref_sp(i-1,2))*6894.7)*(De(i,j)-De(i-
1,j))*delta_d*(sqrt((Tube_d/2)^2-((Tube_d/2)-j*delta_d)^2)+sqrt((Tube_d/2)^2-
((Tube_d/2)-(j-1)*delta_d)^2))/2;
%         A(i)=B(j)+A(i);
%     end
%     egy(i)=A(i);
% end
%
% % calculate the energy increase between every frame and initial frame
% for i=1:n0
%     A1=0;
%     for j=1:i
%         B1=egy(j);
%         A1=A1+B1;
%     end
%     energy(i,1)=A1;
% end
%
% DFLE(:,1)=t;
% DFLE(:,2)=energy(:,1);
%
% Figure(4),plot(t,energy(:,1),'r','linewidth',3);
% xlabel('Time (s)');
% ylabel('Energy (J)');
% % axis tight;
% grid on;
%
% Figure(5),plot(De(:,50),energy(:,1),'r','linewidth',3);
% xlabel('Deflection (m)');
% ylabel('Energy (J)');
% grid on;
Figure(1)
plot(Strain(:,1),Strain(:,2),'r','linewidth',3), hold on
xlabel('Time (\mus)')
ylabel('Strain')
grid on;
filename=input('Please input the filename you want to save final data into: ','s');
 save strain.mat;
eval(['save ',filename,'_Strain.DAT',' Strain',' /ascii'])

clc
```

Code to Filter Measurement Data

```
% This code can be used to appy a low-pass filter to the measured data.

% data_name1 = 'Resistance_Data_Filter_2';
% eval(['load ',data_name1,';'])
%
% eval(['x = ',data_name1])

x = resistance_2;

fn=0.03;
n=2;
[bb,a] = butter(n, fn );
xx = filtfilt(bb,a,x);
Figure(1)
plot(x)
Figure(2)
plot(xx)

save Filtered_Data_Resistance_2 xx -ascii
```

BIBLIOGRAPHY

Ajayan, P. M. and J. M. Tour (2007). "Materials Science: Nanotube composites." *Nature* 447(7148).

Alexopoulos, N. D., C. Bartholome, et al. (2009). "Structural health monitoring of glass fiber reinforced composites using embedded carbon nanotube (CNT) fibers." *Composites Science and Technology* 70(2): 260-271.

Allaoui, A., S. Bai, et al. (2002). "Mechanical and electrical properties of a MWNT/epoxy composite." *Composites Science and Technology* 62(15): 1993-1998.

Bauhofer, W. and J. Z. Kovacs (2009). "A review and analysis of electrical percolation in carbon nanotube polymer composites." *Composites Science and Technology* 69(10): 1486-1498.

Bezryadin, A., A. R. M. Verschueren, et al. (1998). "Multiprobe Transport Experiments on Individual Single-Wall Carbon Nanotubes." *Physical Review Letters* 80(18): 4036-4039.

Bianco, A., H.-M. Cheng, et al. (2013). "All in the graphene family - A recommended nomenclature for two-dimensional carbon materials." *Carbon* 65(0): 1-6.

Cai, W.-Z., S.-T. Tu, et al. (2005). "A Physically Based Percolation Model of the Effective Electrical Conductivity of Particle Filled Composites." Journal of Composite Materials 40(23): 2131-2142.

Cardoso, S. M., V. B. Chalivendra, et al. (2012). "Damage detection of rubber toughened nanocomposites in the fracture process zone using carbon nanotubes." *Engineering Fracture Mechanics* 96(0): 380-391.

Chakrabarti, M. H., C. T. J. Low, et al. (2013). "Progress in the electrochemical modification of graphene-based materials and their applications." *Electrochimica Acta* 107(0): 425-440.

Dalton, A. B., S. Collins, et al. (2004). "Continuous carbon nanotube composite fibers: properties, potential applications, and problems." *Journal of Materials Chemistry* 14(1): 1-3.

Dash, M., M. Tripathy, et al. (2010). "Poly(anthranilic acid)/multi-walled carbon nanotube composites: spectral, morphological, and electrical properties." *Journal of Materials Science* 45(14): 3858-3865.

Du, J., L. Zhao, et al. (2011). "Comparison of electrical properties between multi-walled carbon nanotube and graphene nanosheet/high density polyethylene composites with a segregated network structure." *Carbon* 49(4): 1094-1100.

Eswaraiah, V., K. Balasubramaniam, et al. (2011). "Functionalized graphene reinforced thermoplastic nanocomposites as strain sensors in structural health monitoring." *Journal of Materials Chemistry* 21(34): 12626-12628.

Evora, V. M. F. and A. Shukla (2003). "Fabrication, characterization, and dynamic behavior of polyester/TiO2 nanocomposites." *Materials Science and Engineering: A* 361(1-2): 358-366.

Fang, M., K. Wang, et al. (2009). "Covalent polymer functionalization of graphene nanosheets and mechanical properties of composites." *Journal of Materials Chemistry* 19(38): 7098-7105.

Fim, F. d. C., J. M. Guterres, et al. (2009). "Polyethylene/graphite nanocomposites obtained by in situ polymerization." *Journal of Polymer Science Part A: Polymer Chemistry* 48(3): 692-698.

Frazier, R., D. Daly, et al. (2009). Recent progress in graphene-related nanotechnologies. Recent Patents on Nanotechnology. 3: 164-176.

Gao, L., T.-W. Chou, et al. (2010). "A comparative study of damage sensing in fiber composites using uniformly and non-uniformly dispersed carbon nanotubes." *Carbon* 48(13): 3788-3794.

Gao, L., E. T. Thostenson, et al. (2009). "Coupled carbon nanotube network and acoustic emission monitoring for sensing of damage development in composites." *Carbon* 47(5): 1381-1388.

Godovsky, D. Y. (2000). Device Applications of Polymer-Nanocomposites. Biopolymers · PVA Hydrogels, Anionic Polymerisation Nanocomposites, Springer Berlin Heidelberg. 153: 163-205.

Goncalves, G., P. A. A. P. Marques, et al. (2010). "Graphene oxide modified with PMMA via ATRP as a reinforcement filler." *Journal of Materials Chemistry* 20(44): 9927-9934.

Guo, P., X. Chen, et al. (2007). "Fabrication and mechanical properties of well-dispersed multiwalled carbon nanotubes/epoxy composites." *Composites Science and Technology* 67(15-16): 3331-3337.

Heeder, N., A. Shukla, et al. (2012). "Sensitivity and dynamic electrical response of CNT-reinforced nanocomposites." *Journal of Materials Science* 47(8): 3808-3816.

Heeder, N., A. Yussuf, et al. (2013). "Highly conductive graphene-based segregated composites prepared by particle templating." *Journal of Materials Science* 49(6): 2567-2570.

Heeder, N. J., A. Shukla, et al. (2012). "Electrical Response of Carbon Nanotube Reinforced Nanocomposites Under Static and Dynamic Loading." *Experimental Mechanics* 52(3): 315-322.

Heeder, N., A. Yussuf, et al. (2014). "Fixed-Angle Rotary Shear as a New Method for Tailoring Electro-Mechanical Properties of Templated Graphene-Polymer Composites." *Journal of Composites Science and Technology* (Submitted).

Herrera-Alonso, M., A. A. Abdala, et al. (2007). "Intercalation and Stitching of Graphite Oxide with Diaminoalkanes." *Langmuir* 23(21): 10644-10649.

Hu, H., G. Zhang, et al. (2012). "Preparation and electrical conductivity of graphene/ultrahigh molecular weight polyethylene composites with a segregated structure." *Carbon* 50(12): 4596-4599.

Huang, X., X. Qi, et al. (2011). "Graphene-based composites." *Chemical Society Reviews* 41(2): 666-686.

Inukai, S., K.-i. Niihara, et al. (2011). "Preparation and Properties of Multiwall Carbon Nanotubes/Polystyrene-Block-Polybutadiene-Block-Polystyrene Composites." *Industrial & Engineering Chemistry Research* 50(13): 8016-8022.

Jordan, J., K. I. Jacob, et al. (2005). "Experimental trends in polymer nanocomposites - a review." *Materials Science and Engineering: A* 393(1-2): 1-11.

Kabir, M. E., M. C. Saha, et al. (2007). "Effect of ultrasound sonication in carbon nanofibers/polyurethane foam composite." *Materials Science and Engineering: A* 459(1-2): 111-116.

Kalaitzidou, K., H. Fukushima, et al. (2007). "Multifunctional polypropylene composites produced by incorporation of exfoliated graphite nanoplatelets." *Carbon* 45(7): 1446-1452.

Kang, I., Y. Y. Heung, et al. (2006). "Introduction to carbon nanotube and nanofiber smart materials." *Composites Part B: Engineering* 37(6): 382-394.

Khan, U., P. May, et al. (2011). "Development of stiff, strong, yet tough composites by the addition of solvent exfoliated graphene to polyurethane." *Carbon* 48(14): 4035-4041.

Kim, H., A. A. Abdala, et al. (2010). "Graphene/Polymer Nanocomposites." *Macromolecules* 43(16): 6515-6530.

Kim, H. and C. W. Macosko (2008). "Morphology and Properties of Polyester/Exfoliated Graphite Nanocomposites." *Macromolecules* 41(9): 3317-3327.

Kim, H. and C. W. Macosko (2009). "Processing-property relationships of polycarbonate/graphene composites." *Polymer* 50(15): 3797-3809.

Kim, H., Y. Miura, et al. (2010). "Graphene/Polyurethane Nanocomposites for Improved Gas Barrier and Electrical Conductivity." *Chemistry of Materials* 22(11): 3441-3450.

Kim, I.-H. and Y. G. Jeong (2010). "Polylactide/exfoliated graphite nanocomposites with enhanced thermal stability, mechanical modulus, and electrical conductivity." *Journal of Polymer Science Part B: Polymer Physics* 48(8): 850-858.

Kogut, P. M. and J. P. Straley (1979). "Distribution-induced non-universality of the percolation conductivity exponents." Journal of Physics C: Solid State Physics 12: 2151-2159.

Kolsky, H. (1949). "An Investigation of the Mechanical Properties of Materials at very High Rates of Loading." *Proceedings of the Physical Science* 62: 676-700.

Kuilla, T., S. Bhadra, et al. (2010). "Recent advances in graphene based polymer composites." *Progress in Polymer Science* 35(11): 1350-1375.

Leyva, M. E., G. M. O. Barra, et al. (2003). "Electric, dielectric, and dynamic mechanical behavior of carbon black/styrene-butadiene-styrene composites." *Journal of Polymer Science Part B: Polymer Physic*s 41(23): 2983-2997.

Li, B. and W.-H. Zhong (2011). "Review on polymer/graphite nanoplatelet nanocomposites." *Journal of Materials Science* 46(17): 5595-5614.

Li, C., E. T. Thostenson, et al. (2008). "Sensors and actuators based on carbon nanotubes and their composites: A review." *Composites Science and Technology* 68(6): 1227-1249.

Li, J., J.-K. Kim, et al. (2005). "Conductive graphite nanoplatelet/epoxy nanocomposites: Effects of exfoliation and UV/ozone treatment of graphite." *Scripta Materialia* 53(2): 235-240.

Li, M., C. Gao, et al. (2013). "Electrical conductivity of thermally reduced graphene oxide/polymer composites with a segregated structure." *Carbon* 65(0): 371-373.

Li, W., A. Dichiara, et al. (2013). "Carbon nanotube-graphene nanoplatelet hybrids as high-performance multifunctional reinforcements in epoxy composites." *Composites Science and Technology* 74(0): 221-227.

Liang, J., Y. Huang, et al. (2009). "Molecular-Level Dispersion of Graphene into Poly(vinyl alcohol) and Effective Reinforcement of their Nanocomposites." *Advanced Functional Materials* 19(14): 2297-2302.

Lim, A. S., Q. An, et al. (2011). "Mechanical and electrical response of carbon nanotube-based fabric composites to Hopkinson bar loading." *Composites Science and Technology* 71(5): 616-621.

Liu, Y.-T., X.-M. Xie, et al. (2011). "High-concentration organic solutions of poly(styrene-co-butadiene-co-styrene)-modified graphene sheets exfoliated from graphite." *Carbon* 49(11): 3529-3537.

Lu, M.-D. and S.-M. Yang (2005). "Syntheses of polythiophene and titania nanotube composites." *Synthetic Metals* 154(1-3): 73-76.

Ma, P.-C., N. A. Siddiqui, et al. (2010). "Dispersion and functionalization of carbon nanotubes for polymer-based nanocomposites: A review." *Composites Part A: Applied Science and Manufacturing* 41(10): 1345-1367.

Mamunya, Y. (2011). Carbon Nanotubes as Conductive Filler in Segregated Polymer Composites - Electrical Properties. Carbon Nanotubes-Polymer Nanocomposites. D. S. Yellampalli, InTech.

Nofar, M., S. V. Hoa, et al. (2009). "Failure detection and monitoring in polymer matrix composites subjected to static and dynamic loads using carbon nanotube networks." *Composites Science and Technology* 69(10): 1599-1606.

Novoselov, K. S., A. K. Geim, et al. (2005). "Two-dimensional gas of massless Dirac fermions in graphene." *Nature* 438(7065): 197-200.

Novoselov, K. S., A. K. Geim, et al. (2004). "Electric Field Effect in Atomically Thin Carbon Films." *Science* 306(5696): 666-669.

Pang, H., Y. Bao, et al. (2012). "Segregated Conductive Ultrahigh-Molecular-Weight Polyethylene Composites Containing High-Density Polyethylene as Carrier Polymer of Graphene Nanosheets." *Polymer-Plastics Technology and Engineering* 51(14): 1483-1486.

Pantelic, R. S., J. W. Suk, et al. "Oxidative Doping Renders Graphene Hydrophilic, Facilitating Its Use As a Support in Biological TEM." *Nano Letters* 11(10): 4319-4323.

Paredes, J. I., S. Villar-Rodil, et al. (2008). "Graphene Oxide Dispersions in Organic Solvents." *Langmuir* 24(19): 10560-10564.

Park, C., Z. Onuaies, et al. (2010). Polymer-Single Wall Carbon Nanotube Composites for Potential Spacecraft Applications. Material Research Society. *Material Research Society* 706.

Paulson, S., M. R. Falvo, et al. (1999). "In situ resistance measurements of strained carbon nanotubes." *Applied Physics Letters* 75(19): 2936-2938.

Pedroni, L. G., M. A. Soto-Oviedo, et al. (2009). "Conductivity and mechanical properties of composites based on MWCNTs and styrene-butadiene-styrene block™ copolymers." *Journal of Applied Polymer Science* 112(6): 3241-3248.

Peng, H. (2007). "Aligned Carbon Nanotube/Polymer Composite Films with Robust Flexibility, High Transparency, and Excellent Conductivity." *Journal of the American Chemical Society* 130(1): 42-43.

Potts, J. R., D. R. Dreyer, et al. (2011). "Graphene-based polymer nanocomposites." *Polymer* 52(1): 5-25.

Pramoda, K. P., H. Hussain, et al. (2010). "Covalent bonded polymer–graphene nanocomposites." *Journal of Polymer Science Part A: Polymer Chemistry* 48(19): 4262-4267.

Qi, X.-Y., D. Yan, et al. (2011). "Enhanced Electrical Conductivity in Polystyrene Nanocomposites at Ultra-Low Graphene Content." *ACS Applied Materials & Interfaces* 3(8): 3130-3133.

Qu, S. and S.-C. Wong (2007). "Piezoresistive behavior of polymer reinforced by expanded graphite." *Composites Science and Technology* 67(2): 231-237.

Ramanathan, T., A. A. Abdala, et al. (2008). "Functionalized graphene sheets for polymer nanocomposites." *Nat Nano* 3(6): 327-331.

Ramirez, C., F. M. Figueiredo, et al. (2012). "Graphene nanoplatelet/silicon nitride composites with high electrical conductivity." *Carbon* 50(10): 3607-3615.

Rath, T. and Y. Li (2011). "Nanocomposites based on polystyrene-b-poly(ethylene-r-butylene)-b-polystyrene and exfoliated graphite nanoplates: Effect of nanoplatelet loading on morphology and mechanical properties." *Composites Part A: Applied Science and Manufacturing* 42(12): 1995-2002.

Sahrim, H., A. Mou'ad, et al. (2011). Reinforced Thermoplastic Natural Rubber (TPNR) Composites with Different Types of Carbon Nanotubes (MWNTS). Carbon Nanotubes - Synthesis, Characterization, Applications. S. Yellampalli, InTech.

Sengupta, R., M. Bhattacharya, et al. (2010). "A review on the mechanical and electrical properties of graphite and modified graphite reinforced polymer composites." *Progress in Polymer Science* 36(5): 638-670.

Singh, V., D. Joung, et al. (2011). "Graphene based materials: Past, present and future." *Progress in Materials Science* 56(8): 1178-1271.

Soldano, C., A. Mahmood, et al. (2010). "Production, properties and potential of graphene." *Carbon* 48(8): 2127-2150.

Stankovich, S., D. A. Dikin, et al. (2006). "Graphene-based composite materials." *Nature* 442(7100): 282-286.

Stankovich, S., D. A. Dikin, et al. (2007). "Synthesis of graphene-based nanosheets via chemical reduction of exfoliated graphite oxide." *Carbon* 45(7): 1558-1565.

Stankovich, S., R. D. Piner, et al. (2006). "Stable aqueous dispersions of graphitic nanoplatelets via the reduction of exfoliated graphite oxide in the presence of poly(sodium 4-styrenesulfonate)." *Journal of Materials Chemistry* 16(2): 155-158.

Sumfleth, J., S. Buschhorn, et al. (2011). "Comparison of rheological and electrical percolation phenomena in carbon black and carbon nanotube filled epoxy polymers." *Journal of Materials Science* 46(3): 659-669.

Tang, Q.-Y., Y.-C. Chan, et al. (2010). "Surfactant-assisted processing of polyimide/multiwall carbon nanotube nanocomposites for microelectronics applications." *Polymer International* 59(9): 1240-1245.

Tang, W., B. Liu, et al. (2011). "Processing-dependent high impact polystyrene/styrene-butadiene-styrene tri-block copolymer/carbon black antistatic composites." *Journal of Applied Polymer Science* 123(2): 1032-1039.

Thostenson, E. T. and T. W. Chou (2006). "Carbon Nanotube Networks: Sensing of Distributed Strain and Damage for Life Prediction and Self Healing." *Advanced Materials* 18(21): 2837-2841.

Thostenson, E. T., Z. Ren, et al. (2001). "Advances in the science and technology of carbon nanotubes and their composites: a review." *Composites Science and Technology* 61(13): 1899-1912.

Tibbetts, G. G., M. L. Lake, et al. (2007). "A review of the fabrication and properties of vapor-grown carbon nanofiber/polymer composites." *Composites Science and Technology* 67(7-8): 1709-1718.

Tjong, S. C. (2006). "Structural and mechanical properties of polymer nanocomposites." *Materials Science and Engineering: R: Reports* 53(3-4): 73-197.

Vadlamani, V. K., V. Chalivendra, et al. (2012). "In situ sensing of non-linear deformation and damage in epoxy particulate composites." *Smart Materials and Structures* 21(7).

Vadlamani, V. K., V. B. Chalivendra, et al. (2012). "Sensing of damage in carbon nanotubes and carbon black-embedded epoxy under tensile loading." *Polymer Composites* 33(10): 1809-1815.

Vadukumpully, S., J. Paul, et al. (2011). "Flexible conductive graphene/poly(vinyl chloride) composite thin films with high mechanical strength and thermal stability." *Carbon* 49(1): 198-205.

Venkateswara Rao, C., C. R. Cabrera, et al. (2011). "Graphene-Supported Pt-Au Alloy Nanoparticles: A Highly Efficient Anode for Direct Formic Acid Fuel Cells." *The Journal of Physical Chemistry C* 115(44): 21963-21970.

Verdejo, R., M. M. Bernal, et al. (2010). "Graphene filled polymer nanocomposites." *Journal of Materials Chemistry* 21(10): 3301-3310.

Viculis, L. M., J. J. Mack, et al. (2005). "Intercalation and exfoliation routes to graphite nanoplatelets." *Journal of Materials Chemistry* 15(9): 974-978.

Wang, B., H. Li, et al. (2013). "Electrostatic adsorption method for preparing electrically conducting ultrahigh molecular weight polyethylene/graphene nanosheets composites with a segregated network." *Composites Science and Technology* 89(0): 180-185.

Wang, L., J. Hong, et al. (2010). "Comparison study of graphite nanosheets and carbon black as fillers for high density polyethylene." *Polymer Engineering & Science* 50(11): 2176-2181.

Xie, S. H., Y. Y. Liu, et al. (2008). "Comparison of the effective conductivity between composites reinforced by graphene nanosheets and carbon nanotubes." *Applied Physics Letters* 92(24): -.

Xiong, Y., Y. Xie, et al. (2012). "Reduced graphene oxide/hydroxylated styrene-butadiene-styrene tri-block copolymer electroconductive nanocomposites: Preparation and properties." *Materials Science and Engineering: B* 177(14): 1163-1169.

Yang, S., W. Lin, et al. (2011). "Synergetic effects of graphene platelets and carbon nanotubes on the mechanical and thermal properties of epoxy composites." *Carbon* 49(3): 793-803.

Yasmin, A. and I. M. Daniel (2004). "Mechanical and thermal properties of graphite platelet/epoxy composites." *Polymer* 45(24): 8211-8219.

You, K., S. Park, et al. (2011). "Preparation and characterization of conductive carbon nanotube-polyurethane foam composites." *Journal of Materials Science* 46(21): 6850-6855.

Zhang, H.-B., W.-G. Zheng, et al. (2010). "Electrically conductive polyethylene terephthalate/graphene nanocomposites prepared by melt compounding." *Polymer* 51(5): 1191-1196.

Zhu, Y., S. Murali, et al. (2010). "Graphene and Graphene Oxide: Synthesis, Properties, and Applications." *Advanced Materials* 22(35): 3906-3924.